RELATIONSHIP BETWEEN PORE GEOMETRY, MEASURED BY

PETROGRAPHIC IMAGE ANALYSIS, AND PORE-THROAT GEOMETRY,

CALCULATED FROM CAPILLARY PRESSURE, AS A MEANS TO PREDICT

RESERVOIR PERFORMANCE IN SECONDARY RECOVERY PROGRAMS

FOR CARBONATE RESERVOIRS

A Thesis

by

CHRISTINA MARIE DICUS

Submitted to the Office of Graduate Studies of
Texas A&M University
in partial fulfillment of the requirements for the degree of

MASTER OF SCIENCE

December 2007

Major Subject: Geology

RELATIONSHIP BETWEEN PORE GEOMETRY, MEASURED BY

PETROGRAPHIC IMAGE ANALYSIS, AND PORE-THROAT GEOMETRY,

CALCULATED FROM CAPILLARY PRESSURE, AS A MEANS TO PREDICT

RESERVOIR PERFORMANCE IN SECONDARY RECOVERY PROGRAMS

FOR CARBONATE RESERVOIRS

A Thesis

by

CHRISTINA MARIE DICUS

Submitted to the Office of Graduate Studies of
Texas A&M University
in partial fulfillment of the requirements for the degree of

MASTER OF SCIENCE

Approved by:

Chair of Committee, Wayne M. Ahr
Committee Members, David S. Schechter
        Hongbin Zhan
Head of Department, Andreas Kronenberg

December 2007

Major Subject: Geology

ABSTRACT

Relationship between Pore Geometry, Measured by Petrographic Image Analysis, and
Pore-Throat Geometry, Calculated from Capillary Pressure, as a Means to Predict
Reservoir Performance in Secondary Recovery Programs for Carbonate Reservoirs.

(December 2007)

Christina Marie Dicus, B.S., Rice University

Chair of Advisory Committee: Dr. Wayne M. Ahr

The purpose of this study was first to develop a method by which a detailed
porosity classification system could be utilized to understand the relationship between
pore/pore-throat geometry, genetic porosity type, and facies. Additionally, this study
investigated the relationships between pore/pore-throat geometry, petrophysical
parameters, and reservoir performance characteristics. This study focused on the
Jurassic Smackover reservoir rocks of Grayson field, Columbia County, Arkansas.

This three part study developed an adapted genetic carbonate pore type
classification system, through which the Grayson reservoir rocks were uniquely
categorized by a percent-factor, describing the effect of diagenetic events on the
preservation of original depositional texture, and a second factor describing if the most
significant diagenetic event resulted in porosity enhancement or reduction. The second
part used petrographic image analysis and mercury-injection capillary pressure tests to
calculate pore/pore-throat sizes. From these data sets pore/pore-throat sizes were
compared to facies, pore type, and each other showing that pore-throat size is controlled

by pore type and that pore size is controlled primarily by facies. When compared with each other, a pore size range can be estimated if the pore type and the median pore-throat aperture are known.

Capillary pressure data was also used to understand the behavior of the dependent rock properties (porosity, permeability, and wettability), and it was determined that size-reduced samples, regardless of facies, tend to show similar dependent rock property behavior, but size-enhanced samples show dispersion. Finally, capillary pressure data was used to understand fluid flow behavior of pore types and facies. Oncolitic grainstone samples show unpredictable fluid flow behavior compared to oolitic grainstone samples, yet oncolitic grainstone samples will move a higher percentage of fluid. Size-enhanced samples showed heterogeneous fluid flow behavior while the size-reduced samples could be grouped by the number of modes of pore-throat sizes.

Finally, this study utilized petrographic image analysis to determine if 2-dimensional porosity values could be calculated and compared to porosity values from 3-dimensional porosity techniques. The complex, heterogeneous pore network found in the Grayson reservoir rocks prevents the use of petrographic image analysis as a porosity calculation technique.

DEDICATION

". . . I usually don't like thinking about the future. I mean, let's face it, you can't predict what's gonna happen. But sometimes, the thing you didn't expect is what you really wanted after all. Maybe the best thing to do is just stop trying to figure out where you're going, and just enjoy where you're at . . ."

John Dorian

ACKNOWLEDGEMENTS

NOMENCLATURE

MMSTB   Million stock tank barrels (of oil)

MCF   Thousand cubic feet (of gas)

PIA   Petrographic Image Analysis

MICP   Mercury-Injection Capillary Pressure

k   Permeability in μ^2 or md ($1md = 9.871 * 10^{-4}$)

ϕ Phi, porosity as a fraction or as a percent

PTS (PTA)   Pore-throat size in μ or mm (or pore-throat area, μm^2 or mm^2)

PS (PA)   Pore size in μ or mm (or pore area in μm^2 or mm^2)

TABLE OF CONTENTS

LIST OF FIGURES

Page

LIST OF TABLES

INTRODUCTION

Oil and gas fields comprising of carbonate reservoir rocks have complex heterogeneities in reservoir quality due to the inherent complexity of carbonate sediments. These complexities are the result of the unique attributes that distinguish carbonates from other sedimentary rocks types. Such attributes include: sediment formation within the basin of deposition by biological, chemical, and detrital processes, dependence on biological activity as a source of constituent grain types, complex mineralogical composition of grains, and the susceptibility to extensive diagenetic change and brittle rock behavior before, during, and after deposition. These unique attributes dictate that secondary rock properties such as porosity and permeability are dependent not only on depositional processes but also on diagenetic alterations and fracturing of reservoir rocks. Thus carbonate rocks are traditionally characterized by a variety of complex pore types including interparticle, intercrystalline, intraskeletal, vuggy, and moldic pores, thereby preventing the easy prediction of related petrophysical and reservoir performance characteristics. Additionally, since the distribution of porosity does not conform to depositional facies boundaries, it is essential to develop a method by which the spatial distribution of high-quality and low-quality porosity zones can be related to stratigraphic horizons in carbonate fields possessing complex heterogeneities.

_____

This thesis follows the style and format of the American Association of Petroleum Geologists Bulletin.

Such a method would initially require an in depth understanding of the geologic origin of the porosity at different locations throughout the field and in different reservoir rock lithologies. Ahr (2003) suggests that the recognition of different pore types can be especially important for reservoir performance. Therefore an adaptation of the traditional carbonate porosity classifications would be useful to account for the geologic processes that control the creation of different types of porosity, and be directly linked to a descriptive pore type, with the ultimate goal that these pore types can be distinguished by different reservoir performance characteristics.

Two of the most basic yet most important reservoir performance characteristics are the distributions of pore and pore-throat sizes. These two parameters, jointly described as pore/pore-throat geometry, control both the fluid storage capacity of a rock and the ability of the fluid to flow out of pore spaces. For this reason, a second step in this pore-classification method would be to determine the relationship between pore and pore-throat sizes. Determining such a relationship would be essential for field development strategies such as predicting reservoir response to fluid injection, selecting infill well locations, or enhancing the profitability of recovery methods by highlighting areas in carbonate fields where pore and pore-throat size distributions may be related or may be erratic due to several stages of diagenesis.

Hence the final step would be two combine the descriptive pore types and their corresponding pore/pore-throat geometries; the goal being to determine if there is a distinctive relationship between different pore types and their pore/pore-throat geometries in such a way that by identifying and classifying pores their corresponding

petrophysical characteristics can be determined. Knowing the geological causes that created the pore types and geometries, it is also possible to identify corresponding stratigraphic characteristics created by the pore-forming processes, such that it is possible to correlate pore types/characteristics and consequent reservoir quality at field scale. This method should make it possible to map reservoir quality zones in complex carbonate reservoirs by using the genetic links between pore types and their correlative stratigraphic characteristics such as disconformities, unconformities, siliciclastic or evaporite-rich zones, paleosols, etc.

Previous Work

Previous thesis work (Poole, 2006) focused on developing the depositional and diagenetic history of the Grayson field reservoir rocks, identifying, mapping, and ranking flow units, baffles, and barriers throughout the field, and establishing the spatial distribution of the different facies across Grayson field. A fundamental problem in the analysis of all reservoirs is identifying flow units, baffles, and barriers, and assessing which flow units have the greatest potential (highest quality) to produce economic quantities of hydrocarbons. In the Poole (2006) study, flow units are defined as reservoir zones that combine high porosity and permeability with low capillary resistance to fluid flow. Flow units were quality-ranked on the combined numerical values of porosity and permeability as measured by conventional core analyses. Reservoir zones with lower poroperm values that do not readily allow direct fluid transmission but do allow circuitous flow around low poroperm segments are defined as

baffles. True barriers to flow do not allow fluid flow vertically or horizontally.

Additionally, Poole (2006) made basic pore type classifications for the Smackover

reservoir rocks. Poole (2006) states that examination of thin sections and cores reveals

H_{1a} as the main pore type in Grayson field, per the Ahr Genetic Classification of

Carbonate Porosity (Ahr et al., 2005).

Other studies show that a more detailed classification system of pore types can

often provide insight into the fluid-flow properties of different rock units. Kopaska-

Merkel and Mann (1991) developed *pore facies*, rocks units that are defined by certain

proportions of pore types, which contain specific pore-throat-size distributions, and

exhibit certain consequent fluid-flow properties. Pore facies can be made up of one or

more different pore types. Kopaska-Merkel and Mann (1991) recognized that pore

systems are the result of sediment deposition and several stages of diagenetic change,

and the consequent shapes and sizes of the pores directly affects fluid-flow properties.

They also suggest that pore-system geometry exerts greater control on hydrocarbon-

production potential than any other feature of reservoir rock matrix. Thus the work of

Kopaska-Merkel and Mann (1991) supports this present study and its undertaking of the

development of a detailed pore classification system, in which different types of

reservoir rocks can be linked to different pore types, based on diagenetic history,

different pore/pore-throat geometries, and the corresponding petrophysical and reservoir

performance characteristics. Kopaska-Merkel and Mann (1991) were able to classify

pore types and pore facies for Smackover reservoir rocks in southwestern Alabama, with

similar rock units of similar facies and porosity.

A similar study has been conducted on the Smackover Formation in Southern Arkansas at Waller Creek field, which is in same county as Grayson field. Bliefnick and Kaldi (1996) evaluated the hydrocarbon potential of the field with a similar goal to determine the best enhanced recovery technique. The study involved the description of the Smackover reservoir properties based on sedimentological, petrophysical, and capillary pressure data; the goal being to link certain reservoir properties with geological controls (depositional vs. diagenetic) and the production potential of different rock types. Bliefnick and Kaldi (1996) believe that pore geometry controls reservoir quality and they present in their study the qualitative relationship between pore geometry and reservoir quality using thin sections, pore casts, and mercury-injection capillary pressure analysis. Reservoir quality, per Bliefnick and Kaldi, (1996) is indicated by the relationship of pore-throat size distribution, the ratio of pore to pore-throat size, and the degree of pore connectivity.

The main differences between the Bliefnick and Kaldi (1996) Waller Creek field study and the present Grayson field study are in the methods for obtaining pore/pore-throat geometry data. For this study, petrographic image analysis is the focus as a reliable, rapid, and reproducible method to characterize pore geometry. Additionally, this study will not use capillary pressure curves as a means to identify different types of reservoir rocks, rather mercury-injection capillary pressure analysis data will be utilized for the pore-throat aperture, permeability, and saturation data that such an analysis provides. Finally, the carbonate pore type classification for the present Grayson field study will be based on a newly devised, adapted version of the Ahr Genetic

Classification for Carbonate Porosity (Ahr et al., 2005) with some incorporation of traditional carbonate porosity classifications such as the Dunham (1962) classification system.

Petrographic image analysis has been extensively documented by Ehrlich et al. (1984, 1991). Ehrlich et al. developed petrographic image analysis (PIA) as a means to relate the petrology of reservoirs to petrophysical and geophysical data. This relationship is based on the idea that the two-dimensional view of porosity from PIA is useful for calculating total optical porosity to represent effective porosity, and for classifying pore types. More recent work has compared the estimation of porosity from PIA to core-measured-porosity methods. Mowers and Budd (1996) performed PIA techniques to quantify porosity and permeability reduction in grain-supported dolostone samples with varying amounts of late-stage calcite cements. The results from this study suggest that PIA is applicable for characterizing pore systems and estimating porosity from thin section for the specific reservoir rocks and formations analyzed in their study. Positive results from their PIA study give support to this study to test if petrographic image analysis is applicable to the Smackover reservoir rocks of Grayson field and if it can assist both in pore type characterization and rapid and reliable porosity estimation.

Definition of Problem

Grayson field in Columbia Country Arkansas is in the advanced development and secondary recovery stage. While the spatial distribution and rank of flow units across the field has been previously established, a detailed analysis of the different types of genetic porosity and the relationships between pore/pore-throat geometry and dependent rock properties has yet to be undertaken. Additionally, unique methods such as petrographic image analysis used to calculate porosity and the relationship between pore/pore-throat geometry and other petrophysical parameters has not been previously determined.

Purpose of Study

The purpose for undertaking this study is first, to develop a method by which a detailed and unique porosity classification system can be utilized to understand the relationship between pore/pore-throat geometry, genetic porosity type, and facies. Second, this study proposes to investigate the relationships, if any, between pore/pore-throat geometry and petrophysical parameters just as permeability and porosity. For the calculation of porosity, an innovative image analysis approach will be used to determine if such a method, based on thin section photomicrographs, is both time-effective and adequately compares to other porosity calculation methods from cores and core plugs. Finally, suggestions will be made in regards to determining either pore/pore-throat size, permeability, or to qualify the fluid flow behavior in different samples from different

wells and depths across the field by knowing either the pore type or the facies of the sample.

Grayson Field Details

Grayson field is located in Columbia County, Arkansas in Township 16 South, Range 21 West (Figure 1). The field was discovered in March 1993 with the drilling of the Alexander #1 well by Petro-Chem Operating Co., Inc. (Netherland et al., 1996). The reservoir covers an area of 800 – 900 acres (Takach et al., 1998) and has produced over 13.25 MMSTB from the Smackover limestone (Jurassic) formation. Figure 2 shows field production from 1993 to present. A reservoir simulation study by Netherland, Sewell, and Associates, Inc. (1996) suggests that the original oil-in-place is estimated to be 41.9 MMSTB. At the time of the study, the reservoir pressure was below the oil bubblepoint pressure, allowing for gas cap formation, and the reservoir drive mechanism was primarily solution-gas drive with minimal aquifer influx.
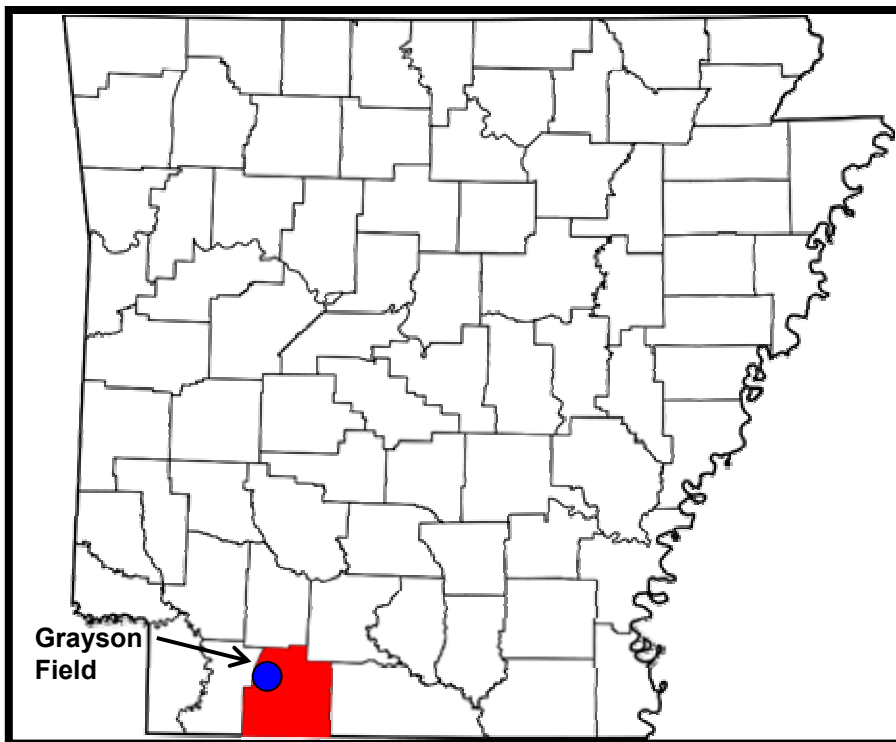
Figure 1: Grayson field, Columbia County, Arkansas. Township 16 South, Range 21 West (redrawn from Benbennick, 2007).
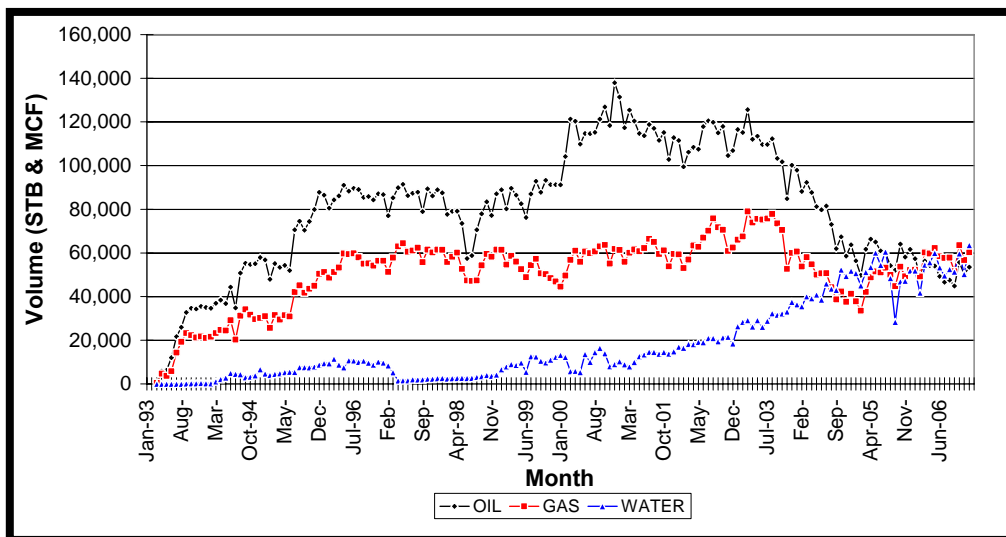
Figure 2: Grayson field production from 1993 to present.

In Grayson field, oil is produced from the Upper Jurassic Smackover limestones. The Netherland et al. (1996) reservoir simulation study suggests that there is at most 100ft of net pay thickness in the Smackover lime unit on top of the structural high, thinning to <25ft at the field perimeter. Average porosity from log analysis is estimated at about 26%. In the reservoir simulation study the Smackover formation was divided into 3 major intervals. Interval A is the most massive and is the best developed reservoir unit containing the majority of the oil reserves in the field. Intervals B and C are predominantly wet, although interval C has been completed and produced in 2 wells. Within these 3 units Netherland et al. (1996) found geologically distinguishable layers. For example in interval A they state that there are 5 layers with significantly different core porosities and permeabilities and are identifiable through out all of the wells analyzed in their study. Hence, the variability within the Smackover formation at Grayson field and the uniqueness of different layers within the Smackover reservoir rocks warrants a detailed study of the potentially heterogeneous petrophysical and reservoir performance characteristics such as pore and pore-throat systems and pore types in these reservoir units at Grayson field.

Netherlands et al. (1996) additionally suggested that development wells should be drilled and completed in the central area of the field, or the drilling and completion of horizontal wells in the low permeability Smackover units to increase recovery from the underdeveloped central field area. This present Grayson field study aims to show the value of a detailed petrographic and petrophysical study for determining the proper

course of action to increase and enhance recovery of the oil reserves in the Smackover

limestone reservoir units.

REGIONAL GEOLOGIC SETTING

Structural Setting

Tectonism along the Arkansas-Louisiana border during the Triassic-Jurassic was controlled by west northwest-east southeast rifting and block faulting associated with the opening of the Gulf of Mexico during this time period. South of the state line graben, northern Louisiana was a region of active subsidence, while southern Arkansas remained stable and is termed the South Arkansas shelf. The negative area south of the state line where subsidence was active is termed the North Louisiana Salt basin, which is bordered on the west by the Sabine Uplift and on the east by the Monroe Uplift (Moore and Druckman, 1981) (Figure 3). Thus the State Line Fault System running parallel along the Arkansas-Louisiana state line is bordered to the south by this North Louisiana Salt Basin, and is underlain by the thick Jurassic Louann salt that extends midway up the South Arkansas shelf before pinching out (Kalbacher and Sartin, 1986). Grayson field is located immediately updip of the State Line Fault system. The producing Smackover (Jurassic) reservoir rocks dip to the southwest across southern Arkansas (Troell and Robinson, 1987).
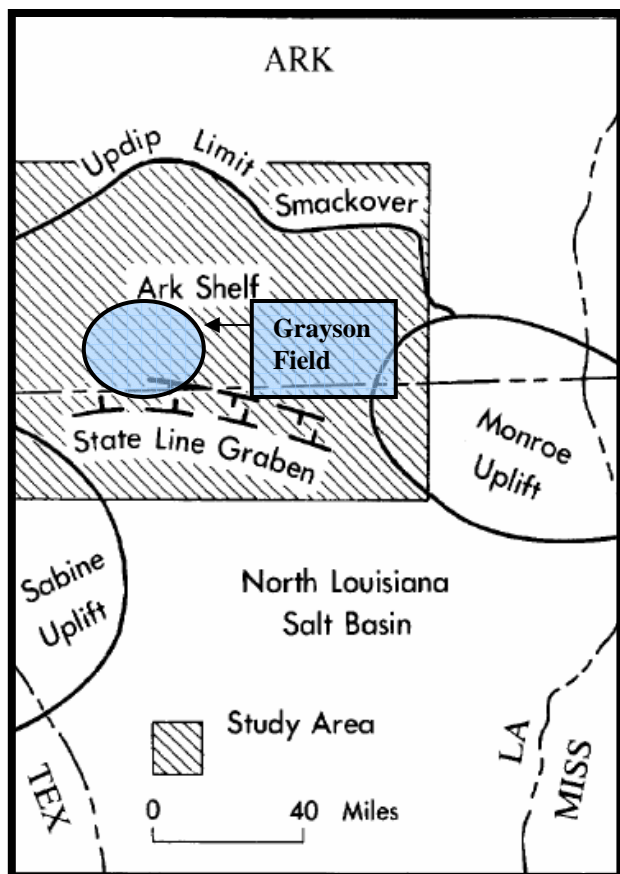
Figure 3: Structural setting of Grayson field. The "study area" indicated on this figure corresponds to the study area in this present Grayson field stud (redrawn from Moore and Druckman, 1981).

Smackover oil production in this region has been predominantly from salt-cored anticline structures (Bornhauser, 1958), and fields exemplifying this characteristic, such as Dorcheat- Macedonia, Atlanta, and Magnolia Fields, were discovered as early as the late 1930's. Production in the Smackover formation along the State Line Fault System began as early as the late 1940's (Troell and Robinson, 1987). As suggested by Bornhauser (1958), these salt-cored anticlines were generated by the thickening of the Louann salt formation in the folds of beds of younger depositional units. The movement

of salt that created these folds in the younger strata was the result of gravity-flow folding as younger strata were deposited on top of the Louann salt (Troell and Robinson, 1987). Hughes (1968) explains the evolution of salt anticlinal structures beginning with the deposition of the Norphlet sandstone on top of the Louann salt. The movement of salt also created the South Arkansas Fault System by gravity sliding and the State Line Fault System is associated with salt tectonics during the Smackover-Buckner and younger strata deposition (Troell and Robinson, 1987).

Grayson field is an elongated, east-west striking, salt-cored anticline, south of a down-to-the-south normal fault (Netherlands et al., 1996) with a combination structural-stratigraphic trap. The salt-cored anticline structure of Grayson field has few internal faults; however, Netherlands et al. (1996) identified a small normal fault on the southeast portion of the salt-cored feature.

Stratigraphic Setting

The Smackover formation in Southern Arkansas is Oxfordian in age and is conformably overlain by the Kimerigdian Buckner formation that consists of a sequence of evaporates and intercalated dolomite beds, and serves as the seal for the Smackover reservoir rocks in Grayson field (Poole, 2006). Throughout southern Arkansas, the Smackover is underlain by either the Norphlet sandstone formation or by the Louann salt (Moore and Druckman, 1981). Grayson field, however, is located north of the Norphlet quartzose clastics pinchout and thus is underlain by the Louann salt, composed of halite

and some siliciclastics and anhydrite (Poole, 2006). Figure 4 shows the simplified

stratigraphy of the Jurassic section in southern Arkansas.
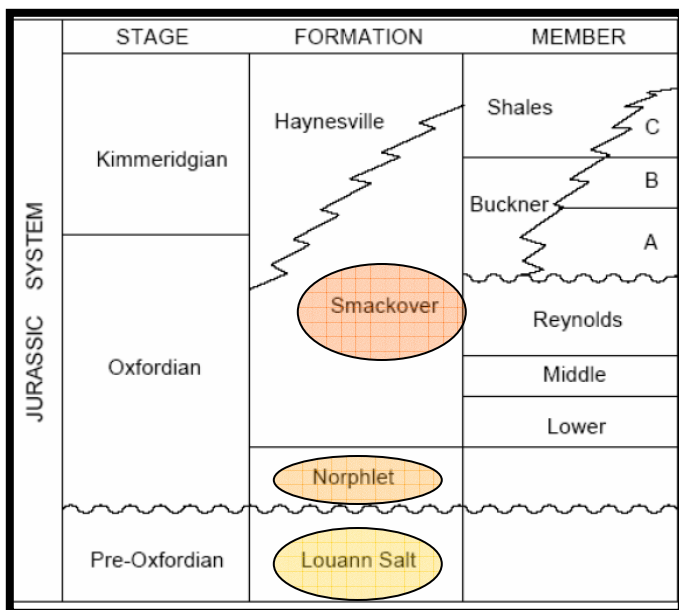
Figure 4: Simplified stratigraphy for the Jurassic section in southern Arkansas. Units of interest are highlighted (redrawn from Bliefnick and Kaldi, 1996).

The upper Smackover of Grayson field is interpreted to be a prograding ooid

shoal complex deposited on a carbonate ramp. The primary ramp surface is the Louann

salt that thickens basin ward and was deposited on a flat basinward dipping surface (Ahr,

1973; Hughes, 1968). However, pre-Jurassic salt movement and paleo-highs controlled

variability in carbonate sedimentation. Poole (2006) suggests that grain-supported facies

and microbial boundstone facies are located at the top and flanks of salt highs, Buckner

thins, and Smackover structural highs. The work by Poole (2006) confirms that the

present day Smackover structure is similar in both size and shape to the bathymetry of

the Buckner-Smackover ocean at the time of Buckner deposition (Poole, 2006). The

paleo-highs allowed shallow, agitated waters to form ooid grainstone shoals and

microbialites. On the other hand, fine-grained packstones and wackestones were

deposited off-structure toward paleo-lows, and wackestone and mudstones facies were

deposited directly in paleo-lows. These structurally negative areas allowed for the

development of quiescent, deepwater environments associated with fine-grained

sediment deposition (Poole, 2006).

These findings are consistent with the Jurassic carbonate ramp model and

comparable to the Campeche Bank of the Pleistocene, grainy rocks along the updip

margin and muddy rocks deposited basinward (Ahr, 1973). Figure 5 shows the extent

and the facies pattern for the Jurassic Smackover ramp deposits (Ahr, 1973). The basinal

mudstones are dark colored, organic rich deposits considered to serve as the source rock

for many Smackover reservoirs. Most of the Smackover reservoirs are found in the

grainstone units because of the potential for high depositional porosity and

diagenetically enhanced flow units with high storage capacity and connectivity (Morgan,

2003).

Poole (2006) also described in detail the diagenetic history of Grayson field.

Figure 6 is a summary of the diagenetic history of the study area from Poole (2006).

Thin section petrography showed micritization of grains as the first diagenetic event

occurring in the marine environment, along with early isopachus rim cement. Leaching,

compaction, and blocky cementation events were the dominant events occurring in the

meteoric phreatic and mixing zone environments. Poole (2006) considers the meteoric

leaching event to be the dominant porosity and permeability enhancement mechanism.

The dominant porosity and permeability reduction mechanism is considered to be the

freshwater phreatic, blocky cementation, and late-stage anhydrite and dolomite pore-

filling events.
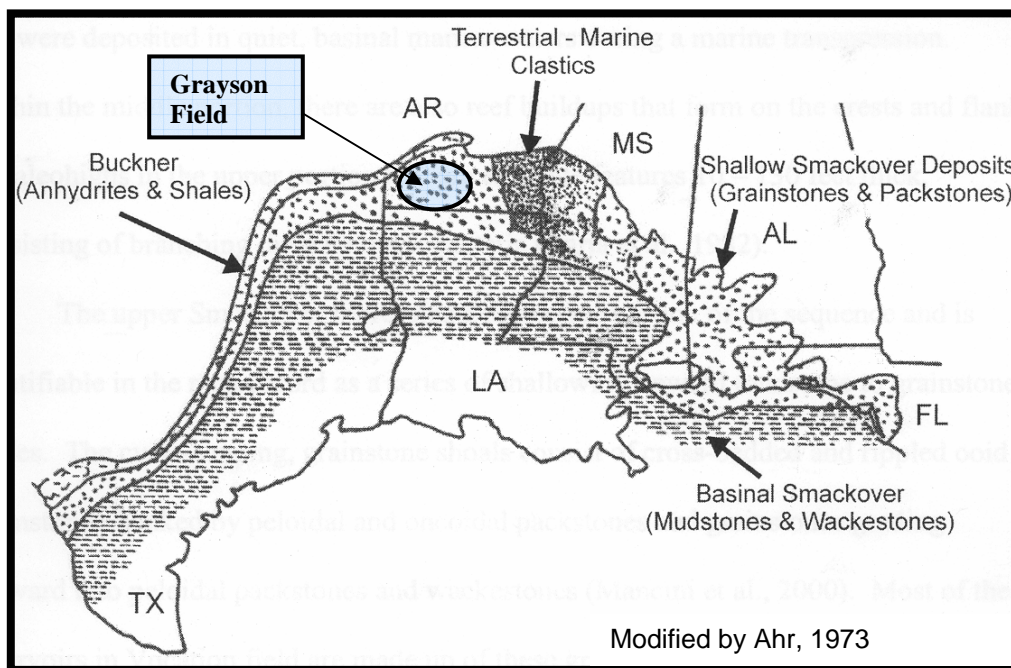
***Figure 5: Extent and facies patterns for Jurassic Smackover ramp deposits (redrawn
from Ahr, 1973 and Poole, 2006).***
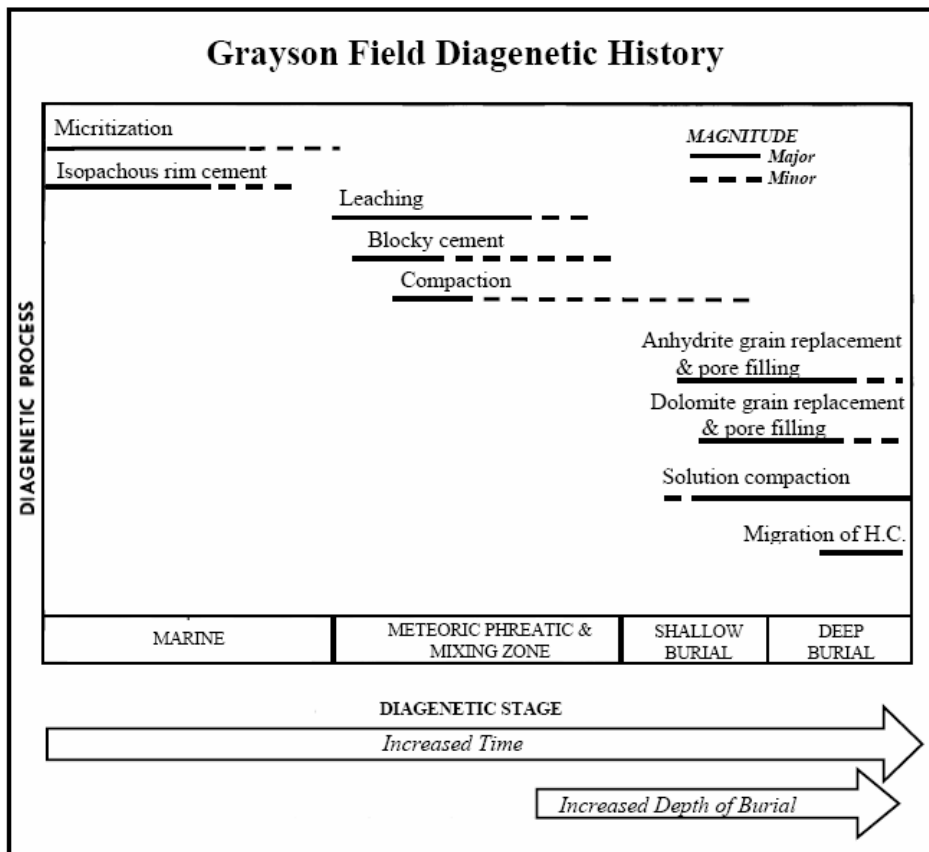
Figure 6: Diagentic history for the study area (redrawn from Poole, 2006).

METHODS

The evaluation of pore and pore-throat characteristics for Grayson field Smackover reservoir rock consists of three procedures: 1) classification of pore types, 2) petrographic image analysis, and 3) mercury-injection capillary pressure testing. Thirty-nine thin sections (professionally prepared with Alizarin Red S stain and impregnated with epoxy to identify pore space) from trimmed end segments of one-inch diameter core plugs collected from 10 wells across Grayson field were provided by Poole (2006). These thin sections were utilized for both classification of pore types and petrographic image analysis. Descriptions of depositional textures, mineralogy, grain and cements types, and diagenetic history based on thin section petrography compiled by Poole (2006) were reevaluated and used in conjunction with detailed pore type characterization, based on an adaptation of the genetic classification of carbonate porosity developed by Ahr et al. (2005). Digital photographs of thin sections were obtained for petrographic image analysis and utilized with image analysis software to measure pore area and total visible porosity. Core plugs provided by Poole (2006) were cleaned prior to mercury-injection capillary pressure testing, which was performed by PetroTech Associates.

Classification of Pore Types

The goal of pore type classification in this study is to determine the spatial distribution of different petrophysical parameters throughout the Smackover reservoir

rock. A porosity classification scheme that considers both the products (pore types) and the processes (depositional and diagenetic) of pore-formation is therefore essential. For this reason the Ahr genetic classification of carbonate porosity (Ahr et al., 2005) has been used as the general basis for the pore type classification procedures in this study. This genetic classification system is based on the principle that carbonate pores are more effectively distinguished by a combination of their geologic origin and their pore geometry such as interparticle, intercrystalline, molds, vugs, and fenestral pores, for example. The Ahr system utilizes some elements of the more common carbonate porosity classifications such as Choquette and Pray (1970), while enhancing the characterization of the pores with links to formative geologic processes and thus adapting carbonate porosity for subsurface mapping and the identification of flow units.

Explanation of Adapted Pore Type Classification

Diagenetic processes can alter the original depositional texture by dissolution of grains and mud-matrix, by cementation due to crystal precipitation around grain boundaries, by the replacement of precursor carbonate minerals by anhydrite or dolomite, and by mechanical compaction due to overburden stress that causes individual grains to penetrate surrounding grains and matrix thus destroying depositional features. Additionally, post-depositional processes may result in reduced or enhanced pore space. Porosity reduction by diagenetic processes includes mechanical compaction by increasing grain contacts, pore filling and grain replacement by anhydrite and dolomite that transgress grain boundaries and pore walls, and precipitation of cements that coat

the perimeter of grains, filling pore space. Porosity enhancing processes present in the Grayson samples are dissolution of pore-filling cements and solid rock by undersaturated waters, and replacement by dolomite crystals.

Based on the Ahr genetic classification of carbonate porosity, traditionally, carbonate rocks with evidence of some original depositional porosity but a diagenetic influence on that porosity are called hybrid 1 pore types (Figure 7). For the Grayson samples, the observation in thin section of the above mentioned alterations to original depositional grain texture combined with the diagenetic enhancement or reduction of porosity warranted the adaptation of the Ahr classification. Therefore a more detailed scale for assigning a specific pore type label within the more general hybrid 1 pore type group was designed based on two factors. The first factor qualifies the preservation of the depositional texture based on recognition of the original depositional character of the grains and matrix in thin section. A value that represents an increasing diagenetic imprint on the depositional character of the grains and matrix (solid rock) is assigned, based on a scale of 10, 30, 60, and 90% diagenetic influence. The second factor is whether the post-depositional diagenetic processes enhanced or reduced porosity. Hence, the pore type labels formulated for the Grayson samples are written as H1-10e, H1-10r, H1-30e, H1-30r, etc. For each percent value of diagenetic influence on depositional texture (10, 30, 60, 90%) there are two pore types- either enhanced "e" or reduced "r" (porosity).

In conclusion, the numerical value in the pore type label refers to preservation of the depositional texture (increasing influence of diagenesis on depositional texture) and

the label "e" or "r" refers to the affect of post-depositional processes on porosity, either

enhancing or reducing the porosity. Finally, samples labeled depositional (depo) and

diagenetic (diag) indicate pore types that are the end members on the Ahr genetic

carbonate porosity classification (Figure 7).
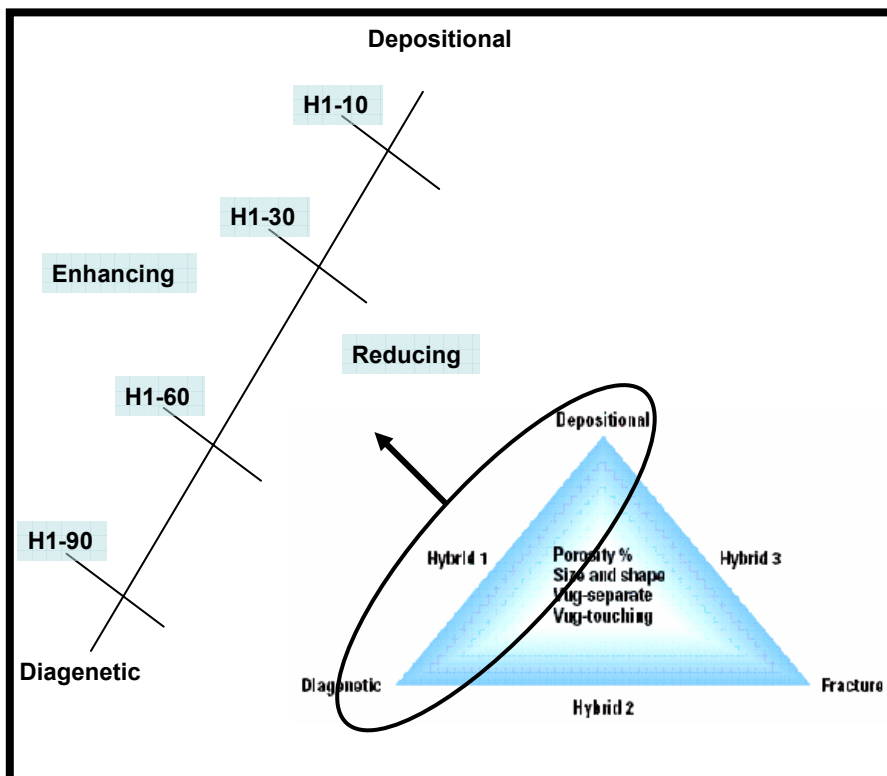
Figure 7: Adapted pore type classification based on the Ahr genetic classification of
carbonate porosity (redrawn from Ahr et al., 2005).

Petrographic Image Analysis

Petrographic image analysis (PIA) is a computer-based imaging technique

utilized in the measurement of pore characteristics from thin section. It allows for the

rapid compilation of pore geometry data, such as pore area, and the calculation of total

visible porosity in 2-D. Ehrlich et al. (1984) developed PIA as a means of relating the

petrology of reservoirs to petrophysical and geophysical data, thus improving the

assessment of reservoir quality and more effectively linking pore networks to spatial

data such as well logs and seismic. Specifically, Ehrlich et al. (1984, 1991) suggests that

the two-dimensional view of porosity from PIA is useful for not only calculating total

optical porosity, which can be related to effective porosity, but also for classifying pore

types. Although the use of pore casts, created by impregnating samples with epoxy and

dissolving away solid rock (Bliefnick and Kaldi 1996), provide a greater understanding

of pore networks in three-dimensions, PIA is considered a less destructive and more cost

efficient method to make pore geometry observations.

Concern over the change in the observational dimension of porosity between 2-D

(PIA) and 3-D pore casts (for example) has been addressed by Ehrlich et al. (1984,

1991). For the purposes of evaluating thin section porosity, Ehrlich developed the idea

of a "porel" or porosity element that relates a discrete patch of porosity as observed in a

2-D thin section view to its equivalent pore (and pore-throats in highly permeable rocks)

in a 3-D volume (Ehrlich et al., 1991 pg1550). Additionally, Ehrlich states that it can be

assumed that the pore system captured by a 2-D slice has some relationship to the 3-D

network form which it was extracted (Ehrlich et al., 1984 p.1366). The assumption that

there is some relationship between a 3-D pore network and the pore/pore-throat complex

that intersects a plane (thin section view, for example) requires some simplification, such

as spherical, hexagonally packed grains, yet any significant changes in 3-D pore

networks will still be captured by proportional changes in 2-D views. Furthermore, changes to original porosity, such as post-depositional diagenetic processes, that influence the 3-D pore network will be reflected in the 2-D slice by some relationship termed "transfer function". On the basis of PIA procedures established by Ehrlich et al. (1984, 1991), it can therefore be assumed that the complexity of the relationship between 2-D and 3-D observations of pores system increases as pores lose their original depositional character (spherical grains and intergranular pores).

PIA in This Study

Petrographic image analysis in this study was based on procedures outlined by Adams (2005), and performed with the image software package *Image-Pro® Plus v6.0 by Media Cybernetics*, *Inc*. Photographs of thin section samples for use with the imaging software must be acquired in digital format. In this study a Zeiss Axioplan II microscope with an Axiocam digital camera and Axiovision imaging software were used. It is suggested by Adams (2005) that 20-30 adjacent rectangular camera viewfields (approximately 4 x 5 mm) at 25x magnification (2.5x objective and 10x ocular) are sufficient to ensure that the entire thin section is photographed and that individual pores are neither too large nor too small for observation with PIA. Additional care must be given to the light intensity and exposure time for each thin section sample; the desired end result is maximum color contrast between the grains and the pore space so that the blue epoxy (in plane light) that represents pore space can be identified and selected for false color assignment during the PIA. Adjusting the light and exposure

time when cements and replacement mineral grains are in abundance is the most

challenging step of PIA, as it directly affects the measured pore areas if the blue epoxy

cannot be easily differentiated from cements that appear with a bluish hue due to

improperly adjusted light. The digital image data are then transferred to a computer for

processing with the imaging software.

In this study petrographic image analysis (PIA) is used to gather data on only one

measurement criteria, object area. The "objects" are representative of pores and thus

pore areas (mm^2) are measured (Adams, 2005). The PIA procedure simply involves:

first, for each viewfield the solid rock and pore space are selected as the "area of

interest" to exclude the unwanted space surrounding the actual rock sample. Second, the

blue epoxy "pore space" pixels are selected and assigned a false color. During false color

assignment objects (micropores) of less than $1.66x\ 10^{-5}\ mm^2$ are below detection by the

imaging software and are excluded from the object area measurements. Third, distinct

object area categories are assigned so that the software can automatically sort the objects

and their areas into bins. The ranges of pore areas for the different bins were assigned

based on suggestion from Adams (2005). Finally, the objects with false color are

measured according to the criteria (i.e. area). The software provides the criteria data

(Table 1) as total area that the objects in each category cover for a selected view, as

mean area, and as percent of total objects for each designated object area category.

Additional useful data that was collected includes a list of each area in mm^2 for each

pore identified, outlines of the false color assignments for each viewfield, and sorted

objects image files where each pore shape can be viewed apart from the solid rock.

Table 1: Sample of imaging software data output. "Total area" values for each pore area bin and the entire viewfield are highlighted, as well as the 2-D porosity calculation and four examples of individual pore area measurements.

Pore Area View 10								
Pore Area Bin mm^2	Objects	% Objects	Total Area mm2	% Area	Mean Area mm2	Std.dev.	Min Area mm2	Max Area mm2
< 0.02	382	96.4646	**0.2751**	6.3306	0.0007	0.0022	0.0000	0.0165
0.02 - 0.5	13	3.2828	**0.6911**	15.9020	0.0532	0.0393	0.0219	0.1595
0.5 - 1	0	0.0000	**0.0000**	0.0000	0.0000	0.0000	0.0000	0.0000
> 1	1	0.2525	**3.3796**	77.7675	3.3796	0.0000	3.3796	3.3796
			4.3458					
						Total Pore	396	
	Total Pore Area		43.1223	mm2		**Count**		
	Thin Section Area		426.83	mm2		Obj#	Area mm2	
	2-D Porosity		**10.10%**			1	3.4E-05	
						2	3.4E-05	
						3	5E-05	
						4	0.00017	

The collected pore area data are then categorized based on pore type to determine if there is a distinct pore area range for each pore type group. Additionally box plots, a five-number statistical summary depicting the smallest non-outlier observation, the lower quartile, the median, the upper quartile, and the largest non-outlier observation, are created to show the statistical distributions of pore areas for different pore types.

One important calculation that results from the data provided by PIA is total 2-D porosity. This porosity is considered to be effective porosity because the blue epoxy impregnation is limited to interconnected pores and because the micropores are below the detection limits of false color assignment pixel identification. The value for 2-D porosity is calculated for each thin section sample by summing the total area of each pore area category from each of the viewfields and dividing by the total area of the thin section solid rock and pore space. Median pore areas were also calculated by compiling the areas of every pore identified for the whole thin section (from the 20- 30 viewfields).

Mercury-Injection Capillary Pressure Analysis

Mercury-injection capillary pressure (MICP) measurements were made on 17 core plug samples by PetroTech Associates, Houston TX. Previous to MICP testing the core plug samples were cleaned at the Department of Petroleum Engineering at Texas A&M University. The cleaning procedure involved a simple distillation to extract hydrocarbons and other pore-filling compounds. Boiled toluene and methanol gases saturate the core plugs and expel the pore-filling compounds. The contaminated solvent is flushed through a siphon and the process is repeated for 72 hrs, at which point the plugs are considered cleaned (and the solvent is clear after flushing). Before shipment to PetroTech, samples were dried at 100°C after 18 hours to remove residual moisture.

Injected mercury was monitored at 118 pressure points from 1.64 to 59,500 psia. The results from MICP testing included: 1) drainage curves for each sample based on wetting phase saturation for each of the 118 incremental mercury injection pressure points, 2) pore aperture diameter distributions based on pore volume percent, 3) mercury-derived porosity, and 4) permeability based on the Swanson equation. Additionally, data such as cumulative mercury intrusion were used for calculating other pore throat properties.

Supplemental MICP Data Calculations

Based on the MICP data, the J-function is calculated using the equation:

$$J(S_w) = \frac{Pc}{\sigma \cos\theta} \sqrt{(k/\phi)}$$ (Amyx, Bass, & Whiting, 1960)

where Pc is capillary pressure in psia, k is permeability in md, ϕ is porosity, θ is the contact angle, and σ is the interfacial tension in dynes/cm. The values for J are plotted against wetting phase saturation provided from the MICP measurements.

The Lorenz curve reflects the joint storage and flow capacity of a reservoir rock. It indicates how the pore-throat sizes are associated with fluid capacity, i.e. are the biggest pore-throats concentrated in a small volume of the rock or are they evenly spread throughout the sample. Additionally, the Lorenz curve can indicate if there are preferred fluid pathways through different pore-throat distributions.

The Lorenz coefficient is a number between 0 and 1 which measures how unevenly the flow capacity is distributed through the rock, compared to the storage capacity. A Lorenz coefficient of 0 would indicate a perfectly homogeneous distribution of both flow and storage capacity, while a value nearly 1 indicates that only a very small percentage of the rock is responsible for most of the flow capacity and the remaining pore throats contain immobile fluids.

Figure 8 is an idealized example of Lorenz curves showing different flow and storage capacities. The flow capacity is based the cumulative pore-throat areas and the storage capacity is calculated from the wetting phase saturation.
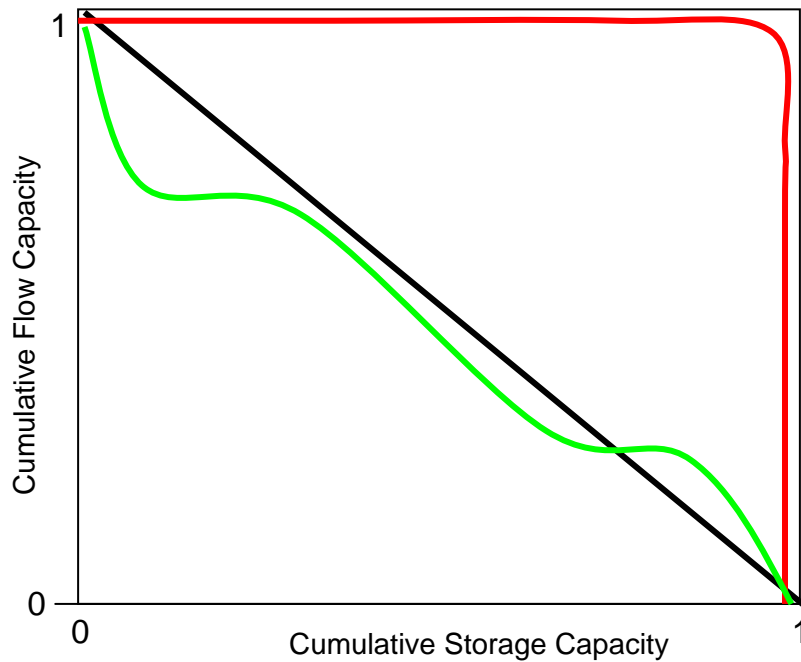
Figure 8: Idealized Lorenz curves.

The three idealized curves show different flow and storage capacity relationships. The black curve represents a sample that has a uniform pore-throat distribution and each pore throat is contributing equally to the fluid flow capacity. The red curves represents a sample where there are only a few large pore-throats representing most of the fluid flow capacity and fluid can only be drained from about 5% of the satiable rock. The remaining 95% of the fluid in the red sample would be immobile. The green curve represents a sample with a multi-modal pore-throat distribution. Each plateau along this curve is a different pore-throat mode that is gradually adding to the flow capacity of the rock. The largest pore-throats contribute ~25% of flow capacity, middle pore-throats

contribute another 40-50% with the remaining 25% capacity held by the smaller pore-throat modes until all the fluid in the satiable rock has been transmitted out of the rock.

Lorenz curves can also be utilized for rock typing and flow unit identification (Gunter et al., 1997). By comparing the slopes of the curves, it can be determined if the reservoir flow capacity or storage capacity is greater. In the case where flow capacity is greater than storage capacity, the unit is expected to have a high reservoir process speed, termed a speed zone by Gunter et al. (1997). On the other hand, if storage capacity is greater than flow capacity a reservoir barrier may be identified. Neither flow nor storage capacity most likely signifies a baffle.

Supplemental Data

For purposes of comparing thin section 2-D porosity with various 3-D porosity measurements, porosity values obtained during conventional core analysis (CAMP) was provided by Poole (2006) for all of the thirty-nine corresponding thin section samples. Additionally, helium core-plug porosity was measured for twelve samples in the Department of Petroleum Engineering at Texas A&M University.

RESULTS

This section presents results from the three main pore and pore-throat measurement and descriptive techniques outlined in the methods section. This includes: classification and occurrence of pore types and example thin section photomicrographs of pore types, pore and pore-throat size measurements and their correspondence with pore types and facies, relationships between pore and pore-throat sizes, capillary property measurements of permeability, J-function, and Lorenz curves, and porosity estimations and porosity measurement technique comparisons. Numerical values for pore and pore-throat sizes and porosity are provided in the appendices. Graphical representation of pore and pore-throat size using box plots are presented in this results section and are used to determine if there is a distinct relationship between pore/pore-throat geometry and pore type. Pore and pore-throat size are also plotted together to determine if pore and pore-throat geometry are related and if pore-throat size can be used as a proxy for determining pore size. Plots of permeability and pore-throat size, J-function, and Lorenz curves are also provided in this section to determine the behavior of reservoir performance characteristics of the different pore types.

Description of Rock Types

Based on core descriptions from 10 wells, Poole (2006) identified five facies within the Smackover interval of Grayson field. The dominant facies is the grainstone/packstone 1 (G/P 1), which accounts for 67% of rocks described (Poole,

2006). This grainstone/packstone facies is moderately sorted and composed of 65% ooids and peloids ranging in size from 2mm to 0.25mm and 5mm to 0.1 mm respectively. A second grainstone/packstone facies (G/P 2) composed of poorly sorted pisoids (rare), ooids and peloids (~50%), and greater than 2% oncoids. Ooids range in size from 2mm to 0.25mm, oncoids range in size from 10mm to 2mm, and peloids range from 7mm to 0.125mm.

The packstone/wackestone (P/W) facies comprises 3% of the rocks described. This facies is made up of poorly sorted ooids and peloids ranging from 0.5mm to 0.25mm and 5mm to 0.1mm respectively. The wackestone/packstone facies (W/P) also accounts for 3% of rocks described, and is composed of oncoids and pisoids, less than 20% ooids and peliods, and less than 2% quartz grains. Ooids and peloids range from 0.5mm to 0.25mm and 0.25mm to 0.125mm respectively. Oncoids range from 8mm to 2mm. The wackestone/packstone facies is commonly poorly sorted. Eleven percent of the rocks described are from the microbial boundstone facies that is composed of sparse fossils, such as gastropods, bryozoans, echinoderms, and various shell fragments as well as ooids and greater than 70% peloids. Ooids range in size from 1mm to 0.5mm and peliods are 1mm to 0.1mm in size.

Classification of Pore Types

To ensure reproducibility, 82 thin sections were classified using the adapted Ahr genetic porosity classification (as outlined in the Methods section). Only 39 samples will be discussed in detail because they correspond to the samples analyzed with

petrographic image analysis. Of the 39 samples, the following pore types were observed: depositional, H1-10e, H1-30e, H1-30r, H1-60e, H1-60r, H1-90e, H1-90r, and diagenetic.

Two of the 39 samples exhibited 'purely' depositional pores, meaning that the grains reflect original depositional texture formed during detrital sedimentation during and immediately after which depositional porosity was preserved (Appendix C, Figure C.1). This sample shows an example of interparticle porosity in a moderately to poorly sorted oolitic grainstone. Interparticle pores range in size from 0.0000166 to 0.22 mm^2. Although this sample shows evidence of slight dissolution or minimal grain replacement or pore filling, the degree of diagenetic alteration to the grains is less than 10%, the 'cutoff' value used for minimally-altered diagenetic pore types. The depositional pores occur in different facies because digenesis did not affect all facies equally depending in part on the paleostructural position of the sampled segment of the facies at different times of diagenesis. One of the facies exhibiting depositional pores is the oolitic grainstone facies (G/P 1, Appendix C, Figure C.1); another is the oncolitic grainstone facies (G/P 2). The sorting and packing of these two different facies types has an effect on the size of the interparticle pores, with the moderately sorted oolitic grainstone having pores that are slightly larger than those of the oncolitic, poorly sorted, grainstone sample. Figure 9 shows the effects of different packing orientations and the pore volume reduction due to poorly sorted sediments. Cubic packing with equidimensional spherical grains results in 47.6% porosity. The more stable rhombohedral packing of equidimensional spherical grains reduces porosity to 26% due to a decrease in the pore

volume. Further pore volume reduction results with the presence of smaller spherical

grains that fill the pore space created by cubic packing. In the situation of poorly sorted

sediments with two different grain sizes of uniformly spherical shape, the maximum

possible porosity is 12.5%. In 2-D thin section view, pore volume is related to pore size

and therefore smaller pores are expected in poorly sorted grainstones where pore volume

is reduced by the presence of smaller grains.

Cubic Packing equal
Grain size ϕ=47.6%

Rhomdohedreal Pack-
ing equal grain size
ϕ=26%

Cubic Packing twin
grain size ϕ=12.5%
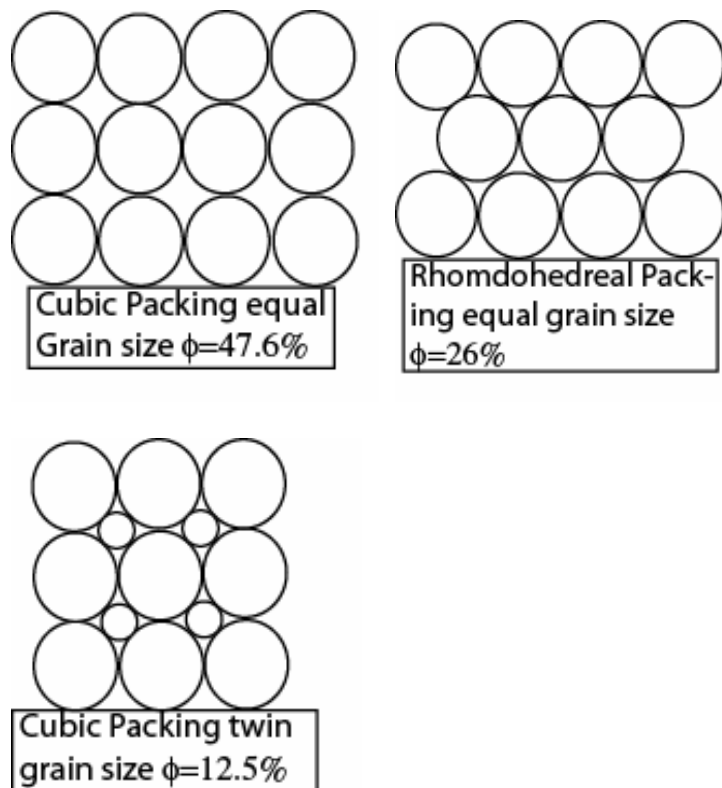
*Figure 9: The effect of different packing orientations and pore volume reduction due
to poorly sorted grains.*

H1 hybrid pore types are created by combined depositional and diagenetic processes. The occurrence of the different hybrid pore types categorized by the porosity enhancing or reducing factor is presented in Table 2. Additionally, the hybrid pore types and pore-modifying processes can be divided based on whether the original depositional texture was grain or mud-supported (Table 2).

Table 2: Pore type- categorized by porosity factors and facies.

Pore Type- Porosity Factors	Causes (in order of abundance)	Facies		Pore Type	Pore Type Occurrence
Enhanced (e)	A. Dissolution of solid rock, pore filling and rim cements, and replacement mineral grains	Grain Supported	G/P 1	H1-30e	3
				H1-60e	4
				H1-90e	1
			G/P 2	H1-10e	5
				H1-30e	4
			P/W	H1-30e	1
				Diag	1
	B. Dolomite grain replacement	Dolostone		Diag	1
Reduced (r)	A. Grain coating and pore filling cements	Grain Supported	G/P 1	H1-90r	1
			G/P 2	H1-30r	1
			P/W	H1-30r	1
	B. Replacement of solid rock and pore filling by anhydrite and dolomite	Grain Supported	G/P 1	H1-30r	4
				H1-60r	2
			G/P 2	H1-30r	1
				H1-60r	2
		Mud Supported	W/M	H1-60r	1
				Diag	1
	C. Mechanical and pressure-solution compaction of grains	Grain Supported	G/P 1	H1-30r	2
				H1-60r	1

As described in the Methods section of this study, there are two porosity enhancing processes, the primary being dissolution of solid rock, pore filling and rim cements, and replacement mineral grains. Replacement of grains by dolomite crystals is a secondary porosity enhancement process but this process is only considered to be truly pore volume enhancing in diagenetic pores types, which are discussed in a separate subsection.

The dissolution of matrix, cements, and replacement grains enlarges interparticle porosity, forming pores that transgress grain boundaries or creating oomoldic pores that, with several stages of leaching, can form extensive interconnectivity of large pore spaces and large pore-throats. Dissolution can also be accompanied by varying degrees of grain and matrix original texture alteration. Oolitic grainstone samples tend to have a higher degree of grain and matrix alteration than do the oncolitic grainstone samples, however H1-10e pore types only occur in the oncolitic grainstone facies samples. The reason for the higher degree of solid rock alteration to the oolitic grainstone facies samples is probably related to the abundance of smaller ooid grains in the oolitic grainstone facies as compared to the fewer but coarser oncoid grains of the oncolitic grainstone facies, i.e. the dissolution of a large percent of smaller ooid grains appears visually as a more significant solid rock alteration than does the dissolution of portions of very coarse oncolitic grains.

There are three causes of porosity reduction in the Grayson field samples: cementation that coats grains and fills pore spaces, replacement and pore filling by anhydrite and/or dolomite replacement mineral grains, and mechanical or pressure-

solution compaction of grains and rim cements. For this study the most prominent

porosity reducing factor was selected as the main cause of pore space reduction for each

sample, however for almost every case the sample underwent more than one porosity

reduction process.

Based on the 'main cause' identification, the most common porosity-reducing

process is replacement and pore filling by anhydrite and/or dolomite. This is a process

by which the recrystallization of dolomite grains and the formation of anhydrite nodules

replaces portions of original depositional grains and matrix or fills pore spaces

surrounding grains, thereby reducing fluid storage space (pore volume) and limiting the

transmissivity of fluids by blocking pore-throat passages. The replacement of grains,

matrix, and pore space by anhydrite can be extensive but because anhydrite crystals

generally occur in 'felted' clusters, or nodules, only portions of a core plug or thin

section sample may be 'blocked' due to the presence of anhydrite. Thus, replacement by

anhydrite or dolomite that can affect only portions of a sample causes distinct alterations

to reservoir performance characteristics compared to cementation which tends to be

more uniform, as seen in thin section petrography. Cementation is the second most

common porosity reduction process. Simply stated this is the precipitation of crystal

cements around grain boundaries that reduce the storage capacity and block pore-throat

passages. As previously stated, cementation tends to affect greater portions of a thin

section sample because cements are not 'isolated' to distinct nodules, therefore causing a

more uniform porosity reduction. Finally, compaction due to mechanical stress and

pressure-solution increases grain-grain contacts to reduce pore volume, and is the
primary cause of porosity reduction in a few samples.

Diagenetic pore types occur in fine-grained grain-supported and mud-supported
facies (packstone, wackestone, and mudstone) or in dolostone. The original texture of
these pore types has been completely destroyed by anhydrite and dolomite grain
replacement and pore filling. Because the porosity of the dolostone sample is
intercrystalline and vuggy the sample is considered enhanced. Replacement by dolomite
may not be enough to enhance porosity, such as the packstone/wackestone sample where
50% dolomite does not fully allow for the enhanced intercrystalline porosity but
extensive late-stage dissolution of remaining grains and pores places this sample in the
enhanced porosity category. However, replacement and pore filling by anhydrite and
dolomite is the controlling porosity reducing factor for the wackestone/mudstone
diagenetic pore type sample.

Examples of H1 Hybrid Pore Types

For H1-10 pores (Appendix C, Figure C.2) the original grain type is clearly
visible with slight cementation or dissolution of grain boundaries, or minimal grain
replacement, and the sample can be described as having strong depositional attributes as
viewed in thin section. If, for example, few of the ooid grains have been dissolved,
leaving some molds, the sample is considered a H1-30 hybrid pore type (Appendix C,
Figure C.3a). Moderate grain replacement also occurs in H1-30 samples (Appendix C,
Figure C.3b). It is only when grain dissolution becomes widely dispersed (greater

abundance of ooid molds), or when grains are so highly compacted that the original

grain types are difficult to recognize, that the sample is labeled a H1-60 pore type

(Appendix C, Figure C.4a). Additionally if some dissolved grains underwent late-stage

cementation or extensive grain replacement, the sample is labeled H1-60 (Appendix, C

Figure C.4b). A sample with grain texture that is beyond recognition and the grains no

longer appear as individual textural components is labeled a H1-90 pore type (Appendix

C, Figure C.5). This, however, is distinct from a purely diagenetic sample, where

original grain and matrix fabrics are entirely replaced by crystalline mineral grains

(Appendix C, Figure C.6).

Pore and Pore-Throat Properties

<u>Pore Size and Pore Type</u>

Table 3 shows the categorization of pore size for the Grayson field samples.

Both the pore area categories (Table 3) and the box plots (Figure 10) show that pore area

is not dependent on pore type, i.e. both enhancing and reducing pore types can have a

similar range in pore area and similar median values. Pore size (area, mm^2) was

determined by petrographic image analysis and the median pore area for each sample

was calculated.
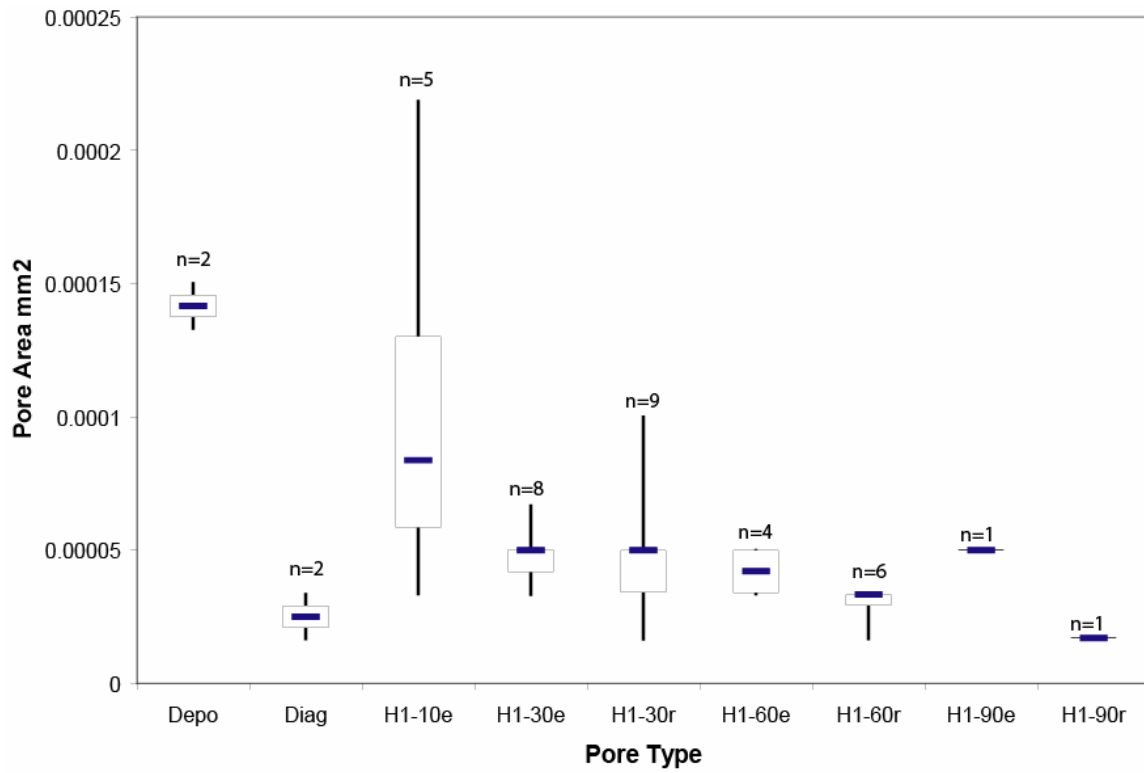
Figure 10: Box plots showing the ranges (vertical black line) and median values (blue horizontal line) of pore area (mm^2) for each pore type.

Table 3: Facies and pore type correspondence by pore area (mm^2) categories.

Pore Size (Area mm^2) Categories
(Ranges are based on median pore area data from petrographic image analysis)

1	2	3	4	5
< 5x 10^{-5}	5x 10^{-5} to 7x 10^{-5}	7x 10^{-5} to 9x 10^{-5}	9x 10^{-5} to 1x 10^{-4}	> 1x 10^{-4}

Pore Size (Area mm^2) Categories by Facies and Pore Type

	Grainstone/ Packstone 1	Grainstone/ Packstone 2	Packstone/ Wackestone	Wackestone/ Mudstone	Dolostone
Depo	5	5			
H1-10e		1 to 5			
H1-30e	1	1 to 2	1		
H1-30r	1 to 4	1 to 2	1		
H1-60e	1				
H1-60r	1				
H1-90e	1				
H1-90r	1				
Diag			1		1

Depositional pores are only preserved in the two grainstone/packstone facies and they contain the largest pores with areas greater than 1x 10^{-4} mm^2. The H1-10e (oncolitic grainstone) and H1-30r (oolitic grainstone) pore type samples both have very large ranges in pores areas, 1.85x 10^{-4} and 8.3x 10^{-5} mm^2 respectively. These large ranges in pores area are evident because pores from samples of both 10e and 30r pore types fall within the both smallest and the largest pore area categories (Table 3). The smallest range in pore areas, 1.64x 10^{-5} mm^2, is for the H1-60e pores, which are found in the oolitic grainstone facies. These H1-60e pores are within pore area category 1. The H1-90e and r pore types have only one representative sample; therefore, a range in pore areas cannot be determined and the reliability of the pore area categorization is negatively influenced by the small number of samples. All of the packstone/wackestone

pore types have pores in category 1. The wackestone/mudstone samples are composed of pores below the resolving power of the imaging software (values, Appendix B).

Many of the pore types for the oncolitic grainstone do not fall into one pore area category (Table 3 and Appendix B). This can be explained by the poorly sorted grains of this facies and the effect of poor sorting on dissolution and cementation patterns. For example, dissolution of very coarse-grain oncoids will result in large pores, but if smaller ooid or peloid grains undergo dissolution the pore areas will not be as large. Depending on the coarseness of grains present in the rock, the median pore area for that rock could potentially fall within several different pore area categories.

Both the pore area categories (Table 3) and the box plots (Figure 10) show that pore area is not dependent on pore type, i.e. both enhancing and reducing pore types can have a similar range in pore area, and similar median values. The H1-10e pores show an especially large range in pore areas, and due to the fact that they are found in only the oncolitic grainstone facies, there must be some control on pore area by the facies of the sample. Depositional pores, however, have the largest pore areas of all the pore types for both the oolitic and oncolitic grainstone facies. In these cases, diagenetic alteration to original grain texture destroys the relationship between pore area and pore type.

Pore-Throat Size and Pore Type

Box plots (Figure 11) show that depositional and size-enhanced pore types have larger pore-throat areas than reduced and purely diagenetic pores. It is clear that pore type does have a control on pore-throat size and that diagenetic alteration to both grains

and pore space controls the pore-throat area category of each sample. Porosity

enhancing events did not enlarge pore-throats beyond their original depositional size, but

the processes did prevent the pore-throats from being closed.

Pore-throat size was obtained from the mercury-injection capillary pressure

measurements as median pore aperture diameter in microns. From those values pore-

throat areas (μm^2) were calculated to compare the distribution of pore-throat areas with

pore type and to their corresponding pore areas (mm^2). Figure 11 shows box plots with

the median pore-throat area highlighted for each of the different pore types, and Table 4

shows the categorization of pore-throat size by pore type and facies.

Pore-throats have also been grouped into categories (Table 4). Diagenetic pore

types have pore-throat areas in size category 1 for both the wackestone/mudstone and

dolostone facies. Size-reduced samples have smaller pore-throat areas (μm^2) than size-

enhanced pore types, and they are within pore-throat area categories 1 and 2 for the

oolitic grainstone facies and the packstone/wackestone facies. Compared to size-

enhanced pore types, the range of pore-throat areas in reduced pores is small, i.e. 0.054

μm^2 for the H1-60r pore type and 1.814 μm^2 for the H1-30r pore type. The range in

pore-throat areas for the H1-30e pore type is 21.702 μm^2 and 647.25 μm^2 for H1-10e

pore type. The depositional pore type samples of both grainstone/packstone facies 1 and

2 are within pore-throat area category 3 (values, Appendix B).

The observation that pore type controls pore-throat size and that diagenetic

alteration to both grains and pore space controls the pore-throat area category of each

sample can be clearly explained because small pore-throats have a large surface area to

volume ratio and thus there will be a more dramatic response to dissolution or

cementation.
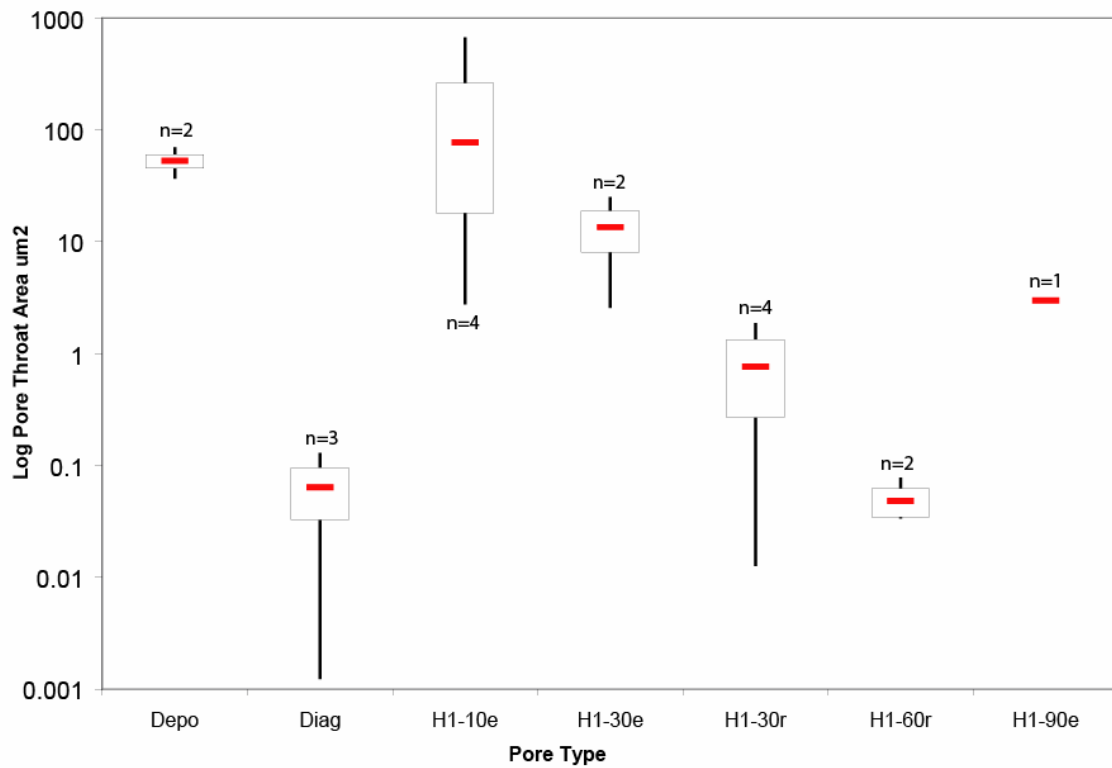
Figure 11: Box plots showing the ranges (vertical black line) and median values (red horizontal line) of pore-throat area (μm^2) for each pore type.

Table 4: Facies and pore type correspondence by pore-throat area (mm^2) categories.

Pore-Throat Area (μm^2) Categories
(Ranges are based on median pore aperture data from mercury-injection capillary pressure analysis)

1	2	3	4	5
<1 μm^2	1 to 20 μm^2	20 to 100 μm^2	100 to 200 μm^2	>200 μm^2

Pore-Throat Area Categories by Facies and Pore Type

	Grainstone/ Packstone 1	Grainstone/ Packstone 2	Packstone/ Wackestone	Wackestone/ Mudstone	Dolostone
Depo	3	3			
H1-10e		2 – 5			
H1-30e		3	2		
H1-30r	2		1		
H1-60r	1				
H1-90e	2				
Diag				1	1

Pore Area and Pore-Throat Area

It is most important to understand the relationship between pore-throat size and pore size. In general, the correlation between pore area and pore-throat area is strong. Figure 12 shows a plot of log pore area (μm^2) vs log pore-throat area (μm^2). The correlation between these two data sets is based on equal probability intervals from the cumulative distribution functions for both properties. The pore area and pore-throat area correlations are clustered by depositional, enhanced, or reduced pore types. This division is obvious for pore- throat area, reduced pore types have smaller pore-throat areas, and enhanced pore-throats can show a wide range in values, particularly for the H1-10e pore type where all of the samples are oncolitic grainstone. The depositional pores show moderate values for pore-throat area. In regards to pore area, however, size-

reduced samples can have large pores (interparticle porosity, $> 3000 \ \mu m^2$), yet the

largest pores (consistently $> 100 \ mm^2$) are found only in the depositional and enhanced

pore types. Therefore, pore-throat area is controlled by enhancement or reduction of

porosity, but pore area can vary independently such that diagenetically- reduced pores

may be especially large ($> 3000 \ \mu m^2$).
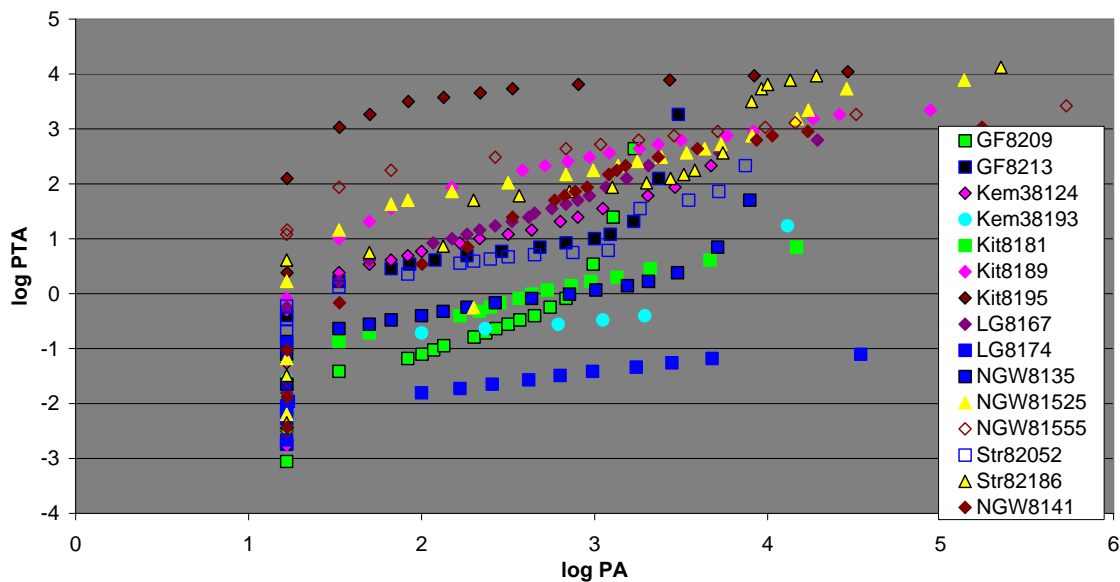
Figure 12: Log of pore area vs log of pore-throat area in μm² categorized by pore type (size-enhanced samples with diamond markers, size- reduced with squares, depositional with triangles, and diagenetic with circles).

The coefficients of determination for pore-throat area vs. pore-area range from

0.65 to 0.99 (values, Appendix B). Size-reduced sample GF8213 and diagenetic pore

type sample Kem38193 have the lowest R^2 values, however there is no dominant

correlation between pore type and a stronger coefficient of determination (although H1-

30e pore type samples tend to have stronger R^2 values (Kit8189, 0.94 and Kem38124,

0.98).

Porosity

Two-dimensional porosity was calculated as total pore area from petrographic

image analysis (PIA) and compared to pore volume as effective porosity from core

analysis. Calculation of porosity from PIA shows a consistent "underestimation" of

porosity when compared to the values obtained from 3-D methods such as conventional

core analysis, core-plug analysis, and mercury-injection capillary pressure porosity

measurements. By comparing the different types of 3-D porosity measurements the

concern that sample volume could affect porosity values in complex heterogeneous

porosity systems can be disregarded. Values for individual samples can be found in

Appendix B.

PIA Porosity and Core Analysis Porosity

Figure 13 shows a plot of PIA porosity and core analysis porosity in percent.

This shows clearly that 2-D porosity for the Grayson samples underestimates 3-D

porosity measured from whole core. For some reduced and diagenetic pore type samples

it was not possible to calculate PIA porosity because either the dolomite replacement

crystals made false-color assignment impossible or the pores were below the resolving

power of the imaging software. PIA porosity is more easily calculated for the size-

enhanced samples. Sample Kit8195, from the H1-10e pore type (oncolitic facies),

underestimates core porosity by about 34%. The other samples underestimate porosity from 39 to 98%.
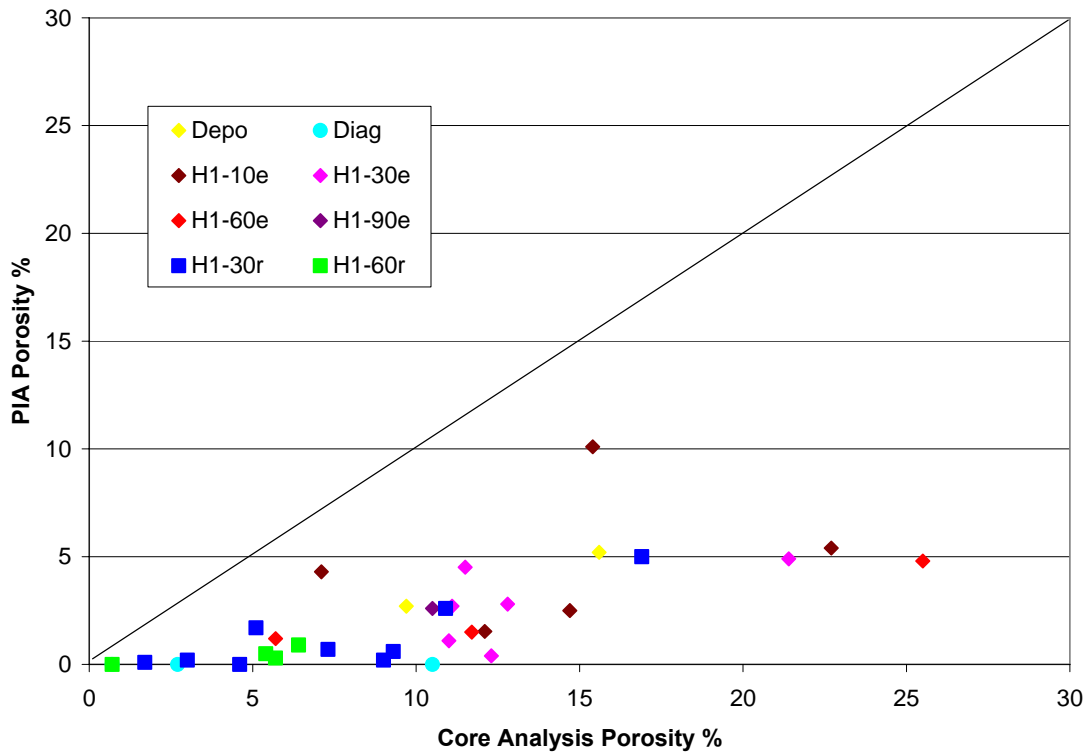
Figure 13: Conventional core analysis porosity compared to PIA porosity in percent.

To understand if the porosity underestimation is due to the difference in sample volume, full core analysis porosity was compared with capillary pressure-derived porosity (core plug) and helium core plug porosity. Sample volume is a concern for diagenetically altered porosity types such as solution-enhanced interparticle, oomoldic, and vuggy porosity because a 1x1in core plug may not be representative of the distribution of porosity seen in a full length core, or it may highlight a high porosity zone

and ignore intervals of low porosity. Figure 14 shows the plot of capillary pressure-derived core plug porosity and the full core analysis porosity. There is a nearly one-to-one correlation between these two different 3-D porosity measurement methods, with core plug porosity being slightly greater than core analysis porosity.
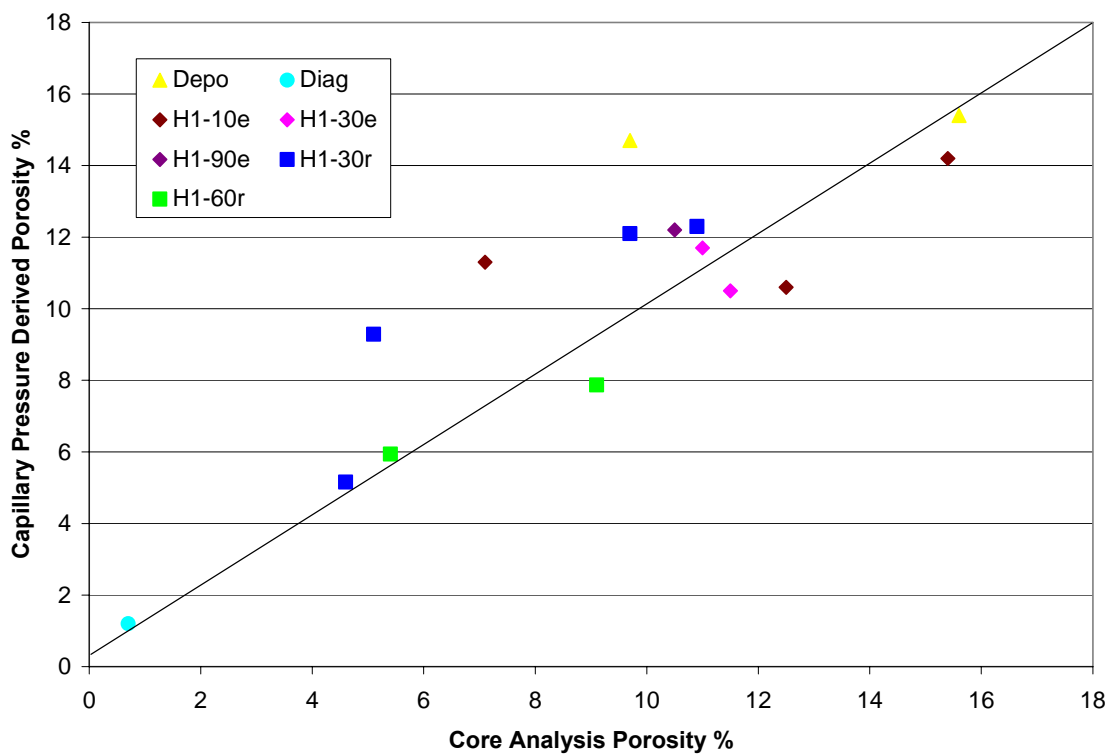
Figure 14: Conventional core analysis porosity compared to capillary pressure derived porosity in percent.

The plot of helium core plug porosity against full core analysis porosity (Figure 15) also shows that core plugs are a valid representation of pore space for the Grayson samples. Thus the concern lies in the ability to compare 2-D to 3-D porosity

calculations. The important issue to consider is how a 2-D slice through a core plug represents porosity. For example, consider a tear-shaped vug, sampling a 2-D slice through the larger end of this vug will show a larger pore in the PIA viewfield, and the calculated total visual porosity will be greater then the porosity calculated for a 2-D slice through the smaller end of the tear-shape vug.
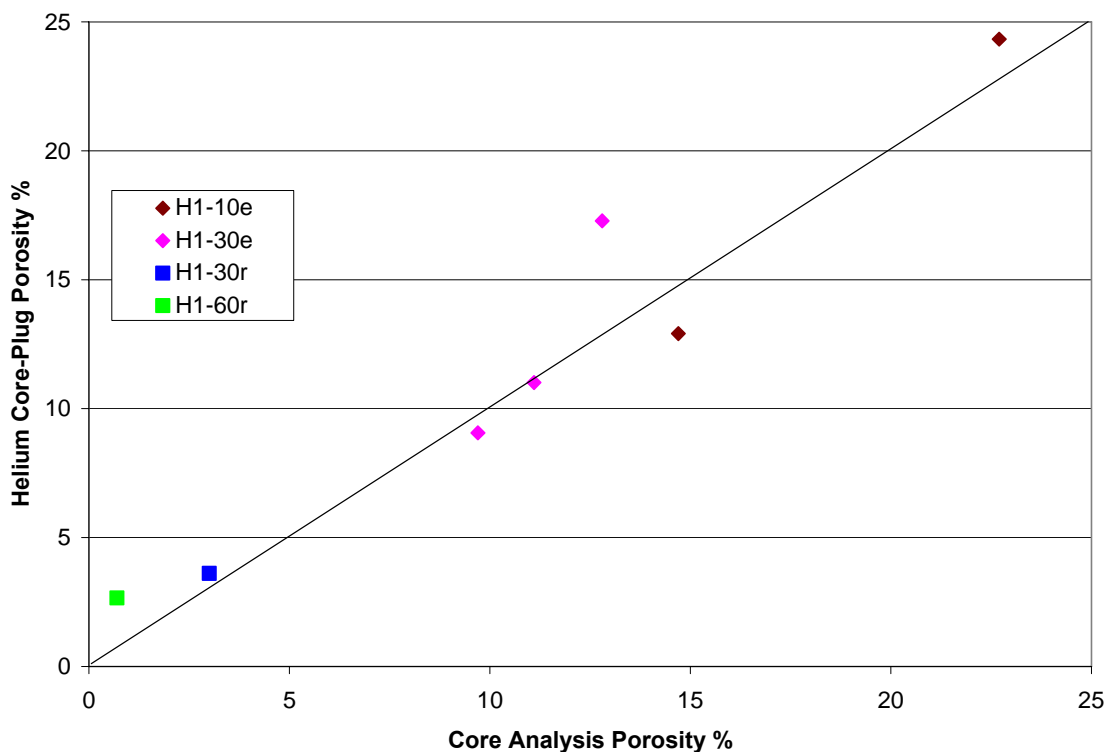
Figure 15: Conventional core analysis porosity compared to helium core plug porosity in percent.

Therefore the underestimation from 2-D to 3-D porosity was not unexpected. Adams (2005) describes the same obstacles between the correspondence of 2-D and 3-D

porosity. He explains that this correspondence decreases from depositional, intergranular carbonate porosity to diagenetically altered pores. Thus it is believed that the cause of the poor correspondence in this study is due to the complex pore geometries of the Grayson samples as a result of diagenetic alteration of pore space. From Poole (2006) it was shown that the oolitic and oncolitic grainstone facies have predominantly solution-enhanced interparticle and moldic porosity, and some intraparticle and interparticle porosity. The packstone/wackestone facies is dominated by interparticle and moldic porosity while wackestone/mudstone facies exhibit mostly intercrystalline pores (Poole, 2006). Additionally, it is not just a matter of the degree of diagenetic alteration to the grain texture, but rather of the type of diagenetic alteration and of the depositional texture and fabric of the reservoir rock. The H1-10e sample (Figure 15) from the oncolitic grainstone facies illustrates such a relationship because it shows that large pore sizes allow a more accurate estimation of porosity in two-dimensional views.

Capillary Properties

Median Pore Aperture Diameter (µm) and Square Root Permeability-k (µm)

Figure 16 shows the relationship between median pore (throat) diameter and the square root of permeability by pore type. By taking the square root of permeability the measurements can be converted from flow units to a measurement of length. The size-reduced samples always have the smallest pore-throat diameters and therefore the smallest permeability values. The strong correlation between pore-throat diameter and permeability ($R^2 = .99$) is expected because the ability of fluids to flow through the

reservoir rocks is dependent on the opening of the pore-throats through which they flowing.

The size-enhanced pore types have larger pore-throat diameters attended by higher permeability but the values are more scattered than size-reduced samples within individual pore type groups. For example the H1-10e pores show a range from about 2.5 to 30 µm for pore-throat and from 0.08 to 0.8 µm for square root of permeability. Clearly the enhancement by dissolution did not create a uniform size range of pore-throats as is seen in samples that have undergone pore-space reduction by cement and grain dissolution. This can be explained by the effect of the depositional texture, i.e. whether the dissolution is primarily of very large oncoid grains or of smaller ooid and peloid grains.

Diagenetic pore types plot very low on both the pore-throat diameter and permeability scales because intercrystalline porosity, partial replacement, and pore filling by dolomite and anhydrite do not permit pore-throats to remain open and thus restrict fluid flow (Figure 16). The unaltered depositional pores plot close together showing neither exceptionally large nor very small pore-throats for the range of pore sizes within this sample universe. Permeability values are moderate for the entire population.
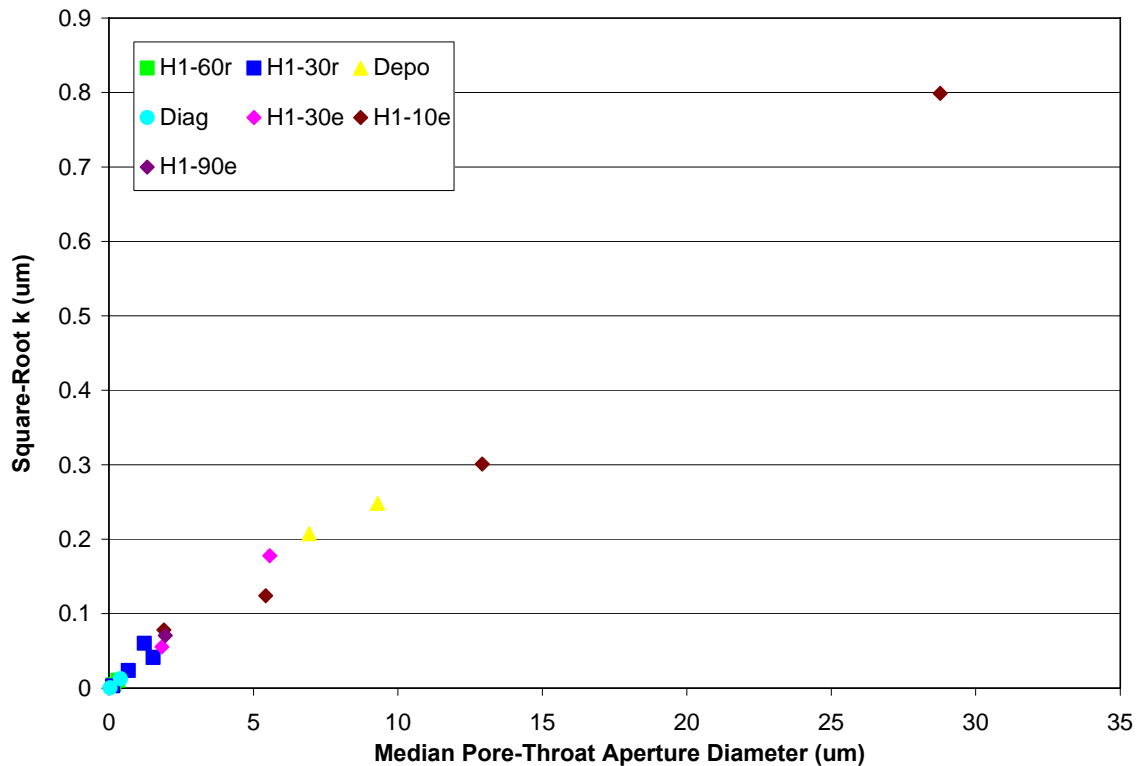
Figure 16: Median pore-throat diameter (μm) compared to permeability (μm).

J-Function Correlations

Figure 17 shows the J-function correlations for 17 of the thin section samples. Similar to the plot of median pore-throat diameter and permeability, the size-reduced pore types cluster in a 'cloud' on the plot but size-enhanced samples do not; they are scattered across the plot. The two diagenetic samples and the two depositional pores plot together.

Dispersion of data points on the J-function curves has been previously observed by Brown (Amyx et al., 1960, p. 156-159). He found that while the trends of the J-function correlations were good, the dispersion of the data points could be improved by

separating the different samples based on their textural features. The limestone core samples, compared to dolomite samples, showed a scattering of data at the range of low water saturation (Amyx et al., 1960). To further improve the correlation, the samples were subsequently subdivided by different grain size. As expected, the dispersion of the data was greater for coarse-grained samples compared to microgranular limestone. The explanation for this is the presence of unique porosity types, solution cavities, vugs, and channels, in the coarse-grained limestone. These pore types are not capillary in size, and thus show deviations from the trends of the capillary pressure data.

Based on the elements of the equation (see Methods), the J-function is a combination of permeability, porosity, and wettability. Between these three characteristics, called dependent rock properties because they depend on definitive properties such as texture and fabric, it would be expected that different types of rocks show different J-function correlations (Tiab and Donaldson, 2004). Therefore based on this expectation, the diagenetically reduced pore types, while not all from the same rock type (facies), have the same dependent rock properties and therefore may behave similarly in terms of reservoir character.

Diagenetically-enhanced pore types do not show this behavior probably because the pores are combinations of diagenetic enlargement by dissolution and original depositional texture and fabric. Dissolution of large grains (> 2 mm), such as oncoids, from the oncolitic grainstone facies create large pore sizes whereas dissolution of smaller ooid grains or peloids may have a negligible effect on measured porosity and permeability. The effect of dissolution on porosity and permeability (pore and pore-

throat sizes) may be limited because of the over-arching influence of depositional texture and fabric (facies characteristics) on dissolution-produced pore and pore-throat sizes. The two depositional samples show nearly the same J-function correlation (Figure 17), therefore, unaltered grain texture and companion porosity, even though from different facies, show similar rock dependent properties, hence behaving as similar reservoir rocks.

Some anomalies exist, however, for the J-function correlations (Figure 17). One such is the H1-30e sample Kem 38124 that plots in the expected range for reduced pore types. This is interpreted to indicate that dissolution of grains, matrix, and pore walls in a fine-grained, grain-supported rock has a limited effect on the three dependent rock properties (because of originally small pore and pore-throat sizes) and thus this sample shows a behavior similar to the reduced pore types. Again, it is a rock that has undergone more than one stage of dissolution and the reservoir properties represent the sum of these events.
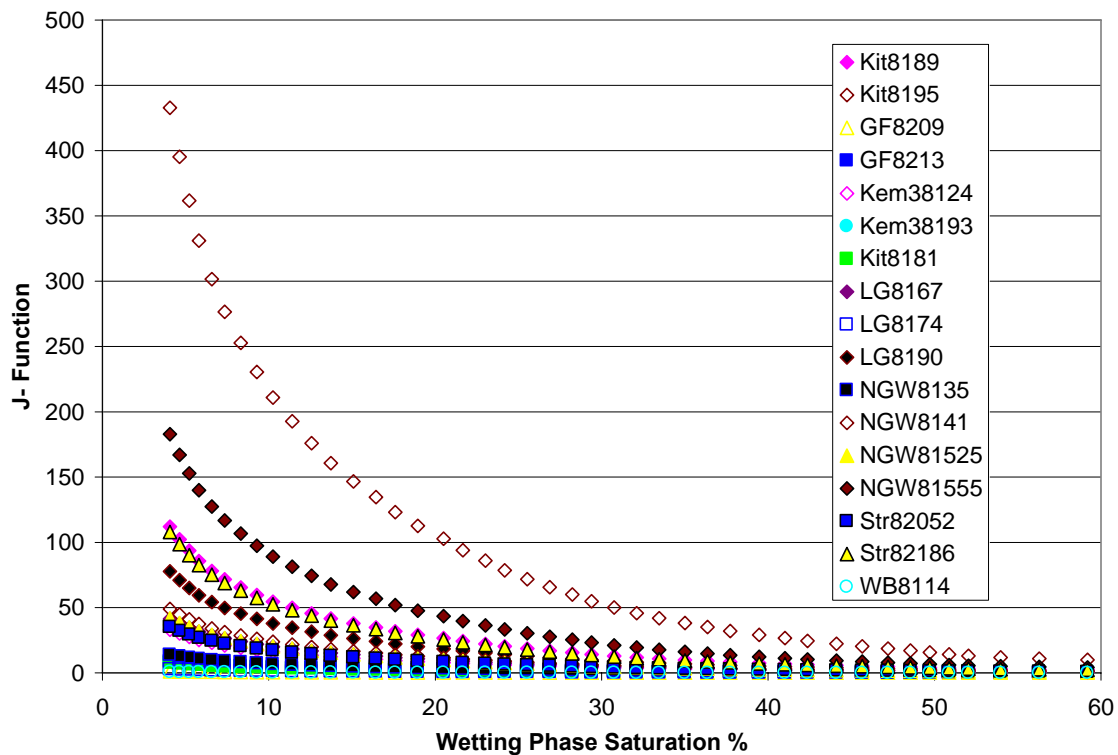
Figure 17: J-function categorized by pore type (size-enhanced samples with diamond markers, size-reduced with squares, depositional with triangles, and diagenetic with circles).

Lorenz Curves

Figure 18 is a Lorenz plot for 17 of the Grayson samples (Lorenz coefficients in Appendix B). The Lorenz plot shows the relationship between flow and storage capacity based on pore-throat diameters and saturation to determine how much fluid can flow through different pore-throat sizes. The Lorenz curves are distinctly grouped by pore type. Size-reduced samples plot in the top right corner and are color-coded in blue and green with square markers. Size-enhanced samples are color-coded in yellow, pink, and

maroon with diamond markers. Diagenetic pore types are turquoise and depositional

samples are yellow.
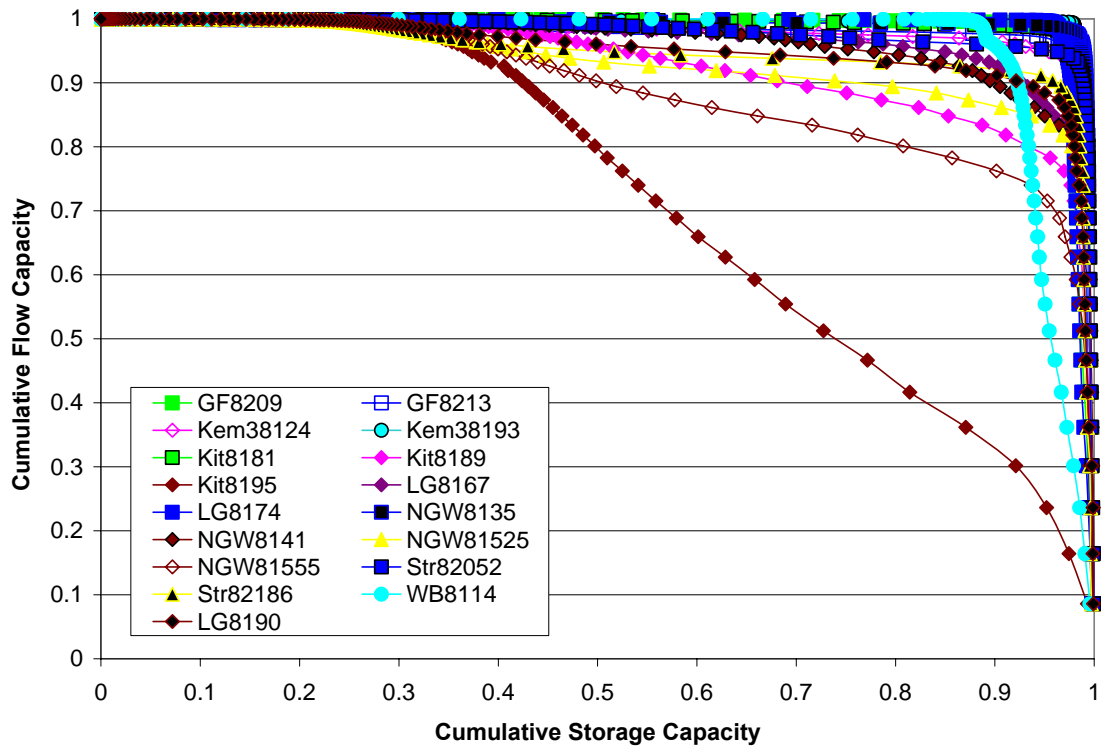
Figure 18: Lorenz curves categorized by pore type (size-enhanced samples with diamond markers, size-reduced with squares, depositional with triangles, and diagenetic with circles).
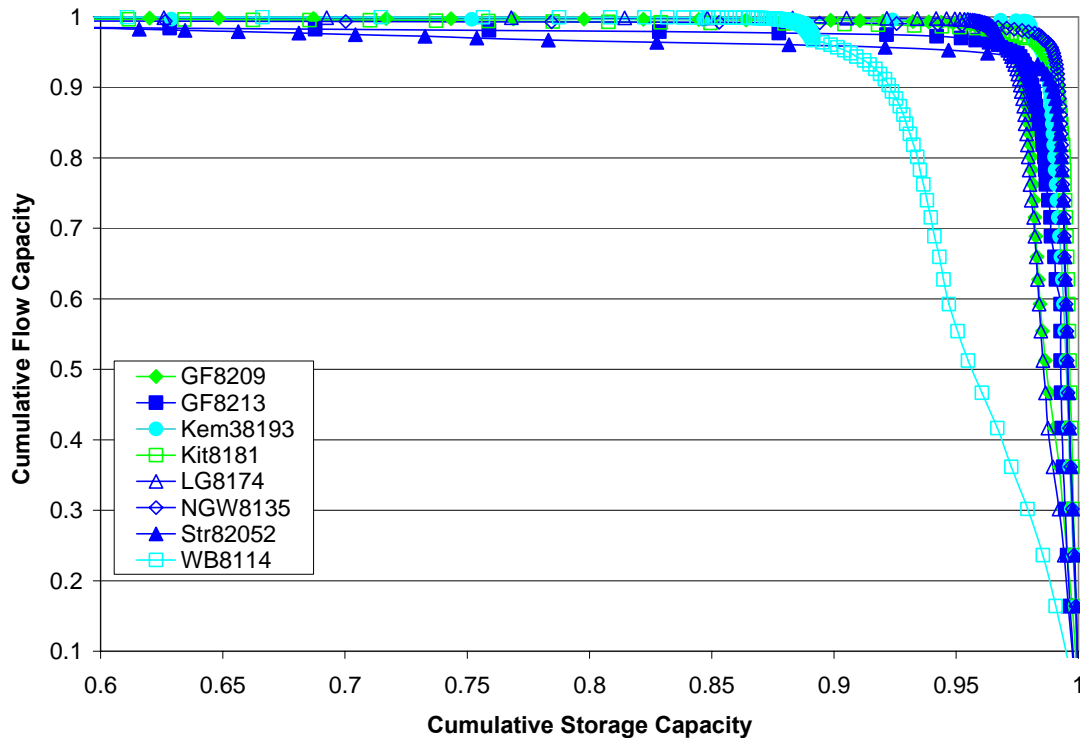
Figure 19: Lorenz curves for size-reduced samples.

The reduced pore type curves are further grouped by those that have a bimodal distribution of pore throats and those with only one mode (Figure 19). The Lorenz curves of reduced pore types with a unimodal pore throat distribution (samples GF8213, Kit8181, LG8174, NGW8135; Figure 19) show that only about 2-4% of the pore throats are controlling about 95% of the fluid flow through the sample. The remaining 98% of pore throats contribute little to flow and are associated with trapped fluid that will not readily flow. The size-reduced samples with bimodal pore throat distributions (samples GF8209, GF8213, Str82052; Figure 19) show a slightly different behavior, in that the larger pore throat area mode (~5% of the pore throats) controls about 8% of fluid flow

capacity, and another 3% of the pore throats controls about 45% of the flow capacity,

and fluid in the remaining 90% of the pore throats will be immobile. Kem38193 (Figure

19) is a diagenetic pore type sample with a unimodal pore throat distribution. It shows a

similar behavior to the size-reduced samples with about 5% of the pore throats

controlling about 95% of the fluid flow capacity. The other diagenetic pore type sample,

WB8114 (Figure 19), shows a Lorenz curve that is clearly segmented, due to a bimodal

pore throat distribution, similar to the bimodal size-reduced samples. However,

WB8114 has about 12% of the pore throats controlling 95% of the fluid flow capacity,

and a second pore throat mode of only about 1% controlling about 2% of the fluid flow

capacity.

Size-enhanced samples always have at least two modes of pore-throat size

distribution (Figure 20). Considering that size-enhanced samples have larger pore-throat

areas than size-reduced samples, the Lorenz curves show how the flow capacity of these

samples differs from the size-reduced samples (Figure 19). While the largest pore throat

mode (~5% of the pore throats) still controls about 80% of the flow capacity, a second or

sometimes third mode of smaller pore throats can control about 10% of the fluid flow

capacity. However the fluid flow and storage capacity behavior of the size-enhanced

samples cannot be as readily stereotyped as can the reduced pore types. For example,

one size-enhanced sample (sample Kit8195; Figure 20) shows fluid flow as nearly

homogeneous through about 60% of the rock, i.e. the fluid flow capacity is distributed

more evenly though different pore-throat sizes and there is not a great a preference for

certain fluid flow pathways as there is for the other size-enhanced samples. The other

size-enhanced samples show that there is still a preferred fluid pathway, although less of the fluid will remain trapped in the smallest pore throats as it will for the size-reduced samples. The two depositional pore types (samples Kem38124 and NGW81525; Figure 20) have Lorenz curves with nearly identical behavior to one size-enhanced sample (LG8190; Figure 20).
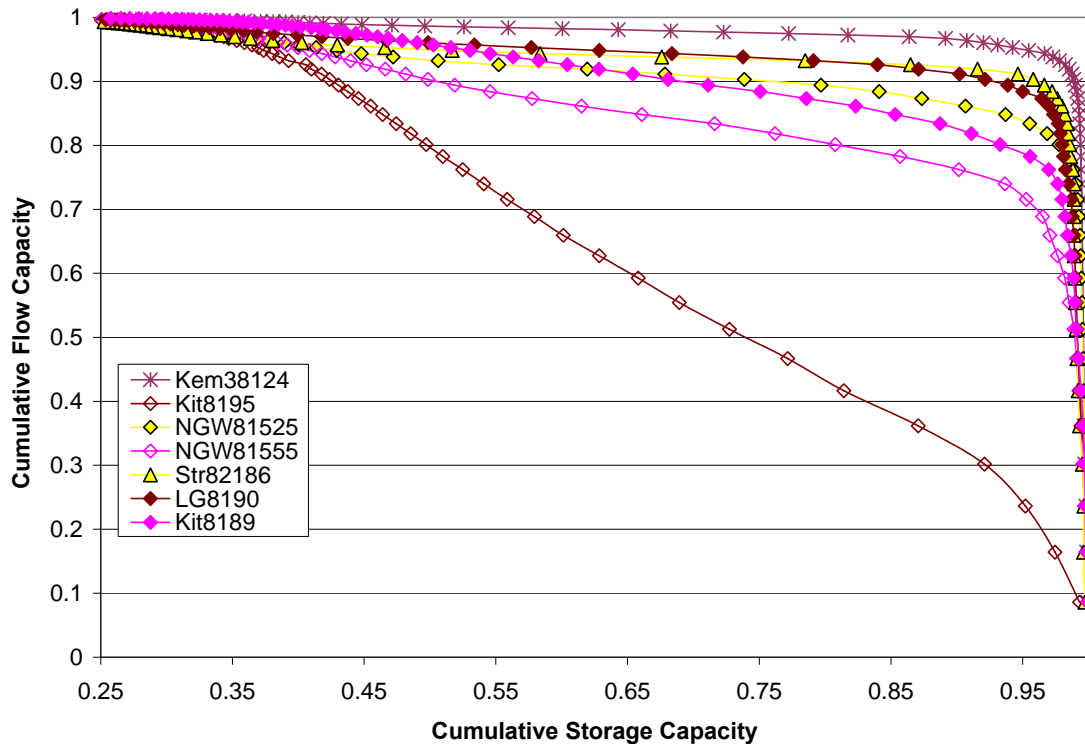
Figure 20: Lorenz curves for size-enhanced samples.

Lorenz curves can also be loosely grouped by facies (Figure 21). The most apparent correlation is the difference between the Lorenz curves for the G/P 1, oolitic grainstone facies and the G/P 2 facies, oncolitic grainstone. The oncolitic grainstone

samples clearly plot in a separate group from the oolitic grainstone facies (Figure 21).
These oncolitic grainstone samples have a much greater potential for fluids to be moved
through the different pore throat distributions, only about 30% of the fluids in the
oncolitic grainstone facies are immobile. In comparison, the oolitic grainstone samples
have between 50 and 90% immobile fluids (Figure 21).
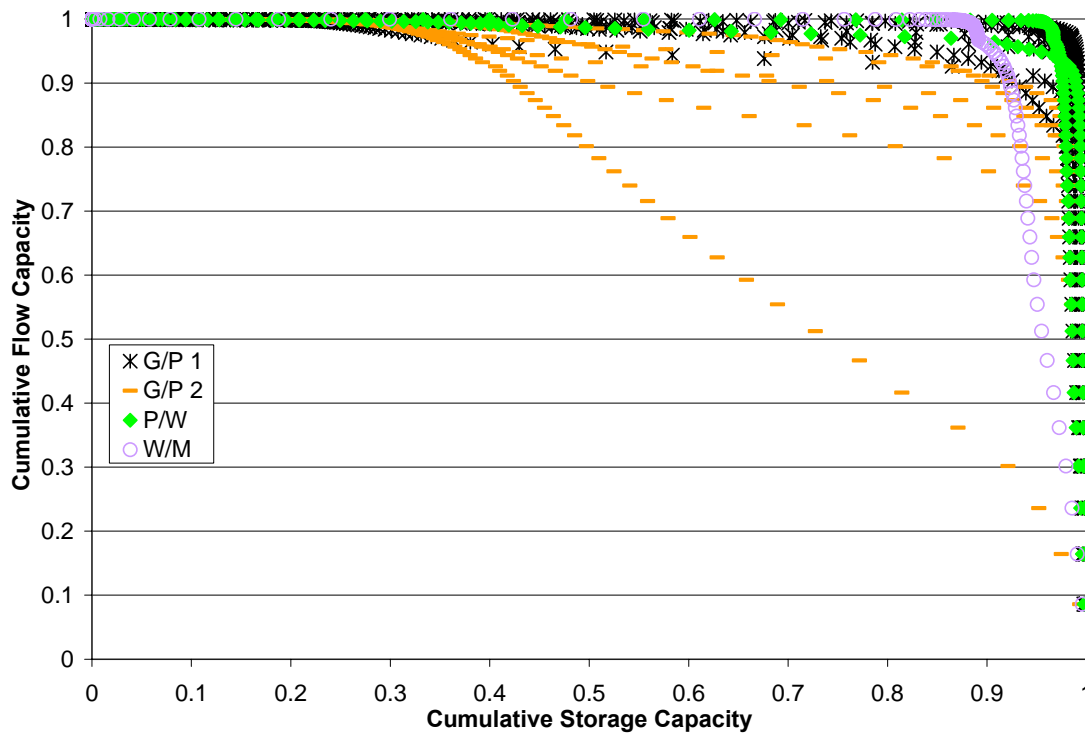
Figure 21: Lorenz curves grouped by facies.

Thus the pore throat distributions of the oncolitic grainstone reservoir rock
samples show a greater capacity to transmit stored fluids. However, there is more
variability in the flow and storage capacity for the oncolitic grainstone facies, where as

the oolitic grainstone facies samples show a more uniform behavior. This is expected as

oncolitic rocks with poorer sorting and a wider range of pore and pore-throats sizes

create an inherently heterogeneous and complex pore system. As expected, the fine-

grained samples, packstone, wackestone, and mudstone have between 5% of the pore-

throats controlling ~10% of the flow, with the remaining 90% of fluids being immobile

(Figure 21).

DISCUSSIONS

Pore and Pore-Throat Geometry

Results of this study reveal relationships between pore types and pore/pore-throat geometry and accompanying reservoir performance characteristics in the Grayson field Smackover reservoir. These relationships enable one to use the data obtained in this study for the design and assessment of enhanced oil recovery techniques. For example, pore type and pore/pore-throat geometry are related in ways that enable genetic pore types and their corresponding petrophysical characteristics to be determined. Furthermore, knowing the geological causes that created the different pore types and their corresponding geometries, it is generally possible to identify associated stratigraphic characteristics created contemporaneously by the pore-forming processes and thus correlate pore types and their attendant reservoir quality at field scale. This method should make it possible to map reservoir quality zones in complex carbonate reservoirs by using the genetic links between pore types and their correlative stratigraphic characteristics such as disconformities, unconformities, siliciclastic or evaporite-rich zones, and paleosols.

Pore Types

Depositional pore types occur in both grainstone facies, the hybrid pore H1-10e occurs only in the oncolitic grainstone facies, purely diagenetic pore types occur in fine-grained, grain-supported and mud-supported facies, and fractures were not found to be

present in the studied thin sections. Based on this first-order pore type and facies categorization, the uniqueness of different pore types to different facies is an important consideration for establishing the spatial distribution of different pore types across Grayson field.

The spatial distribution of pore types, based on the correlation between pore types and the corresponding facies of 81 samples, is determined by plotting the different pore types on stratigraphic cross sections that show the distributions of the facies across different sections of the field; these correlations are illustrated in four different cross sections (Appendix D). Grainstone facies are widely distributed across the field (60% of thin section samples are from the oolitic grainstone facies, and 17% are from the oncolitic grainstone faces), but the spatial distribution of pore types and their relationships to depositional facies is not always clear.

However, the geologic causes of different pore types can be related to the occurrence of unique stratigraphic features such as anhydrite and dolomite beds. Anhydrite and dolomite grain replacement and pore filling is the cause of porosity reduction for 11 samples (The causes of porosity reduction and enhancement were determined for 39 of 81 samples). The detailed core descriptions by Poole (2006) indicate that there is common to abundant anhydrite and/or dolomite present at core depths where these thin section samples were taken. Poole's (2006) descriptions also showed that these samples exhibit ~10% anhydrite and up to 35% dolomite. Thus, the occurrence of anhydrite beds and dolomite can be utilized to locate size-reduced pore samples controlled by anhydrite and dolomite grain replacement and pore filling.

The distribution of all pore types can vary within 6ft vertically in a given facies except when samples are taken at 2ft intervals. Such a small sampling interval provides similar samples that have been exposed to nearly or exactly the same genetic geologic history. In such a case of close-spaced samples, pore types are uniformly distributed in the vertical dimension (e.g. in the Alexander #1 and Reeves#1 boreholes; Appendix D, Figure D.1). In some cases, only one pore type, such as H1-30e, may occupy an entire 10 to 20ft interval within one well (example, Kemmerer #3 from 8124-8143ft, Appendix D, Figure D.2). This predominance of single pore types could not be identified from borehole to borehole however, because sample density varies widely from well to well (See Appendix D for all sample locations and facies distributions).

One goal of the adapted genetic classification for carbonate porosity in this present study (based on Ahr et al., 2005) is that it attempts to fill a gap between the previously existing carbonate porosity classifications and offers as a suggestion to other carbonate porosity researchers that a detailed petrographic and a subsequent petrophysical study adds meaningful value to carbonate porosity classifications and their adaptations for each reservoir. Lonoy (2006) explains that many of the existing classifications either do not sufficiently define poro/perm relationships or if they do, they do not thoroughly integrate sedimentological, diagenetic, and flow-related properties.

Based on his own extensive data base and research, Lonoy (2006) has developed a new pore-type system that extracts elements from the existing carbonate pore-type classification systems while implementing new features such as: the use of pore size rather than particle or crystal size as the criteria for pore class divisions (rather than

interparticle classes), the creation of uniform and patchy porosity distributions, and the creation of mudstone microporosity. Lonoy (2006) was able to demonstrate that both the geological and the petrophysical characteristics of a pore can be integrated in such a way that facilitates the prediction of reservoir performance parameters. Similarly, the Grayson field samples examined in this present study provide further evidence that a classification system that allows for identification of related petrophysical and reservoir performance characteristics is long overdue.

Pore Size

Five pore size categories are found in the Grayson field samples. The biggest pores are found in the depositional pore types in oolitic grainstone facies, and intermediate pores are found in the oncolitic facies hybrid pore types. The smallest pore sizes are found in the hybrid pore type samples of the mud-supported facies. The distribution of different pore sizes in this study indicates that depositional facies is the dominant influence on pore size. Although depositional pores exhibit the largest pore areas ($0.0001mm^2$), hybrid pores from different facies (depositional textures) may fall in different pore size categories. In other words, facies type influences pore sizes more than does genetic pore type. For example, pore areas of H1-10e pores in the oncolitic grainstone facies vary widely while pore areas in packstone/wackestones invariably remain in pore area category 1 (Figure 22) because of the smaller grains associated with the finer-grained facies. Oncolites may be >2 mm in diameter and may have attendant

pore size of >0.0001 mm^2, while packstone/wackestone grains are within the 0.5 to 0.25 mm range and exhibit pores <0.00005 mm^2.
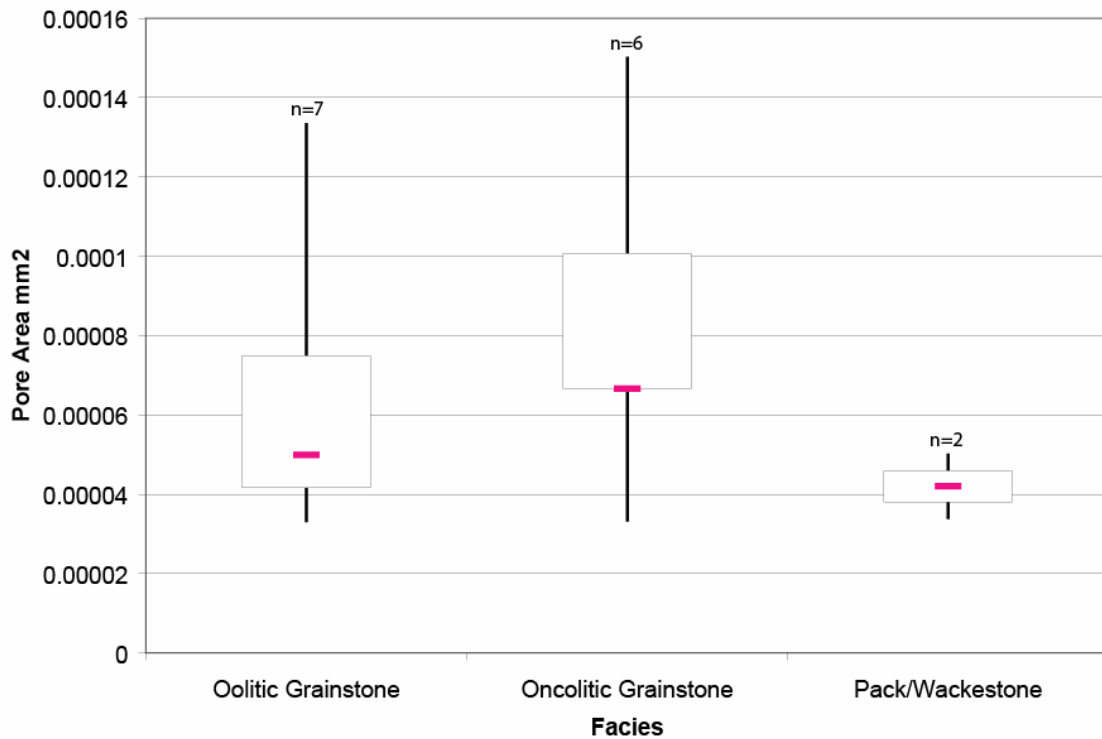
Figure 22: Box plots showing the ranges (vertical black line) and median values (horizontal pink line) of pore area (mm^2) for each facies.

The relationship between pore size (area) and depositional facies is particularly well illustrated in the oncolitic grainstone facies. In this case, the poorly-sorted oncolitic grainstones exhibit the greatest variability in pore size (area) of all depositional facies because the facies includes oncoids up to 10mm in diameter. If the controlling diagenetic process (i.e. grain dissolution, replacement, enhancement, or compaction)

altered large oncoid grains in one sample while contemporaneously altering an adjacent zone of ooids and peloids, 0.1 to 1 mm in diameter, only the oncolitic facies would exhibit 'megapores.' Even poorly sorted packstone/wackestone facies with smaller grain sizes do not exhibit hybrid pore areas larger than original grain dimensions except in the case of vug formation.

Other than depositional pores, which fall into pore size category 5, oolitic grainstone samples have hybrid pores types in category 1 ($<5x\ 10^5\ mm^2$). Where the oncolitic grainstone facies is present the pores are more difficult to categorize, and care was taken to determine the precise pore size category for each sample location (i.e. the location of the well and the depth of the sample). Samples of packstone/wackestone facies with pores that fall within the size range $<5x\ 10^5\ mm^2$, along with mud-supported rocks and dolostones require measurement techniques other than PIA to determine the median pore size.

Because depositional texture was a dominant control factor in determining pore size, it is imperative to understand the spatial distribution of depositional facies across Grayson field. Because variability in pore size may occur within depositional facies, particularly in the oncolitic grainstone facies, there must be statistically reliable sample density to record the variability. Facies distributions in Grayson field have been documented by Poole (2006). Therefore the correspondence between pore size categories and different facies can be determined. For example, there are only two samples with truly depositional pore types found in this study. The oolitic facies sample median pore size is $6.66x10^{-5}\ mm^2$ and the oncolitic facies depositional pore type

median sample is 1.33×10^{-4} mm^2. By increasing the sample density to determine a specific size range for the oncolitic depositional pore type the expected spatial distribution of a certain pore size category can be mapped from well to well.

The same method can be applied for other facies. Packstone/Wackestone samples in this study exhibit pore size category 1. Therefore the pores in that facies can be assumed to have a pore size $<5 \times 10^{-5}$ mm^2. Mud-supported and dolostone samples cannot be imaged by computer-assisted petrographic image techniques; therefore, pore sizes of those samples could not be determined.

Pore-Throat Size

A clear relationship exists between pore-throat size and pore type (Figure 23). Hybrid pores that have been diagenetically size-reduced have pore-throat sizes smaller than those of diagenetically size-enhanced pore types. Depositional pore-throats are larger than all hybrid reduced types, all purely diagenetic types, and some hybrid enhanced types. The H1-10e pore-throats that typically occur in oncolitic facies exhibit greater variability in size than all other genetic pore types, due to the poorly sorted texture and grains >2 mm in size.
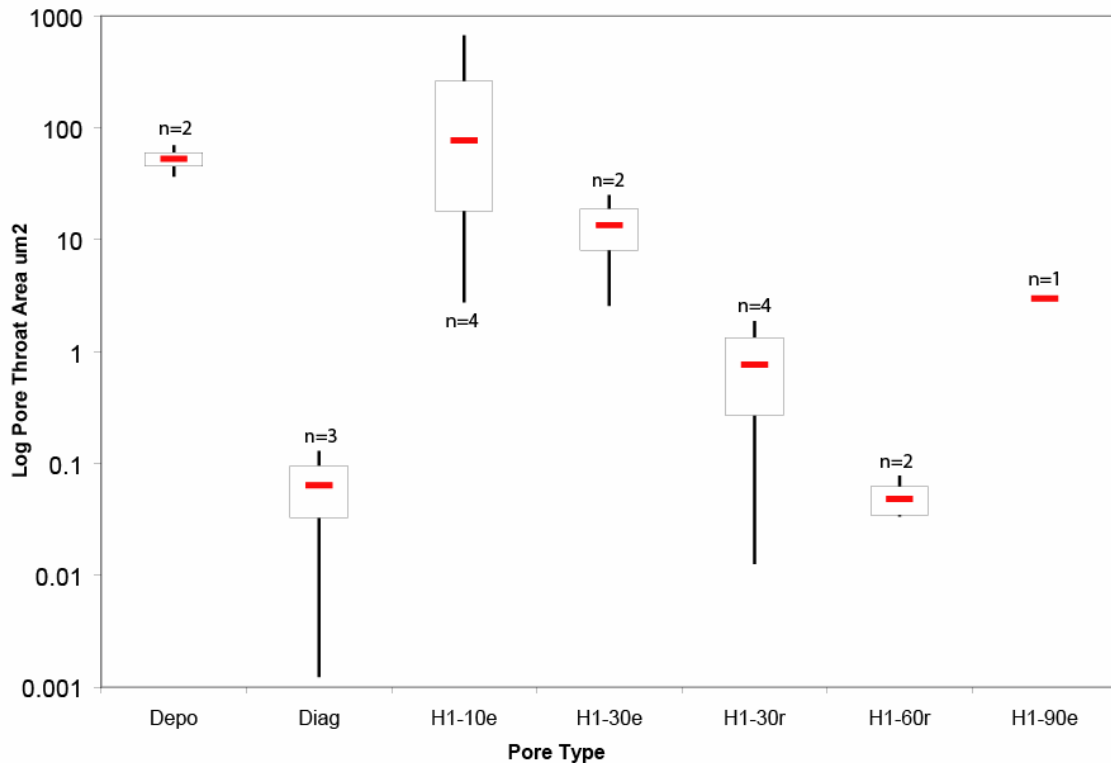
Figure 23: Box plots of pore-throat area (µm²) categorized by pore type. The ranges (vertical black line) and median values (red horizontal line).

Genetic pore type and pore-throat size are related because diagenetic alteration that has affected both grains and pores determines in which pore-throat size category a certain sample will occur. Porosity-enhancing events generally did not create pore-throats larger than their original depositional size, but the processes prevented the pore-throats from being totally closed. This is explained by the fact that small pore-throats have a large surface area to volume ratio; consequently, they were more susceptible to dissolution or cementation.

Pore-throat sizes were determined by mercury-injection capillary pressure measurements. The resulting data were then studied to determine the pore-throat size distribution across Grayson field. Owing to the high cost of the capillary pressure measurements, only 17 samples were studied. This low sample density made it difficult to accurately determine the spatial distribution of pore-throat sizes. The Results section details how pore-throat sizes for each sample can be categorized by pore type.

Because pore-throat size may be controlled by diagenetic processes, it is necessary to correlate pore-throat sizes with pore types and the geologic events that created the system. Typical geologic events include such diagenetic changes as grain and cement dissolution, compaction, grain replacement, and different stages of cementation. For such correlations to be possible, a detailed chronostratigraphic study is needed to determine the depth and location of stratigraphic horizons that exhibit the results of these diagenetic events.

Work by other authors explains the usefulness of pore-throat size and a pore geometry classification system based on pore shapes, particularly for evaluating fluid saturations and predicting well performance. Spain (1992) combines sedimentological, petrophysical, well log, and reservoir engineering data to create a unique reservoir characterization study. Additionally, he was able to utilize a chronostratigraphic correlation of the sandstones to understand the spatial distribution of the different depositional environments. He concluded that, for his sandstone reservoir rocks, both the depositional processes and the subsequent diagenetic changes are the primary factors controlling the pore size distributions, and thus they form different rock types with

unique petrophysical properties. He categorizes the different rock types into a petrophysical rock classification system based on the effective pore-throat size (R_{35}). The different petrophysical rock types are found to be vertically stratified throughout the reservoir section and this information can provide structural height constraints for water-free hydrocarbon production. Additionally, Spain showed that rocks with similar pore geometries and effective pore-throat size show similarity in permeability/porosity ratios, irreducible water saturations, relative permeabilities, and initial flow rates.

The utilization of pore-throat size and pore type categories in this way is support for the work in this present study and for the focus point that the benefits of pore-throat size measurement acquisition go beyond pore classification. Spain (1992) was able to define not only hydrocarbon column heights necessary for water-free oil production, but also calculate accurate water saturations combined with a movable oil analysis and drainage relative permeability/frational-flow curves to predict initial watercuts.

Pore and Pore-Throat Area

Pore geometry of the Grayson field Smackover reservoir rocks is strongly correlated to depositional facies. In turn, genetic pore types correspond to pore-throat sizes. Therefore, by extension, facies and pore types determine pore-throat sizes in Grayson field. Variations from the general pattern can occur as in the case of mega-grain sized oncolitic facies that exhibit reduced pore sizes that are larger than enlarged pore sizes in finer grained facies.
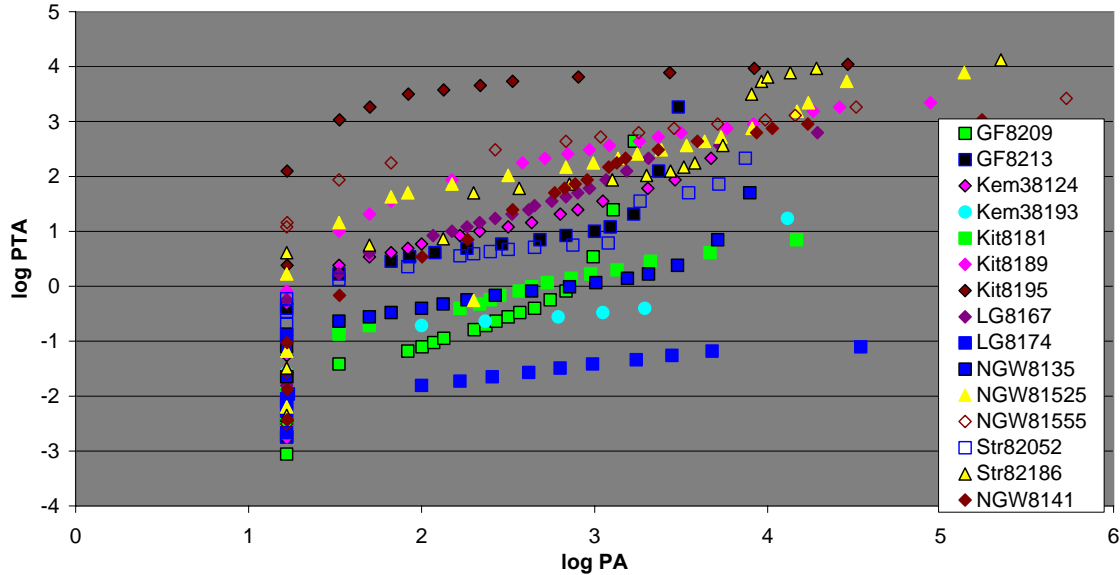
Figure 24: Pore area (μm²) – pore-throat area (μm²) – pore type relationship (size-enhanced samples with diamond markers, size-reduced with squares, depositional with triangles, and diagenetic with circles).

The results from the pore and pore-throat area analysis, Figure 24, show a strong relationship between pore size and pore-throat size, but because of the textural variability in the depositional facies, it is difficult to predict pore and pore-throat size across the field. Though a larger sample base may provide enough information to produce maps of pore and pore-throat sizes, it is probably enough to know that the greatest probability of finding small pores is in mud-supported facies, and locations in the field that have undergone pore space reduction. Conversely, larger pore and pore-throat sizes generally occur in coarser-grained facies and in locations where diagenetic processes created size-enhanced pore types. Fortunately the amount of vuggy porosity is

negligible in Grayson field, therefore the predominant variable related to pore and pore-throat size is original depositional texture.

Capillary Properties

<u>Permeability and Pore-Throat Size</u>

The results of the permeability and pore-throat size analysis show that these two properties have a strong correlation in the Grayson field samples (Figure 25). By extension, because pore-throat size is closely related to pore type, a generalized relationship between pore type and permeability can be made. Size-reduced pore types have lower permeability and small pore-throats. Purely diagenetic pore types have the lowest permeability because these samples have the smallest pore-throat sizes. Size-enhanced pore types have larger pore-throat sizes than reduced pore types and thus higher permeability. Depositional pores have high permeability values but not as high as some H1-10e samples because depositional pores lacked grain leaching to enlarge pore-throats. The H1-10e sample in Figure 25 (Kit8195) has a permeability of >600 md and median pore-throat aperture of nearly 30µm due to the dissolution of oncolites that were as great as 10mm.
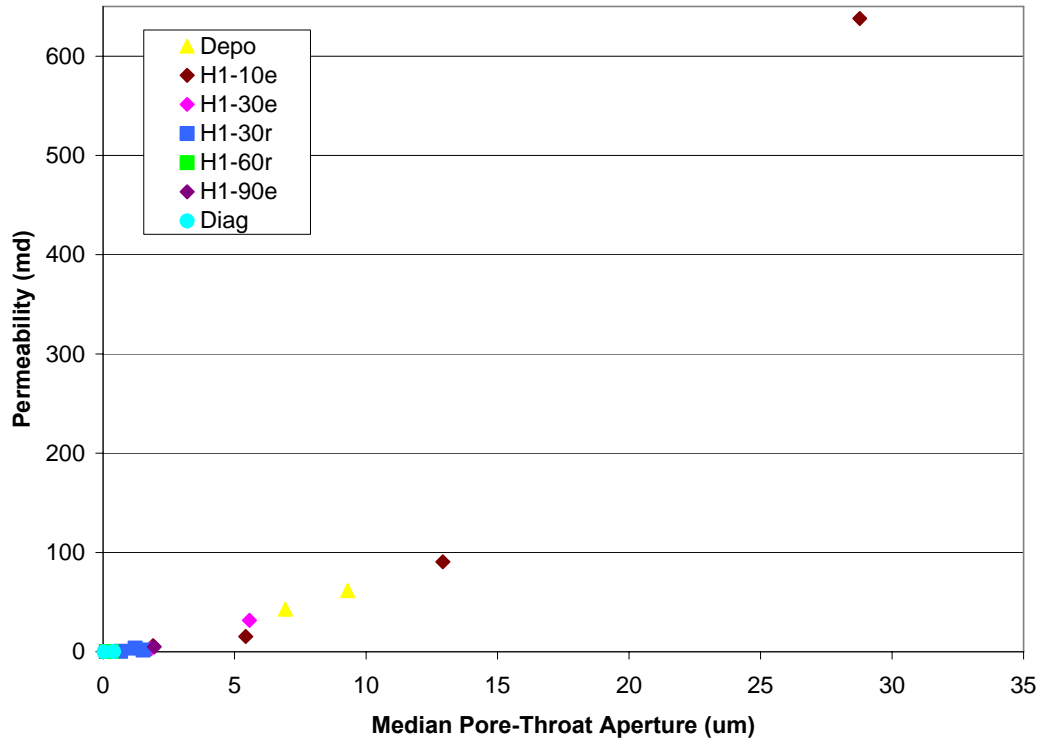
Figure 25: Permeability (md) and median pore-throat aperture (diameter, µm).

The method presented in this study of classifying reservoir rock samples by pore type allows for the prediction of such petrophysical properties as permeability. Based on pore type classifications, different reservoir zones can be identified on a "quick-look" basis for high-quality and low-quality flow units based on the expected high or low permeability values associated with the pore types of the reservoir rocks at specific locations and depths (Table 5).

Table 5: Flow unit ranking based on pore type classification.

Pore Type	Permeability Quality	Flow Unit Quality	Permeability Range (md)	Pore-Throat Size Range (μm)	Notes
Reduced	Low	Poor	0-2	0-1.5	Should apply consistently
Enhanced	Medium	Moderate	2-40	1.5-6	For H1-10e pores depends on the PTS
Depositional and H1-10e	High	High	>40	>6	Should apply consistently for depo and H1-10e PTS >6μm

The J-Function

      Classification of reservoir rock samples by genetic pore type also gives insight into petrophysical characteristics that can also be revealed by the J-function (Figure 26). Results of the J-function analysis show that size-reduced pore types have similar J-function curves and thus behave similarly due to the similarity in their dependent rock properties. On the other hand, size-enhanced pore types show more widely ranging J-function curves because depositional facies has been found to be more important than diagenetic alteration in influencing dependent rock properties of the size-enhanced pore type samples. Additionally, facies changes within one well and between adjacent wells were found to have strong influence on dependent rock properties (i.e. porosity, permeability, and wettability).

By classifying the genetic pore types at different locations and knowing the specific production or enhanced recovery technique to be implemented, it should be possible to identify relationships between reservoir rock zones where the production characteristics and dependent rock properties are closely related. Because consistent permeability values are essential for specific enhanced recovery techniques, despite the fact that the permeability values may be low, an area in the field that consists mostly of reduced pores could still be considered as being potentially "successful" for injection or production as long as the permeability is not below a certain threshold. On the other hand, if the enhanced recovery technique requires permeability be of moderate or high values, even if those permeability (or porosity) values may be heterogeneous, an area of the field with predominantly size-enhanced pores would be an acceptable target.
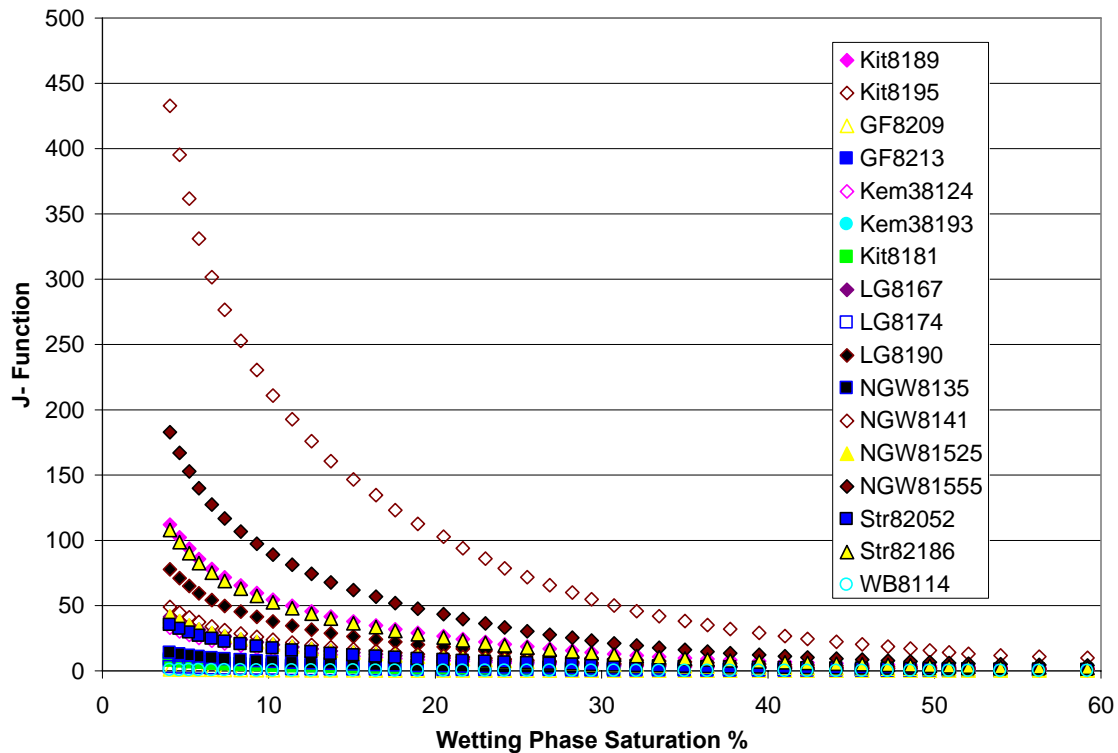
Figure 26: Separation of J-function curves by pore type (size-enhanced samples with diamond markers, size-reduced with squares, depositional with triangles, and diagenetic with circles).

The Lorenz Curve

The Lorenz curves show that the samples from oolitic grainstone facies have a more predictable fluid flow behavior than those of the oncolitic grainstone facies although the latter has a larger range in pore-throat sizes than the oolitic grainstone facies. Fine-grained, grain-supported and mud-supported facies tend to retain about 90% of the fluids trapped in the pore-throats because they have pore-throats that are too small to transmit fluids (Figure 27).
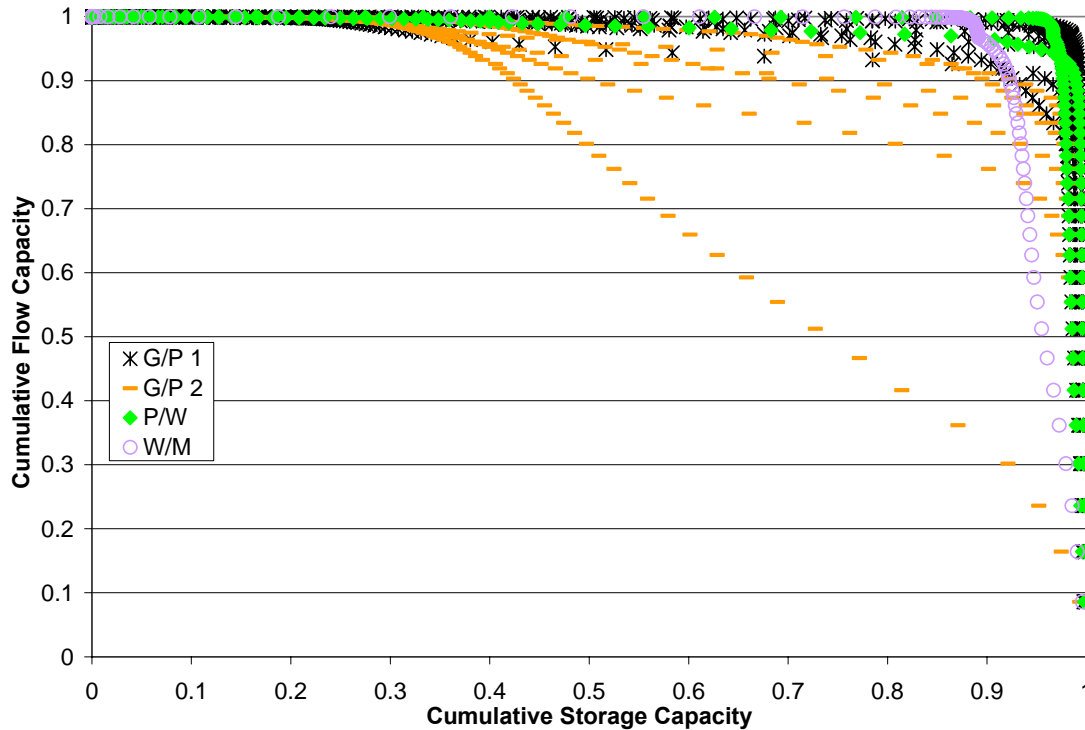
Figure 27: The four different facies have distinct Lorenz curves. Oncolitic grainstone (G/P 2) has the potential to move more fluid through the pore network, but oolitic grainstone (G/P 1) has more predictable fluid flow.

Size-reduced samples show similar fluid flow behavior, and the Lorenz curves for these samples are very different that those showing the fluid flow behavior of the size-enhanced samples (Figure 28). The division of size-reduced samples by their corresponding number of statistical pore-throat size modes shows that for many size-reduced samples there are two dominant pore-throat sizes that contribute to flow. In short, the fluid flow characteristics of samples with size-reduced pores can be grouped according to their corresponding pore-throat size ranges. Samples with size-reduced

pores and the same corresponding number of pore-throat size ranges exhibit similar fluid

flow behavior.
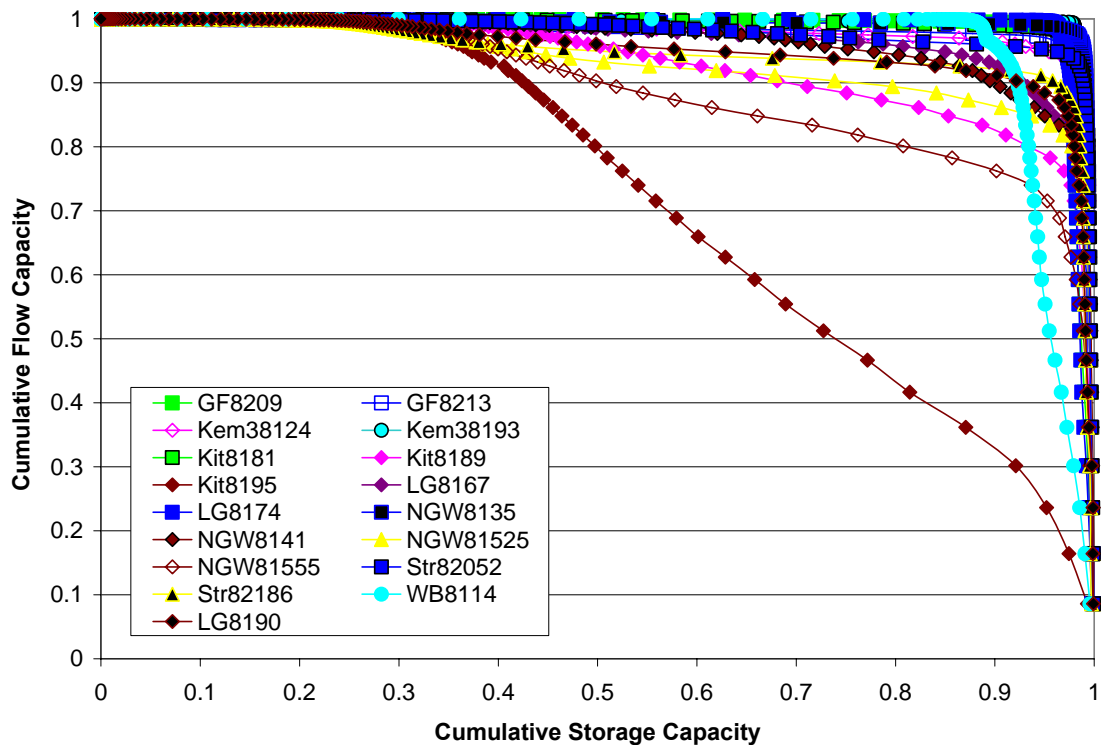
Figure 28: The different pore types also show Lorenz curve division (size-enhanced samples with diamond markers, size-reduced with squares, depositional with triangles, and diagenetic with circles).

Size-enhanced pores show too much variability in fluid flow characteristics to

pinpoint a stereotypical behavior (Figure 29). However, depositional pore types exhibit

fluid flow behavior similar to that of the size-enhanced pores, based on the overlay of

their Lorenz curves, even though the samples come from different facies. It therefore

appears that diagenetic alteration of original depositional texture has affected the

grainstone facies in such a way that the fluid flow characteristics are less predictable

than in the case of depositional pore types. Further study of this problem and the

complexity of fluid flow through the size-enhanced pore type reservoir rocks is advised.
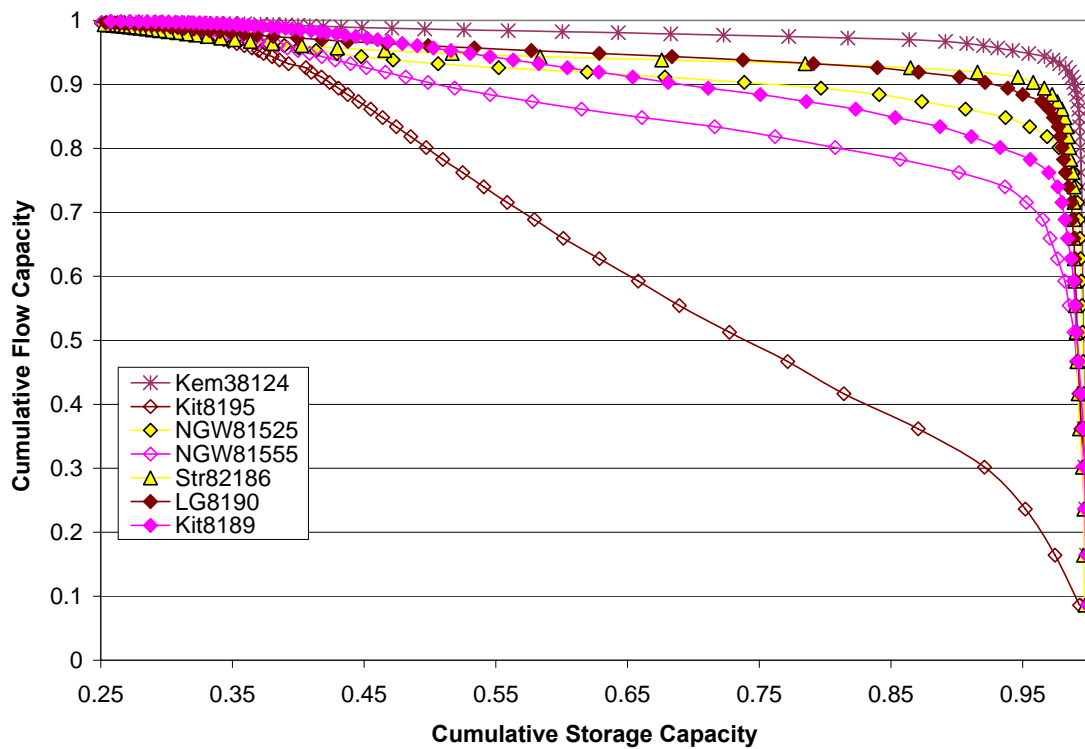
Figure 29: Size-enhanced pore type Lorenz curves are difficult to stereotype and show a wide range of flow and storage capacities.

Modified Lorenz plots have been used by other authors to define flow units for

the upscaling of geological and petrophysical descriptions for reservoir simulation

(Gunter et al., 1997). In their 5-step procedure for quantifying flow units, the authors

create two modified Lorenz curves to define flow units that honor geological data, the

stratigraphic sequence (foot-by-foot data), and that can be used for numerical flow simulation. The first modified Lorenz plot of Gunter et al. (1997) showed the percent of flow capacity versus percent of storage capacity in stratigraphic sequence. This offers a guide to the necessary number of flow units to honor the geologic framework (Gunter et al., 1997). Flow units are selected from inflection points on modified Lorenz curves. The second modified Lorenz plot by Gunter et al. (1997) differs from the original Lorenz plot in that flow capacity and storage capacity is computed on a flow unit basis and maintains stratigraphic position (Gunter et al.'s previously defined flow units were sorted and plotted in decreasing flow speed). Gunter et al. also compare the quality of the flow capacity, storage capacity, and porosity/permeability relations to understand the importance of each flow unit. The key to this method by Gunter et al. (1997) is the inclusion of the geologic framework.

Porosity by Petrographic Image Analysis

The results of this analysis show that petrographic image analysis (PIA) consistently underestimates porosity from routine core analysis by 30 to over 90 % (Appendix B and Figure 30). Underestimation of porosity by PIA techniques has been recognized by a number of other workers including Mowers and Budd (1996), who used PIA techniques to quantify porosity and permeability reduction due to calcite cementation. All samples for their study were grain-supported dolostone. PIA porosity underestimated core-plug porosity in a range of 5 to 52% (mean underestimation ~30%) for 21 samples (two samples had PIA porosity greater than the corresponding core-plug

porosity). Mowers and Budd (1996) suggest two main reasons for the PIA porosity underestimation as compared to the core-plug porosity values. First it is suggested that only pores greater than 1µm in size (i.e. one pixel) can be resolved. Second they suggest that their PIA technique of binary image editing resulted in the loss of some small pores ranging from 1 to 3µm.
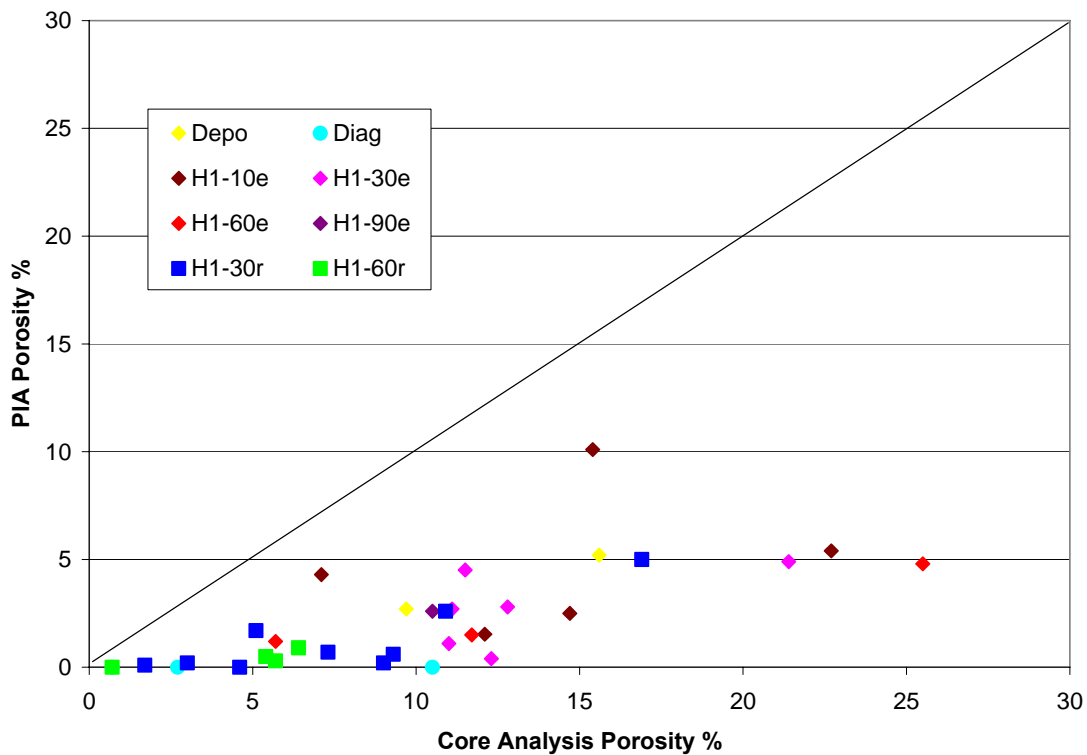
Figure 30: Plot showing underestimation by PIA porosity of conventional core analysis porosity, in percent.

Adams (2005) showed that the correspondence of 2-D and 3-D porosity calculations decreased from depositional intergranular sandstone pores to carbonate

hybrid 1-a pores, to carbonate diagenetic pores (Adams, 2005; Ahr et al., 2005). The reason behind this is that solution-enhanced interparticle, moldic, and vuggy pores have more complex pore geometries in 2-D than intergranular sandstone pores. Adams (2005) also concluded that for cement reduced or diagenetic pores, PIA could not reliably demonstrate a relationship between 2-D and 3-D measured porosity. Again the complications of comparing 2-D and 3-D porosity is somewhat related to the resolving power of the PIA methodology. Thus, the complication with comparing 2-D and 3-D porosity values can be explained in this study by the complex porosity types and the consequently complex pore geometries.

The discrepancies between PIA and routine core analysis porosity values notwithstanding, this study identified firstly that depositional pore areas are greater than $0.1 \ \mu m^2$, enhanced pore areas range between <0.05 to $>0.1 \ \mu m^2$, and reduced pore areas range between <0.05 to $0.1 \ \mu m^2$. The explanation for such a wide range in pore areas within the classification of depositional or the two hybrid porosity types is that the pore area is controlled by facies rather than pore type. Thus using facies to categorize samples by their pore areas, depositional pores of both grainstone facies have median pore area $>0.1 \ \mu m^2$ and both enhanced and reduced median pore areas in the oolitic grainstone facies are $<0.05 \ \mu m^2$ (Table 6). As previously explained, the oncolitic grainstone has a complex influence on pore area due to the tendency for extremely poorly sorted grains, and thus both the enhanced and reduced median pore areas have a very large range from <0.05 to $>0.1 \ \mu m^2$. The mud-supported facies sample pore areas

are consistently <0.05 µm^2 (Table 6). Table 7 shows a pore size category based on pore

diameter in µm.

Secondly it was determined that pore-throat size is strongly influenced by the

pore type; therefore median pore-throat areas can be assigned to the different pore types.

Depositional pore-throat areas are between 20 and 100µm^2, enhanced pore-throats are

from 1 to 100µm^2, and reduced pore-throat sizes range between <1 and 20µm^2.

Diagenetic pore-throats are consistently <1µm^2 (Table 8). Additionally, small pore-

throat diameters correlate with high water saturations from MICP analysis and as a result

correspond to low permeability values. Since pore type is the controlling factor on pore-

throat size, a connection can be made between pore type and water saturation values;

size-reduced samples will have higher water saturations than size-enhanced or

depositional pore types.

Table 6: Quick-look table to determine median pore size (area, µm^2).

Facies	Depositional	Pore Type Enhanced	Reduced	Diagenetic
Oolitic Grainstone	>0.1µm^2	<0.05 µm^2	<0.05 µm^{22}	Below Detection
Oncolitic Grainstone	<0.05 to >0.1 µm^2	<0.05 to 0.1 mm^2	<0.05 to >0.1 µm^2	Below Detection
Packstone/ Wackstone	<0.05 µm^2	<0.05µm^2	<0.05 µm^2	Below Detection
Dolostone	Below Detection	Below Detection	Below Detection	<0.05 µm^2

Table 7: Quick-look table to determine pore size (diameter, µm).

Facies	Pore Type			
	Depositional	Enhanced	Reduced	Diagenetic
Oolitic Grainstone	>13 µm	6.5 to 13 µm	4.5 to 13 µm	Below Detection
Oncolitic Grainstone	>13 µm	6.5 to 20 µm	6.5 to 10 µm	Below Detection
Packstone/ Wackstone	<8 µm	<8 µm	<6.5 µm	Below Detection
Dolostone	Below Detection	Below Detection	Below Detection	<6.5 µm

Table 8: Quick-look table to determine pore-throat size (area, μm^2).

	Pore Type		
	Depositional	Enhanced	Reduced
Pore-Throat Size (μm^2)	20 to 100 μm^2 (5 to 15 µm diameter)	1 to 100 μm^2 (1 to 15 µm diameter)	<1 to 20 μm^2 (<1 to 5 µm diameter)

This study also recognized that pore-throat measurements can be utilized as a proxy for pore size, based on a pore type–pore-throat size–pore size relationship (and also using the reasoning that pore-throat measurements can be obtained from routine mercury-injection capillary pressure analysis, a faster method than PIA). The correlation between pore-throat size and pore size was determined to be strong, such that, if the pore type is known (based on the petrographic pore type classification described in this study, Methods section), and the pore-throat size is known, then the pore size can be identified within a certain range of values. The most striking observations are that size-enhanced pore types have the largest pore-throats and size-reduced pore types consistently have

smaller pore-throats. All pore types show a varied range in pore area, but using pore type and pore-throat size as constraints, a quick-look method for determining pore size has been established by this study (Tables 6 and 7). This established pore/pore-throat relationship shows the correspondence between pore type classification, known pore-throat size, and the estimated pore size. Similarly, knowledge of the pore type and the pore-throat size can be used to estimate both permeability values (and qualify those by low, medium, or high) and flow units rankings.

The J-function was recognized as a useful tool to differentiate that the different pore types (i.e. enhanced, reduced, and depositional) have different correspondence with dependent rock properties. If the pore type classification is known, size-reduced samples can be expected to have a more homogenous behavior, but the size-enhanced pore types require more attention to the grouping of samples both by facies and by stratigraphic location to determine how they will behave according to their dependent rock properties.

By utilizing the different data sets provided by a mercury-injection capillary pressure test, the fluid flow behavior of the reservoir rocks can be qualified (through the Lorenz curve). It was determined that oolitic grainstone samples have a more predictable fluid flow behavior than oncolitic grainstone samples, and that fine-grained samples will retain at least 90% of the flowing fluids due to the small size of the pore-throats. Additionally it is useful to know the number of pore-throat size modes for the size-reduced pore samples; such knowledge tells if the samples will have similar fluid flow behavior. Depositional and enhanced pore type samples show similar behavior, but

this behavior is much more complicated than the size-reduced samples, and thus a quick-

look behavior cannot be identified.

CONCLUSIONS

The goal of this study was to identify relationships between pore types, defined by a genetic carbonate porosity classification, different pore/pore-throat characteristics, and their corresponding petrophysical properties. General conclusions can be made about the distribution of facies, samples, and pore types across Grayson field that can assist in the evaluation of enhanced recovery methods.

- Based on the relationship between pore-throat size, pore size, J-function, Lorenz curves, and the division of pore and pore-throat sizes into specific size categories, the following relationships were identified:
  - o If size-enhanced pore types are identified by petrology, then the pore-throat diameter will be between 5 and 12 µm and the pore area category will depend on the facies of the sample. Size-reduced pore type samples will be <5 µm in diameter.
  - o Size-reduced pore type samples exhibit similar petrophysical characteristics, in regards to the three dependent rock properties, porosity, permeability, and wettability. However, the dependent rock properties of size-enhanced pore type reservoir rock are controlled more by the depositional facies than by pore type and the petrophysical relationship is much more complex.
  - o By knowing both the number of modes of pore-throat sizes and the pore type of each sample, fluid flow behavior can be predicted based on the

fluid and storage capacity. Size-reduced and purely diagenetic pore type samples that have the same number of pore-throat size modes (i.e. unimodal or bimodal pore-throat size distributions) will have the same fluid flow behavior. Size-enhanced pore type samples show too much variability in their fluid flow behavior to pinpoint a distinct stereotype. Depositional pore type samples show the same fluid flow behavior regardless of the number of pore-throat size ranges.

- Of the two grainstone facies, the oolitic grainstone facies has more predictably related pore and pore-throat size categories. In contrast, the oncolitic grainstone facies shows a great variability in both pore size and pore-throat size categories, but the facies has the largest pore and pore-throat sizes. Packstone/wackestone facies samples also have predictable pore and pore-throat categories however the stratigraphic extent of this facies is less than the two grainstone facies.

- Depositional pores tend to have the largest pore and pore-throat sizes for both grainstone facies, and thus pore type classification is especially important. A detailed study of different stratigraphic horizons in which depositional porosity is preserved is essential for mapping pores types because the different pore types are controlled by geological events that should be traceable across stratigraphic boundaries within the Smackover formation.

- In this study it has been difficult to establish the spatial distribution of size-enhanced or size-reduced pore types owing to the low sample density. Preliminary results show that classifying pore type distribution is the solution to

determining the petrophysical behavior of the different Grayson field reservoir rocks. This is confirmed by both J-function and Lorenz curves that show size-enhanced and size-reduced pore types have distinctly different dependent rock properties and fluid flow characteristics. Obtaining more samples, and correlating more pore type locations across the field, should enable a much more reliable spatial distribution of the dependent rock properties and fluid flow behavior.

- Pore types may change over a few feet vertically. This study suggests that in the Nina Grayson Warnock #1 well, at depth interval 8100-8200 ft, a more detailed petrographic and petrophysical analysis is required to determine the lateral extent of the uniqueness of the pore/pore-throat geometry behavior seen at the sample depths of this well. Samples within 20ft vertically in Nina Grayson Warnock #1 exhibit permeability values that range from highest to lowest in the entire study.

- Knowing pore-throat size of the different facies is imperative to evaluate the potential to flow and the potential to store. This study suggests that more MICP data on additional samples throughout Grayson field from different facies and from different depths intervals would provide more accurate representation of flow unit properties across the field.

- PIA is a novel method to determine porosity, but 2-D image slices are not a reliable prediction of 3-D pore volume because of the heterogeneity and complexity of the pore geometries.

REFERENCES CITED

Adams, A. J., 2005, Relationships between observed pore and pore-throat geometries measured porosity and permeability, and indirect measures of pore volume by nuclear magnetic resonance: Ph.D. dissertation, Texas A&M University, College Station, Texas, 277 p.

Ahr, W. M., D. Allen, A. Boyd, H. N. Bachman, T. Smithson, et al, 2005, Confronting the carbonate conundrum: Schlumberger Oilfield Review, Spring 2005, p. 18-29.

Ahr, W. M., 2005, GEOL-624 Carbonate Reservoir, Course Notes, Texas A&M University, 109 p.

Ahr, W. M., 1973, The carbonate ramp: alternative to the shelf model: Gulf Coast Association of Geological Societies Transactions, v. 23, p. 221-225.

Amyx, J. W., D. M. Bass Jr, and R. L. Whiting, 1960, Petroleum Reservoir Engineering Physical Properties: New York, NY, McGraw-Hill Book Company, 610 p.

Benbennick, D., 2007, Map of Columbia County Arkansas: World Wide Web electronic publication, in Wikipedia, The Free Encyclopedia. http://en.wikipedia.org [accessed 09 September 2007].

Bliefnick, D. M., and J. G. Kaldi, 1996, Pore geometry: control on reservoir properties, Walker Creek field, Columbia and Lafayette Counties, Arkansas: American Association of Petroleum Geologists Bulletin, v. 80, p. 1027-1044.

Bornhauser, M., 1958, Gulf Coast tectonics: American Association of Petroleum Geologists Bulletin, v. 42, p. 339-370.

Choquette, P. W., and L. C. Pray, 1970, Geologic nomenclature and classification of porosity in sedimentary carbonates: American Association of Petroleum Geologists Bulletin, v. 54, p. 207-250.

Dunham, R. J., 1962, Classification of carbonate rocks according to depositional texture, *in*: W. E. Ham, ed., Classification of carbonate rocks-a symposium: American Association of Petroleum Geologists Memoir 1: Tulsa, OK, American Association of Petroleum Geologists, p. 108-121.

Ehrlich, R., S. K. Kennedy, S.J. Crabtree, and R. L. Cannon, 1984, Petrographic image analysis I. analysis of reservoir pore complexes: Journal of Sedimentary Petrology, v. 54, p. 1365-1378.

Ehrlich, R., S. J. Crabtree, K. O. Horkowitz, and J. P Horkowitz, 1991, Petrography and reservoir physics I. objective classification of reservoir porosity: American Association of Petroleum Geologists Bulletin, v. 75, p. 1547-1562.

Gunter, G. W., J. M. Finneran, D. J. Hartmann, and J. D. Miller, 1997, Early determination of reservoir flow units using an integrated petrophysical method: SPE Paper 38679, 8 p.

Hughes, D., 1968, Salt tectonics as related to several Smackover fields along the northeast rim of the Gulf of Mexico basin: Gulf Coast Association of Geological Societies Transactions, v. 18, p. 320-330.

Kalbacher, K., and A. A. Sartin, 1986, Diagenetic study of the Upper Member of the Smackover Formation (Upper Jurassic), Columbia County, Arkansas: Gulf Coast Association of Geological Societies Transactions, v. 36, p. 191-199.

Kopaska-Merkel, D. C., and S. D. Mann, 1991, Pore facies of Smackover carbonate reservoirs in southwest Alabama: Gulf Coast Association of Geological Societies Transactions, v. 41, p. 374-382.

Lonoy, A., 2006, Making sense of carbonate pore systems: American Association of Petroleum Geologists Bulletin, v. 90, p. 1381-1405.

Moore, C. G., and Y. Druckman, 1981, Burial diagenesis and porosity evolution, Upper Jurassic Smackover, Arkansas and Louisiana: American Association of Petroleum Geologists Bulletin, v. 65, p. 597-628.

Morgan, D., 2003, Mapping and ranking flow units in reef and shoal reservoirs associated with the paleohighs: upper Jurassic (Oxfordian) Smackover formation, Appleton and Vocation fields, Escambia and Monroe Counties, Alabama: M.S. thesis, Texas A&M University, College Station, Texas, 156 p.

Mowers, T. T., and D. A. Budd, 1996, Quantification of porosity and permeability reduction due to calcite cementation using computer-assisted petrographic image analysis techniques: American Association of Petroleum Geologists Bulletin, v. 80, p. 309-322.

Netherland, Sewell & Associates, Inc., 1996, Reservoir Simulation Study of the Grayson field located in Columbia County, Arkansas, 67 p.

Poole, K. R., 2006, Construction of a diagenetic history and identification with quality ranking of reservoir flow units: Grayson field, Columbia County, Arkansas: M.S. thesis, Texas A&M University, College Station, Texas, 118 p.

Schatzinger, R., 1993, Core description and petrography of three cores from the Smackover of Southern Arkansas: National Institute for Petroleum and Energy Research, 55 p.

Spain, D. R., 1992, Petrophysical evaluation of a slope fan/basin-floor fan complex: Cherry Canyon Formation, Ward County, Texas: American Association of Petroleum Geologists Bulletin, v. 76, p. 805-827.

Takach, J., W. R. Meaney, and K. B. Hill, 1998, The Grayson field Smackover lime oil reservoir Columbia County, Arkansas: Gulf Coast Association of Geological Societies Special Publication, 3-D Seismic Case Histories from the Gulf Coast Basin, p. 131-138.

Tiab, D., and E. C. Donaldson, 2004, Petrophysics: theory and practice of measuring reservoir rock and fluid transport properties, 2nd Ed: Burlington, MA, Gulf Professional Publishing, 880 p.

Troell, A., and D. J. Robison, 1987, Regional stratigraphy of the Smackover limestone (Jurassic) in South Arkansas and North Louisiana, and the geology of Chalybeat Springs oil field: Gulf Coast Association of Geological Societies Transactions, v. 37, p. 255-262.

Supplemental Sources Consulted

Ahr, W. M., and B. S. Hammel, 1999, Identification and mapping of flow units in carbonate reservoirs from the Happy Sprayberry (Permian) field Garza County, Texas USA: Energy Exploration and Exploitation, v. 17, p. 311-334.

Hopkins, T. L., 2002, Integrated petrophysical study of the Smackover Formation, Womack Hill field, Clarke and Choctaw Counties, Alabama: M.S. thesis, Texas A&M University, College Station, Texas, 156 p.

Layman, J. M., 2002, Porosity characterization utilizing petrographic image analysis: Implications for identifying and ranking reservoir flow units, Happy Spraberry field, Garza County, Texas: M.S: thesis, Texas A&M University, College Station, Texas, 114 p.

McCreesh, C. A., R. Ehrlich, and S. L. Crabtree, 1991, Petrography and reservoir physics II: relating thin section porosity to capillary pressure, the association between pore types and pore size: American Association of Petroleum Geologists Bulletin, v. 75, p. 1563-1578.

APPENDIX A

SAMPLE LOCATIONS AND PORE TYPES, PORE AND PORE-THROAT SIZE

CATEGORIZATION DATA

Table A.1
Pore Type and Sample Location by Facies
Grainstone/Packstone 1

Pore Type	Well and Depth of Sample Location
Depo	Alexander 1 (8048.5.5ft)
	Reeves 1 (8072ft)
	Reeves 1 (8077ft)
	Reeves 1 (8080ft)
	Strong 1 (8218.6ft)
H1-10r	Reeves 1 (8084ft)
	Reeves 1 (8085ft)
	Reeves 1 (8091ft)
	Reeves 1 (8098ft)
H1-30e	Alexander 1 (8054ft)
	Kemmerer 3 (8159ft)
	Kitchens 1 (8088ft)
	Kitty Jean 1 (8123.5ft)
	Reeves 1 (8049ft)
	Reeves 1 (8054ft)
	Reeves 1 (8061ft)
	Reeves 1 (8130ft)
H1-30r	Alexander 1 (8020ft)
	Alexander 1 (8022ft)
	Alexander 1 (8024ft)
	Alexander 1 (80285ft)
	Alexander 1 (80305ft)
	Alexander 1 (8038ft)
	Alexander 1 (8056.5ft)
	Alexander 1 (8057ft)
	Genestet Farms 1 (8213ft)
	Kemmerer 2 (8127.5ft)
	Kemmerer 3 (8167ft)
	Nina Grayson Warnock 1 (8135, 8145ft)
	Strong 1 (8205.2ft)
	Reeves 1 (8044ft)

Table A.1 Continued,

Pore Type	Well and Depth of Sample Location
H1-60e	Alice Sydney Crone 1 (8305.5ft) Genestet Farms 1 (8220.5ft) Kemmerer 2 (8070.6ft) Kemmerer 2 (8146.5ft) Reeves 1 (8139ft)
H1-60r	Alice Sydney Crone 1 (8299ft) Genestet Farms 1 (8209ft) Kitchens 1 (8181ft)
H1-90e	Lizzy Grayson 2 (8167ft)
H1-90r	Alexander 1 (8055.5ft) Alice Sydney Crone 1 (8313.5ft) Reeves 1 (8044ft)

Grainstone/Packstone 2

Pore Type	Well and Depth of Sample Location
Depo	Nina Grayson Warnock 1 (8152.5ft)
H1-10e	Kitchens 1 (8195ft) Kitty Jean 1 (8087ft) Lizzy Grayson 2 (8190ft) Nina Grayson Warnock 1 (8141, 8155.5ft)
H1-30e	Kemmerer 3 (8143ft) Kitty Jean 1 (8140.5ft) Kitchens 1 (8184, 8189ft) Reeves 1 (8135ft) Reeves 1 (8136ft)
H1-30r	Kemmerer 2 (8166.8ft) Kemmerer 3 (8155ft)
H1-60r	Kemmerer 2 (8167.5, 8172.1ft)

Packstone/Wackestone

Pore Type	Well and Depth of Sample Location
H1-30e	Kemmerer 3 (8124ft)
H1-30r	Lizzy Grayson 2 (8174ft)
Diag	Kitty Jean 1 (8135.5ft)

Table A.1 Continued,
Wackestone/Mudstone

Pore Type	Well and Depth of Sample Location
H1-60r	Kitchens 1 (8081ft)
Diag	Westbrook 1 (8114ft)

Dolostone

Pore Type	Well and Depth of Sample Location
Diag	Kemmerer 3 (8193ft)

Table A.2
Pore-Throat Sizes and Sample Location by Pore Type
Depositional Pores

Pore-Throat Size (µm)	Well and Depth of Sample Location
6.931	Strong 1 (8218.6ft)
9.3	Nina Grayson Warnock 1 (8152.5ft)

H1-10e

Pore-Throat Size (µm)	Well and Depth of Sample Location
1.9	Nina Grayson Warnock 1 (8141ft)
5.424	Lizzy Grayson 2 (8190ft)
12.92	Nina Grayson Warnock 1 (8155.5ft)
28.77	Kitchens 1 (8195ft)

H1-30e

Pore-Throat Size (µm)	Well and Depth of Sample Location
1.83	Kemmerer 3 (8124ft)
5.566	Kitchens 1 (8189ft)

H1-30r

Pore-Throat Size (µm)	Well and Depth of Sample Location
0.1286	Lizzy Grayson 2 (8174ft)
0.6683	Nina Grayson Warnock 1 (8135ft)
1.22	Strong 1 (8205.2ft)
1.525	Genestet Farms 1 (8213ft)

Table A.2 Continued,

H1-60r

Pore-Throat Size (μm)	Well and Depth of Sample Location
0.1633	Genestet Farms 1 (8209ft)
0.3097	Kitchens 1 (8181ft)

H1-90e

Pore-Throat Size (μm)	Well and Depth of Sample Location
1.948	Lizzy Grayson 2 (8167ft)

Diagenetic

Pore-Throat Size (μm)	Well and Depth of Sample Location
0.0402	Westbrook 1 (8114ft)
0.4006	Kemmerer 3 (8193ft)

Table A.3
Pore-Throat Area (μm^2) Categories
(Ranges are based on median pore aperture data from mercury-injection capillary pressure analysis)

1	2	3	4	5
$<1 \ \mu m^2$	1 to 20 μm^2	20 to 100 μm^2	100 to 200 μm^2	$>200 \ \mu m^2$

Pore-Throat Area Categories by Facies and Pore Type

	Grainstone/ Packstone 1	Grainstone/ Packstone 2	Packstone/ Wackestone	Wackestone/ Mudstone	Dolostone
Depo	3	3			
H1-10e		2 – 5			
H1-30e		3	2		
H1-30r	2		1		
H1-60r	1				
H1-90e	2				
Diag				1	1

Table A.4
Well Locations and Pore-Throat Area Categories by Facies and Pore Type

Grainstone/Packstone 1:

Pore Type	Pore-Throat Area μm^2	Well Location	PTA Category
Depo	37.73	Strong 1 (8218.6ft)	3
H1-30r	1.83	Genestet Farms 1 (8213ft)	2
	0.351	Nina Grayson Warnock 1 (8135ft)	1
	1.17	Strong 1 (8205.2ft)	2
H1-60r	0.021	Genestet Farms 1 (8209ft)	1
	0.075	Kitchens 1 (8181ft)	1
H1-90e	2.98	Lizzy Grayson 2 (8167ft)	2

Grainstone/Packstone 2:

Pore Type	Pore-Throat Area μm^2	Well Location	PTA Category
Depo	67.93	Nina Grayson Warnock 1 (8152.5ft)	3
H1-10e	650.08	Kitchens 1 (8195ft)	5
	23.11	Lizzy Grayson 2 (8190ft)	3
	2.84	Nina Grayson Warnock 1 (8141ft)	2
	131.10	Nina Grayson Warnock 1 (8155.5ft)	4
H1-30e	24.33	Kitchens 1 (8189ft)	3

Packstone/Wackestone:

Pore Type	Pore-Throat Area μm^2	Well Location	PTA Category
H1-30e	2.63	Kemmerer 3 (8124ft)	2
H1-30r	0.013	Lizzy Grayson 2 (8174ft)	1

Wackestone/Mudstone:

Pore Type	Pore-Throat Area μm^2	Well Location	PTA Category
Diag	0.0013	Westbrook 1 (8114ft)	1

Dolostone:

Pore Type	Pore-Throat Area μm^2	Well Location	PTA Category
Diag	0.126	Kemmerer 3 (8193ft)	1

Table A.5
Pore Size (Area mm^2) Categories
(Ranges are based on median pore area data from petrographic image analysis)

1	2	3	4	5
< 5x 10^{-5}	5x 10^{-5} to 7x 10^{-5}	7x 10^{-5} to 9x 10^{-5}	9x 10^{-5} to 1x 10^{-4}	> 1x 10^{-4}

Pore Size (Area mm^2) Categories by Facies and Pore Type

	Grainstone/ Packstone 1	Grainstone/ Packstone 2	Packstone/ Wackestone	Wackestone/ Mudstone	Dolostone
Depo	5	5			
H1-10e		1 to 5			
H1-30e	1	1 to 2	1		
H1-30r	1 to 4	1 to 2	1		
H1-60e	1				
H1-60r	1				
H1-90e	1				
H1-90r	1				
Diag			1		1

Table A.6
Well Locations and Pore Size (Area mm^2) Categories by Facies and Pore Type
Grainstone/Packstone 1:

Pore Type	Pore Size (area mm^2)	Well Location	PS Category
Depo	1.33x 10^{-4}	Strong 1 (8218.6ft)	5
H1-30e	4.99x 10^{-5}	Kitchens 1 (8088ft)	1
	3.33x 10^{-5}	Kitty Jean 1 (8123.5ft)	1
H1-30r	4.99x 10^{-5}	Genestet Farms 1 (8213ft)	1
	4.99x 10^{-5}	Kemmerer 2 (8127.5ft)	1
	4.16x 10^{-5}	Kemmerer 3 (8167)	1
	9.99x 10^{-5}	Nina Grayson Warnock 1 (8135ft)	4
	3.35x 10^{-5}	Nina Grayson Warnock 1 (8145ft)	1
	4.99x 10^{-5}	Strong 1 (8205.2ft)	1
H1-60e	3.35x 10^{-5}	Alice Sydney Crone 1 (8305.5ft)	1
	3.41x 10^{-5}	Genestet Farms 1 (8220.5ft)	1
	4.99x 10^{-5}	Kemmerer 2 (8070.6ft)	1
	4.99x 10^{-5}	Kemmerer 2 (8146.5ft)	1
H1-60r	1.67x 10^{-5}	Alice Sydney Crone 1 (8299ft)	1
	3.33x 10^{-5}	Genestet Farms 1 (8209ft)	1
	3.33x 10^{-5}	Kitchens 1 (8181ft)	1
H1-90e	4.99x 10^{-5}	Lizzy Grayson 2 (8167ft)	1

Table A.6 Continued,
Grainstone/Packstone 2:

Pore Type	Pore Size (area mm^2)	Well Location	PS Category
Depo	1.50x 10^{-4}	Nina Grayson Warnock 1 (8152.5ft)	5
H1-10e	3.35x 10^{-5}	Kitchens 1 (8195ft)	1
	2.18x 10^{-4}	Kitty Jean 1 (8087ft)	5
	1.01x 10^{-4}	Nina Grayson Warnock 1 (8141ft)	5
	6.66x 10^{-5}	Nina Grayson Warnock 1 (8155.5ft)	2
H1-30e	4.99x 10^{-5}	Kemmerer 3 (8143ft)	1
	3.35x 10^{-5}	Kitchens 1 (8184ft)	1
	6.66x 10^{-5}	Kitchens 1 (8189ft)	2
	5.03x 10^{-5}	Kitty Jean 1 (8140.5ft)	2
H1-30r	5.03x 10^{-5}	Kemmerer 2 (8166.8ft)	2
	1.66x 10^{-5}	Kemmerer 3 (8155ft)	1
H1-60r	3.33x 10^{-5}	Kemmerer 2 (8167.5ft)	1
	4.99x 10^{-5}	Kemmerer 2 (8172.1ft)	1

Packstone/Wackestone:

Pore Type	Pore Size (area mm^2)	Well Location	PS Category
H1-30e	4.99x 10^{-5}	Kemmerer 3 (8124ft)	1
H1-30r	3.41x 10^{-5}	Lizzy Grayson 2 (8174ft)	1
Diag	1.67x 10^{-5}	Kitty Jean (8135.5ft)	1

Dolostone:

Pore Type	Pore Size (area mm^2)	Well Location	PS Category
Diag	3.33x 10^{-5}	Kemmerer 3 (8193ft)	1

Table A.7
Pore Size (diameter, µm) Categories
(Ranges are based on median pore area data from petrographic image analysis)

1	2	3	4	5
<8	8 to 9.5	9.5 to 10.5	10.5 to 11.5	>11.5

Pore Size (Diameter, µm) Categories by Facies and Pore Type

	Grainstone/ Packstone 1	Grainstone/ Packstone 2	Packstone/ Wackestone	Wackestone/ Mudstone	Dolostone
Depo	5	5			
H1-10e		1 to 5			
H1-30e	1	1 to 2	1		
H1-30r	1	1	1		
H1-60e	1				
H1-60r	1	1			
H1-90e	1				
H1-90r	1				
Diag			1		1

Table A.8
Well Locations and Pore Size (diameter, µm) Categories by Facies and Pore Type
Grainstone/Packstone 1:

Pore Type	Pore Size (diameter, µm)	Well Location	PS Category
Depo	13.03	Strong 1 (8218.6ft)	5
H1-30e	7.97	Kitchens 1 (8088ft)	1
	6.51	Kitty Jean 1 (8123.5ft)	1
H1-30r	7.97	Genestet Farms 1 (8213ft)	1
	7.97	Kemmerer 2 (8127.5ft)	1
	7.28	Kemmerer 3 (8167)	1
	11.28	Nina Grayson Warnock 1 (8135ft)	5
	6.53	Nina Grayson Warnock 1 (8145ft)	1
	7.97	Strong 1 (8205.2ft)	1
H1-60e	6.53	Alice Sydney Crone 1 (8305.5ft)	1
	6.59	Genestet Farms 1 (8220.5ft)	1
	7.97	Kemmerer 2 (8070.6ft)	1
	7.97	Kemmerer 2 (8146.5ft)	1
H1-60r	4.61	Alice Sydney Crone 1 (8299ft)	1
	6.51	Genestet Farms 1 (8209ft)	1
	6.51	Kitchens 1 (8181ft)	1
H1-90e	7.97	Lizzy Grayson 2 (8167ft)	1

Table A.8 Continued,

Grainstone/Packstone 2:

Pore Type	Pore Size (diameter, μm)	Well Location	PS Category
Depo	13.82	Nina Grayson Warnock 1 (8152.5ft)	5
H1-10e	6.53	Kitchens 1 (8195ft)	1
	16.67	Kitty Jean 1 (8087ft)	5
	11.32	Nina Grayson Warnock 1 (8141ft)	5
	9.21	Nina Grayson Warnock 1 (8155.5ft)	2
H1-30e	7.97	Kemmerer 3 (8143ft)	1
	6.53	Kitchens 1 (8184ft)	1
	9.21	Kitchens 1 (8189ft)	2
	8.00	Kitty Jean 1 (8140.5ft)	2
H1-30r	8.00	Kemmerer 2 (8166.8ft)	2
	4.6	Kemmerer 3 (8155ft)	1
H1-60r	6.51	Kemmerer 2 (8167.5ft)	1
	7.97	Kemmerer 2 (8172.1ft)	1

Packstone/Wackestone:

Pore Type	Pore Size (diameter, μm)	Well Location	PS Category
H1-30e	7.97	Kemmerer 3 (8124ft)	1
H1-30r	6.59	Lizzy Grayson 2 (8174ft)	1
Diag	4.61	Kitty Jean (8135.5ft)	1

Dolostone:

Pore Type	Pore Size (diameter, μm)	Well Location	PS Category
Diag	6.51	Kemmerer 3 (8193ft)	1

APPENDIX B

POROSITY FACTORS AND CAUSES OF POROSITY ENHANCEMENT

/REDUCTION, PORE/PORE-THROAT GEOMETRY DATA, AND CAPILLARY

PROPERTY DATA

Table B.1
Legend I

Well Name	Abbreviation
Alice Sydney Crone #1	ASC
Genestet Farms #1	GF
Kemmerer #2	Kem2
Kemmerer #3	Kem3
Kitchens #1	Kit
Kitty Jean #1	KJ
Lizzy Grayson #2	LG
Nina Grayson Warnock #1	NGW
Strong #1	Str
Westbrook #1	WB

Legend II

Facies	Abbreviation
Oolitic Grainstone	G/P 1
Oncolitic Grainstone	G/P 2
Packstone/Wackestone	P/W
Wackestone/Mudstone	W/M

Legend III

Numbers	Abbreviation
Depth of sample in feet; e.g. 8100ft	8100

Table B.2
Pore Type- Categorized by Porosity Factors and Facies

Pore Type- Porosity Factors	Causes (in order of abundance)	Facies		Pore Type	Pore Type Occurrence
Enhanced (e)	A. Dissolution of solid rock, pore filling and rim cements, and replacement mineral grains	Grain Supported	G/P 1	H1-30e	3
				H1-60e	4
				H1-90e	1
			G/P 2	H1-10e	5
				H1-30e	4
			P/W	H1-30e	1
				Diag	1
	B. Dolomite grain replacement	Dolostone		Diag	1
Reduced (r)	A. Grain coating and pore filling cements	Grain Supported	G/P 1	H1-90r	1
			G/P 2	H1-30r	1
			P/W	H1-30r	1
	B. Replacement of solid rock and pore filling by anhydrite and dolomite	Grain Supported	G/P 1	H1-30r	4
				H1-60r	2
			G/P 2	H1-30r	1
				H1-60r	2
		Mud Supported	W/M	H1-60r	1
				Diag	1
	C. Mechanical and pressure-solution compaction of grains	Grain Supported	G/P 1	H1-30r	2
				H1-60r	1

Table B.3
Major Cause of Porosity Enhancement or Reduction by Sample

Sample	Pore Type	Facies	Porosity Factor (from chart above)
LG8190	H1-10e	G/P 2	Enhanced A
Kit8195	H1-10e	G/P 2	Enhanced A
KJ8087	H1-10e	G/P 2	Enhanced A
NGW8141	H1-10e	G/P 2	Enhanced A
NGW81555	H1-10e	G/P 2	Enhanced A
Kem38143	H1-30e	G/P 2	Enhanced A
Kit8184	H1-30e	G/P 2	Enhanced A
Kit8189	H1-30e	G/P 2	Enhanced A
KJ81405	H1-30e	G/P 2	Enhanced A
Kem38159	H1-30e	G/P 1	Enhanced A
KJ81236	H1-30e	G/P 1	Enhanced A
Kit8088	H1-30e	G/P 1	Enhanced A
ASC83055	H1-60e	G/P 1	Enhanced A
GF82205	H1-60e	G/P 1	Enhanced A
Kem280706	H1-60e	G/P 1	Enhanced A
Kem281465	H1-60e	G/P 1	Enhanced A

Table B.3 Continued,

Sample	Pore Type	Facies	Porosity Factor (from chart above)
ASC8135	H1-90e	G/P 1	Enhanced A
Kem38124	H1-30e	P/W	Enhanced A
KJ81355	Diag	P/W	Enhanced A
Kem38155	H1-30r	G/P 2	Reduced A
Kem281668	H1-30r	G/P 2	Reduced B
Kem281675	H1-60r	G/P 2	Reduced B
Kem381721	H1-60r	G/P 2	Reduced B
GF8213	H1-30r	G/P 1	Reduced C
Kem281675	H1-30r	G/P 1	Reduced B
Kem38167	H1-30r	G/P 1	Reduced B
NGW8135	H1-30r	G/P 1	Reduced B
NGW8145	H1-30r	G/P 1	Reduced B
Str82052	H1-30r	G/P 1	Reduced C
ASC8299	H1-60r	G/P 1	Reduced C
GF8209	H1-60r	G/P 1	Reduced B
Kit8181	H1-60r	G/P 1	Reduced B
LG8167	H1-90r	G/P 1	Reduced A
LG8174	H1-30r	P/W	Reduced A
Kit8081	H1-60r	W/M	Reduced B
WB8114	Diag	P/W	Reduced B

Table B.4
Pore and Pore-Throat Geometry Data

Sample	Facies	Pore Type	Median Pore Area mm^2	Median Pore-Throat Aperture um	Permeability to Air md	√(k) um
ASC8299	G/P 1	H1-60r	1.67E-05	--	--	--
ASC83055	G/P 1	H1-60e	3.35E-05	--	--	--
ASC83135	G/P 1	H1-90r	1.70E-05	--	--	--
GF8209	G/P 1	H1-60r	3.33E-05	0.1633	0.0213	0.0046
GF8213	G/P 1	H1-30r	4.99E-05	1.525	1.7	0.0412
GF82205	G/P 1	H1-60e	3.41E-05	--	--	--
Kem280706	G/P 1	H1-60e	4.99E-05	--	--	--
Kem281275	G/P 1	H1-30r	4.99E-05	--	--	--
Kem281465	G/P 1	H1-60e	4.99E-05	--	--	--
Kem281668	G/P 2	H1-30r	5.03E-05	--	--	--
Kem281675	G/P 2	H1-60r	3.33E-05	--	--	--
Kem281721	G/P 2	H1-60r	4.99E-05	--	--	--
Kem38124	P/W	H1-30e	4.99E-05	1.83	3.07	0.0554
Kem38143	G/P 2	H1-30e	4.99E-05	--	--	--
Kem38155	G/P 2	H1-30r	1.66E-05	--	--	--
Kem38159	G/P 1	H1-30e	--	--	--	--
Kem38167	G/P 1	H1-30r	4.16E-05	--	--	--
Kem38193	Dolostone	Diag	3.33E-05	0.4006	0.159	0.0126
Kit8081	W/M	H1-60r	--	--	--	--
Kit8088	G/P 1	H1-30e	4.99E-05	--	--	--
Kit8181	G/P 1	H1-60r	3.33E-05	0.3097	0.114	0.0107
Kit8184	G/P 2	H1-30e	3.35E-05	--	--	--
Kit8189	G/P 2	H1-30e	6.66E-05	5.566	31.6	0.1778
Kit8195	G/P 2	H1-10e	3.35E-05	28.77	638	0.7987
KJ8087	G/P 2	H1-10e	2.18E-04	--	--	--
KJ81235	G/P 1	H1-30e	3.33E-05	--	--	--
KJ81355	P/W	Diag	1.67E-05	--	--	--
KJ81405	G/P 2	H1-30e	5.03E-05	--	--	--
LG8167	G/P 1	H1-90e	4.99E-05	1.948	4.98	0.0706
LG8174	P/W	H1-30r	3.41E-05	0.1286	0.0094	0.0031
LG8190	G/P 2	H1-10e	--	5.424	15.4	0.1241
NGW8135	G/P 1	H1-30r	9.99E-05	0.6683	0.56	0.0237
NGW8141	G/P 2	H1-10e	1.01E-04	1.9	6.09	0.0780
NGW8145	G/P 1	H1-30r	3.35E-05	--	--	--
NGW81525	G/P 2	Depo	1.50E-04	9.3	61.6	0.2482
NGW81555	G/P 2	H1-10e	6.66E-05	12.92	90.6	0.3010
Str82052	G/P 1	H1-30r	4.99E-05	1.22	3.63	0.0602
Str82186	G/P 1	Depo	1.33E-04	6.931	43	0.2074
WB8114	W/M	Diag	--	0.0402	0.00015	0.0004

Table B.5
Porosity Data

Sample	Facies	Pore Type	Core Analysis Porosity %	PIA Porosity %	Capillary Pressure Derived Porosity %	Core Plug Porosity %
ASC8299	G/P 1	H1-60r	--	2	--	--
ASC83055	G/P 1	H1-60e	--	3.1	--	19.08
ASC83135	G/P 1	H1-90r	--	0.6	--	13.21
GF8209	G/P 1	H1-60r	5.40	0.5	5.94	--
GF8213	G/P 1	H1-30r	5.10	1.7	9.29	--
GF82205	G/P 1	H1-60e	5.70	1.2	--	22.65
Kem280706	G/P 1	H1-60e	25.50	4.8	--	--
Kem281275	G/P 1	H1-30r	16.90	5	--	--
Kem281465	G/P 1	H1-60e	11.70	1.5	--	--
Kem281668	G/P 2	H1-30r	7.30	0.7	--	--
Kem281675	G/P 2	H1-60r	5.70	0.3	--	--
Kem281721	G/P 2	H1-60r	6.40	0.9	--	--
Kem38124	P/W	H1-30e	11.00	1.1	11.7	--
Kem38143	G/P 2	H1-30e	11.10	2.7	--	11.01
Kem38155	G/P 2	H1-30r	3.00	0.2	--	3.61
Kem38159	G/P 1	H1-30e	9.70		--	9.06
Kem38167	G/P 1	H1-30r	1.70	0.1	--	4.08
Kem38193	Dolostone	Diag	10.50	0	8.61	--
Kit8081	W/M	H1-60r	0.70	0	--	2.66
Kit8088	G/P 1	H1-30e	21.40	4.9	--	--
Kit8181	G/P 1	H1-60r	9.10	0.7	7.87	--
Kit8184	G/P 2	H1-30e	12.80	2.8	--	17.28
Kit8189	G/P 2	H1-30e	11.50	4.51	10.5	--
Kit8195	G/P 2	H1-10e	15.40	10.1	14.2	--
KJ8087	G/P 2	H1-10e	22.70	5.4	--	24.33
KJ81235	G/P 1	H1-30e	12.30	0.4	--	12.99
KJ81355	P/W	Diag	2.70	0	--	--
KJ81405	G/P 2	H1-30e	14.70	2.5	--	12.91
LG8167	G/P 1	H1-90e	10.50	2.6	12.2	--
LG8174	P/W	H1-30r	4.60	0	5.16	--
LG8190	G/P 2	H1-10e	12.70	--	10.6	--
NGW8135	G/P 1	H1-30r	9.30	0.6	12.1	--
NGW8141	G/P 2	H1-10e	12.10	1.53	10.6	--
NGW8145	G/P 1	H1-30r	9.00	0.2	--	--
NGW81525	G/P 2	Depo	9.70	2.7	14.7	--
NGW81555	G/P 2	H1-10e	7.10	4.3	11.3	--
Str82052	G/P 1	H1-30r	10.90	2.6	12.3	--
Str82186	G/P 1	Depo	15.60	5.2	15.4	--
WB8114	W/M	Diag	0.70	0	1.2	--

Table B.6
Lorenz Coefficients

Sample	Facies	Pore Type	Lorenz Coefficient
NGW81525	G/P 2	Depo	0.3472
Str82186	G/P 1	Depo	0.3638
Kem38193	Dolostone	Diag	0.4054
WB8114	W/M	Diag	0.3714
Kit8195	G/P 2	H1-10e	0.1388
LG8190	G/P 2	H1-10e	0.3662
NGW8141	G/P 2	H1-10e	0.3783
NGW81555	G/P 2	H1-10e	0.3041
Kem38124	P/W	H1-30e	0.3942
Kit8189	G/P 2	H1-30e	0.3425
NGW8135	G/P 2	H1-30e	0.4046
GF8213	G/P 1	H1-30r	0.3943
LG8174	P/W	H1-30r	0.3994
Str82052	G/P 1	H1-30r	0.3938
GF8209	G/P 1	H1-60r	0.3998
Kit8181	G/P 1	H1-60r	0.4059
LG8167	G/P 1	H1-90e	0.3812

Table B.7
Pore Area vs. Pore-Throat Area Coefficients of Determination

Sample	Facies	Pore Type	R^2
NGW81525	G/P 2	Depo	0.7374
Str82186	G/P 1	Depo	0.8422
Kem38193	Dolostone	Diag	0.6837
Kit8195	G/P 2	H1-10e	0.8269
NGW8141	G/P 2	H1-10e	0.8519
NGW81555	G/P 2	H1-10e	0.9494
Kem38124	P/W	H1-30e	0.9803
Kit8189	G/P 2	H1-30e	0.9391
NGW8135	G/P 2	H1-30r	0.8139
GF8213	G/P 1	H1-30r	0.6496
LG8174	P/W	H1-30r	0.9597
Str82052	G/P 1	H1-30r	0.8862
GF8209	G/P 1	H1-60r	0.7566
Kit8181	G/P 1	H1-60r	0.9856
LG8167	G/P 1	H1-90e	0.9779

APPENDIX C

THIN SECTION PHOTOMICROGRAPHS
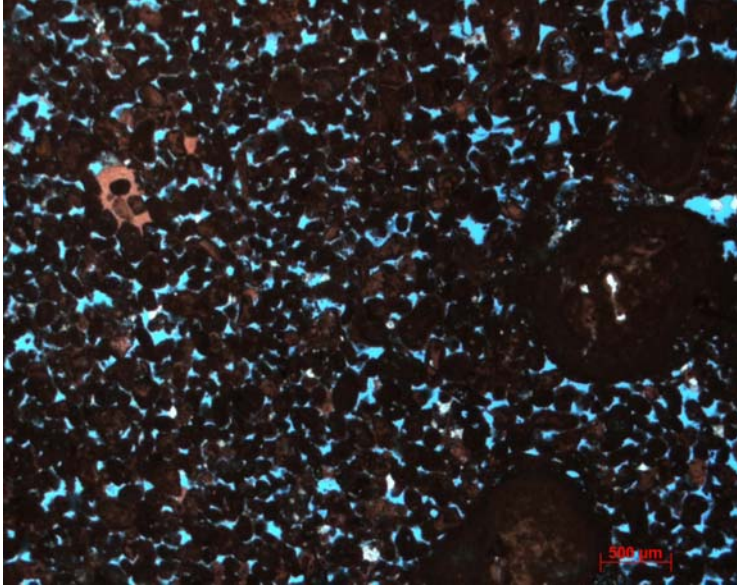
Figure C.1: Sample- Nina Grayson Warnock 1 (8152ft), classified as depositional porosity (scale bar is 500 μm).
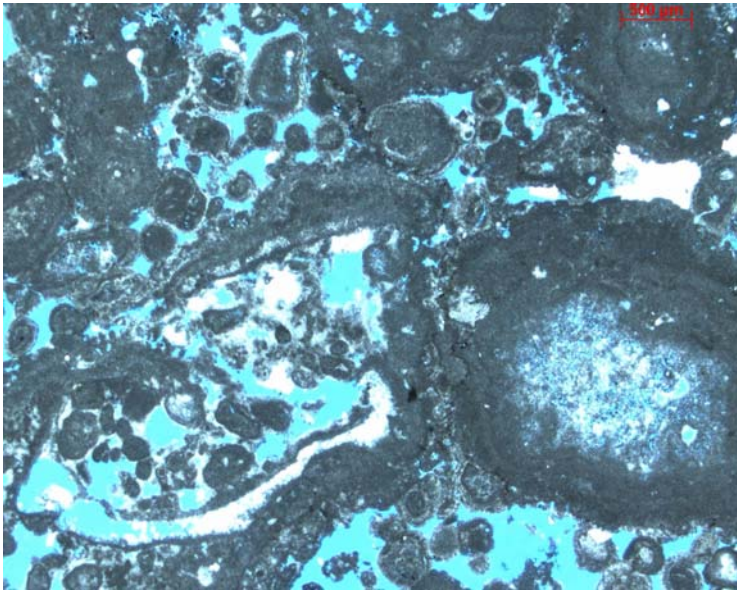
Figure C.2: Sample- Kitchens 1 (8195ft), classified as H1-10e (scale bar is 500 μm).
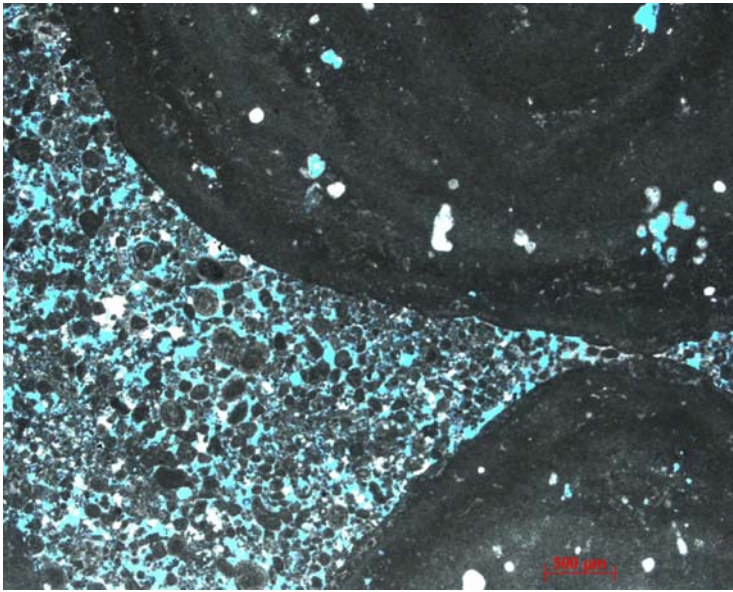
Figure C.3a: Kitchens 1 (8189), classified as H1-30e (scale bar is 500 μm).
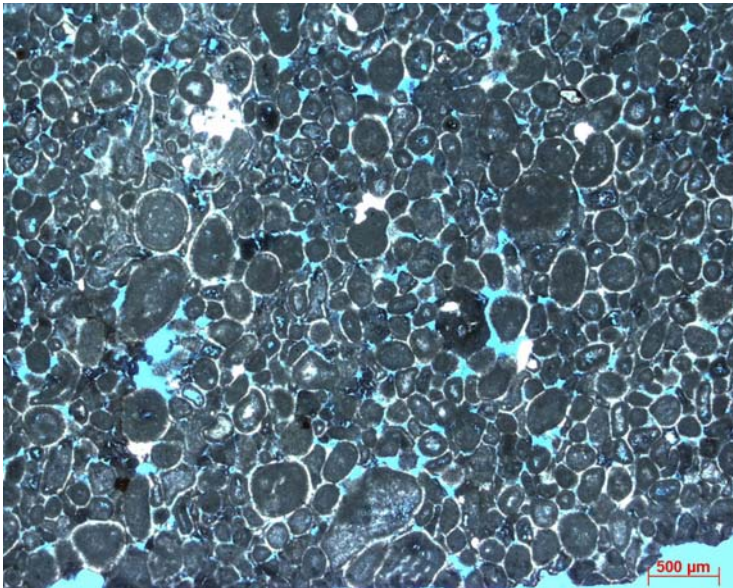
Figure C.3b: Strong 1 (8205.2ft), classified as H1-30r (scale bar is 500 μm).
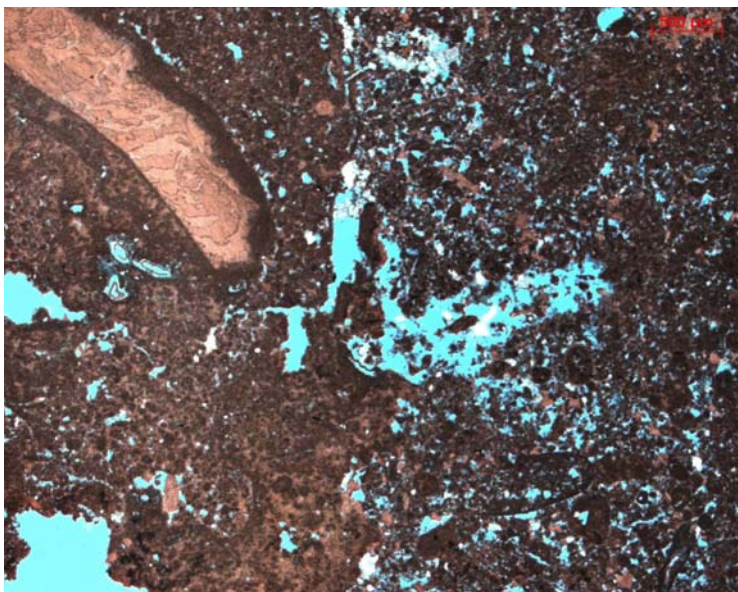
Figure C.4a: Alice Sydney Crone 1 (8305.5ft), classified as H1-60e (scale bar is 500 μm).
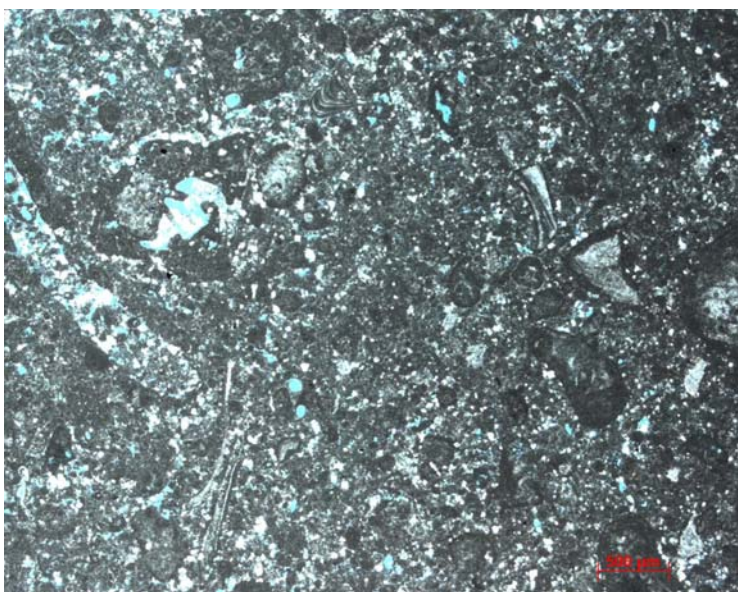
Figure C.4b: Kitchens 1 (8181ft), classified as H1-60r (scale bar is 500 μm).
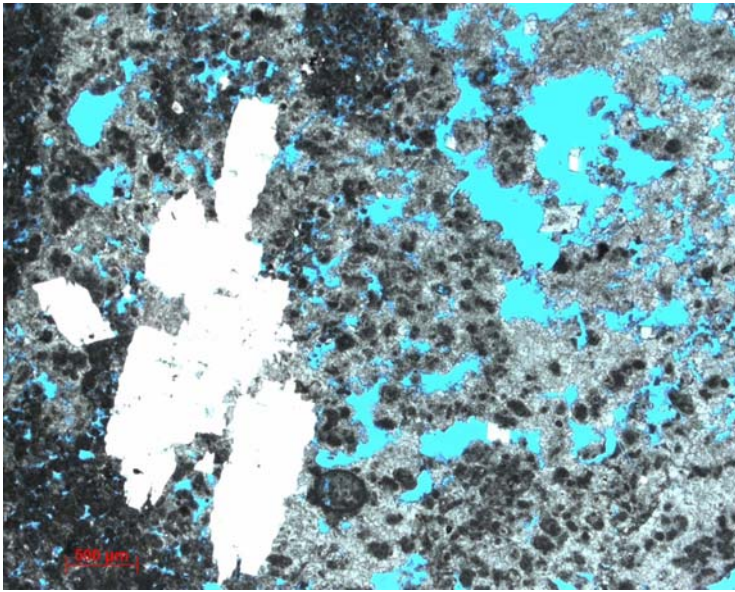
Figure C.5: Lizzy Grayson 2 (8167ft), classified as H1-90e (scale bar is 500 μm).
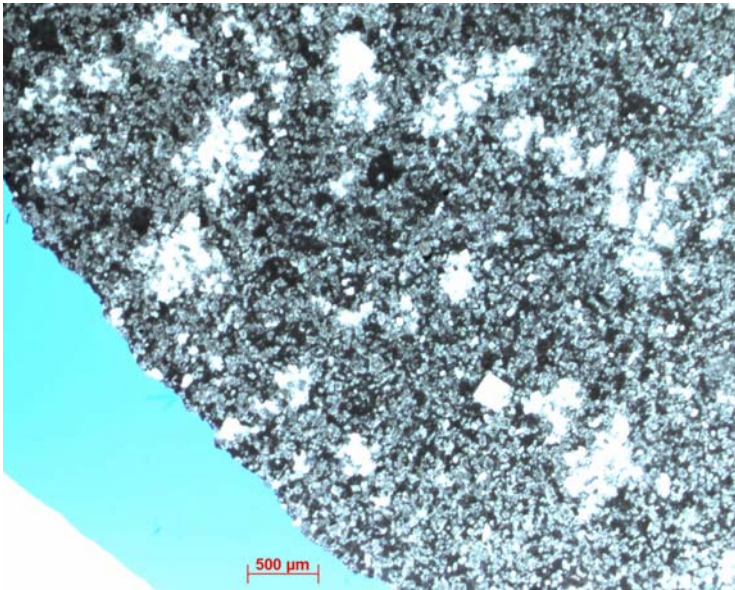
Figure C.6: Westbrook (8114ft), classified as diagenetic porosity (scale bar is 500 μm).

APPENDIX D

CROSS SECTIONS

Cross Section Legend

Sample Legend

Facies Color Codes for Cross Sections

Oolitic Grainstone

Oncolitic Grainstone

Packstone/Wackestone

Wackestone/Mudstone

Microbial Boundstone

Dolostone

Anhydrite

Sample Codes for Cross Sections

☆ Samples used for Petro-graphic Image Analysis

◯ Remaining samples not used for Petro-graphic Image Analysis

Depositional

H1-10e

H1-10r

H1-30e

H1-30r

H1-60e

H1-60r

H1-90e

H1-90r

Diagenetic
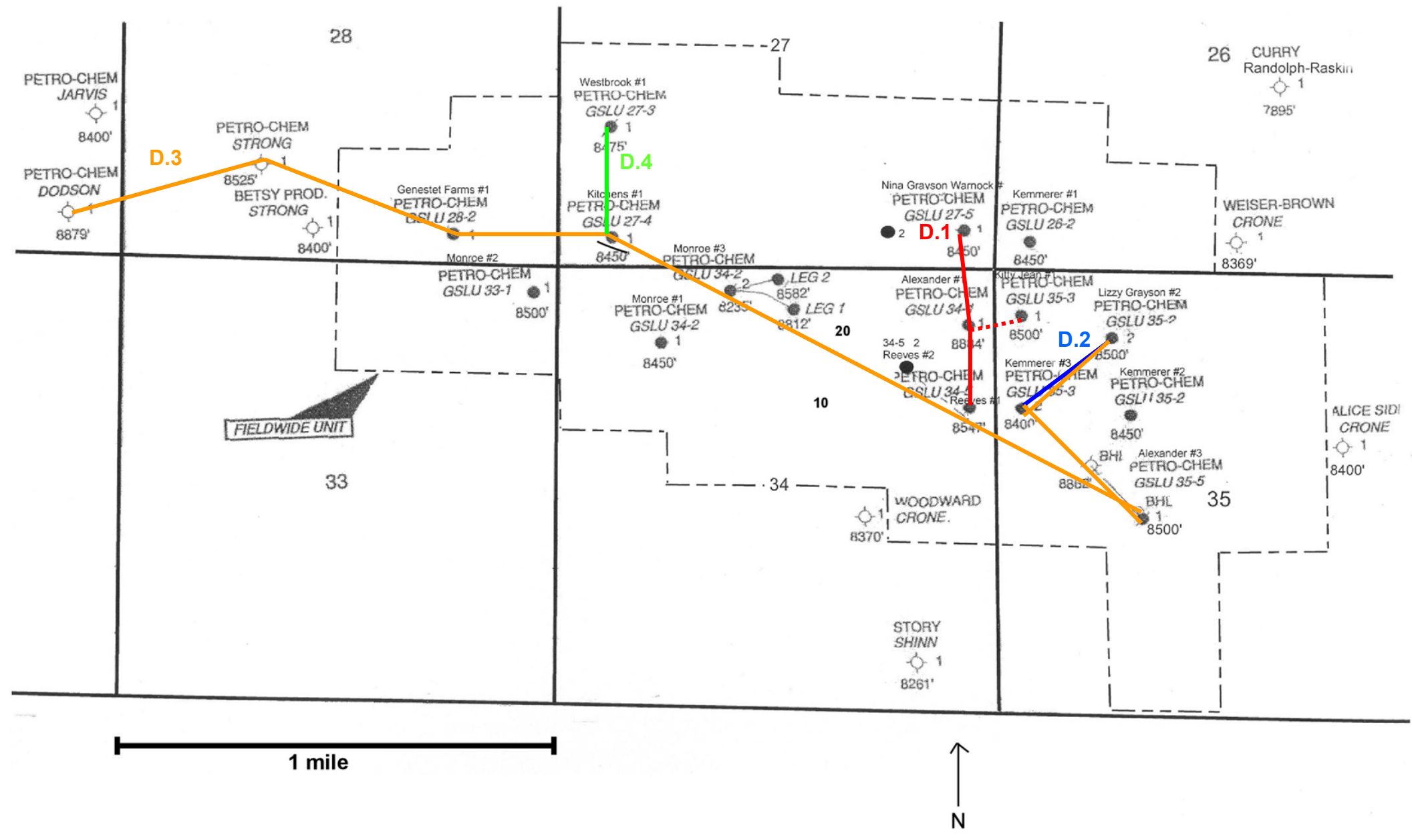
Base Map with Cross Sections and Well Locations Legend

Figure D.1: North-South stratigraphic cross section showing facies distributions (based on Poole, 2006) and sample depths with pore type classification. The cross section is flattened on Top Smackover. See legend for facies color codes and sample color codes. Depths (ft) are marked.

Figure D.2: Southwest to Northeast stratigraphic cross section showing facies distributions (based on Poole, 2006) and sample depths with pore type classification. The cross section is flattened on Top Smackover. See legend for facies color codes and sample color codes. Depths (ft) are marked.

Figure D.3: West to East stratigraphic cross section showing facies distributions (based on Poole, 2006) and sample depths with pore type classification. The cross section is flattened on Top Smackover. See legend for facies color codes and sample color codes. Depths (ft) are marked.
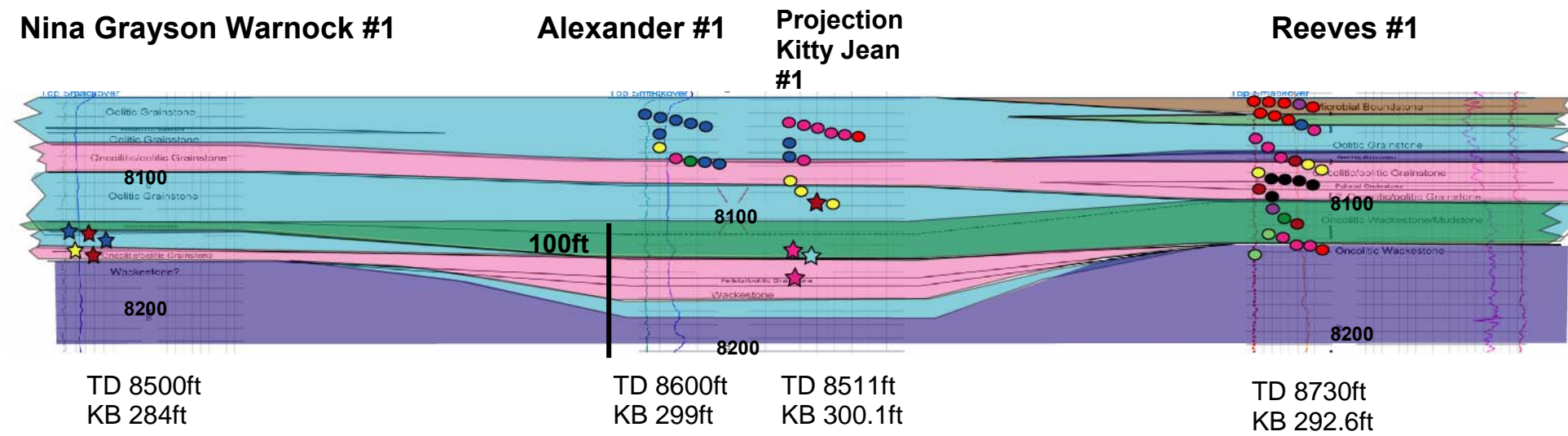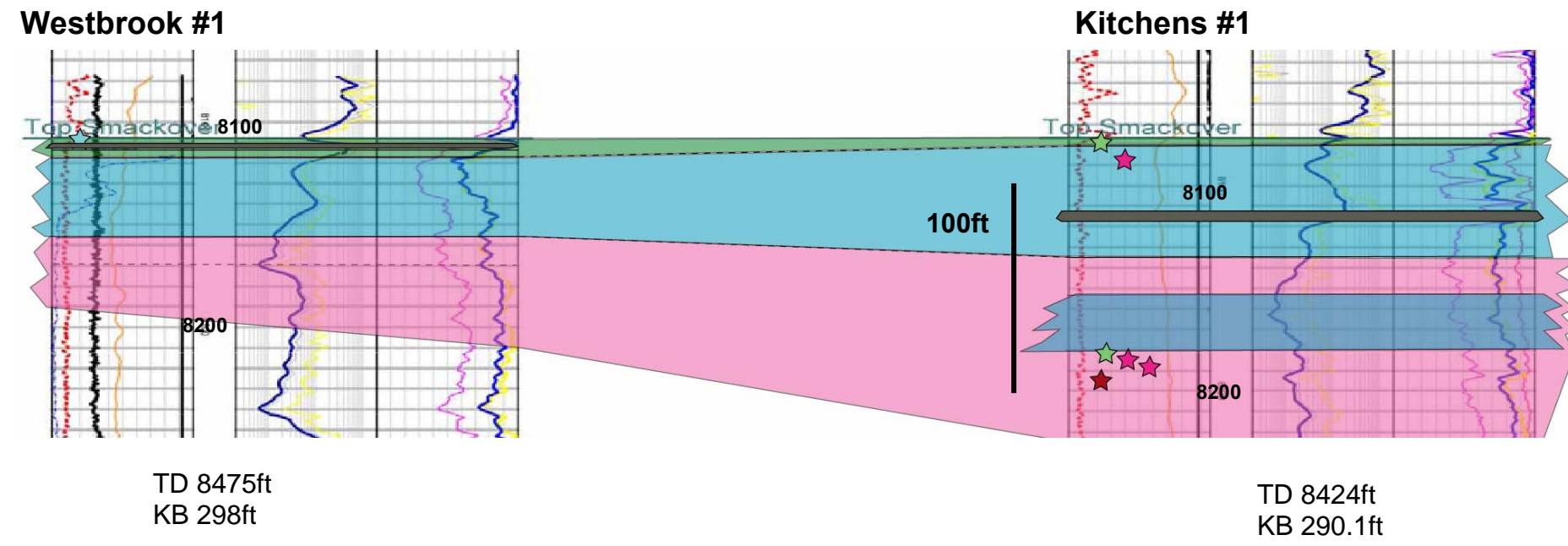
Figure D.4: North to South stratigraphic cross section showing facies distributions (based on Poole, 2006) and sample depths with pore type classification. The cross section is flattened on Top Smackover. See legend for facies color codes and sample color codes. Depths (ft) are marked.

VITA

Name   Christina Marie Dicus

Address   1218 St. Andrews Dr.
                                Dunedin, FL 34698

Email Address   christina.dicus@yahoo.com

Education   B.S., Earth Science, Rice University, 2005
                                M.S., Geology, Texas A&M University, 2007
                                M.S., Reservoir Geoscience and Engineering, IFP School,
                                Rueil Malmaison, France, 2007

Professional Affiliations   American Association of Petroleum Geologists

Professional Experience   Burlington Resources, Houston, TX- Intern
                                Schlumberger, Greenwood Village, CO- Intern
                                BP America, Houston, TX- Intern
                                ConocoPhillips, Houston, TX- Petrophysicist